FINAL REPORT
SATCOM ELECTRONIC SCAN ANTENNA

SBIR PHASE II
MRA P354-F
For the Period Covering: 04/05/00 - 10/31/00

31 October 2000

Prepared By:

Malibu Research Associates
26670 Agoura Road
Calabasas, CA 91302

Prepared For:

Commander
Space and Naval Warfare
Systems Command (SPAWAR)
4301 Pacific Highway
Bldg. OT-1, Room 2721
San Diego, CA 92110-3127

Under:

SBIR Phase II Program
Topic No. N95-111
Contract No. N00039-97-C-0069
CLIN 0002
CDRL Data Item A002
Contract Value: $579,842.00
Competitive Award

Distribution Statement: "Approved for public release; distribution is unlimited."

Malibu Research

26670 Agoura Road
Calabasas, CA 91302–1974
(818) 880-5494   Fax 880-5499

20001106 022

TABLE OF CONTENTS

TABLE OF FIGURES

This is the final report on the experimentation, design and test of a C/Ku-band electronic scan antenna for Space and Naval Warfare Systems Command based on a concept using gas-discharge plasma display technology.

1.0 INTRODUCTION

In this final report is presented the progression of the electronic scan antenna research highlighting the key results and stumbling blocks throughout this SBIR phase II period.

The original premise was to use the FLAPS™ technology, a Malibu Research patent product, and merge it to plasma in order to generate a dynamic phased array antenna. The FLAPS™ technology consists of generating a reflective surface from dipoles of various lengths placed over a ground plane in an array configuration. The dipoles reflect incident RF energy with a phase shift that is dependent on the dipole configuration in relation to the RF frequency. By generating the dipoles via plasma, the reflective surface thus becomes a dynamically steerable antenna. The major advantage of such an antenna is the hysteresis property of the plasma. The hysteresis enabled such an array antenna to be addressed in a latching technique thus considerably reducing the driver requirements and its complexity. To use plasma as the RF reflective element, its conductive properties within the proposed environment and plasma conditions must be sufficient.

The Phase I result of this SBIR demonstrated that plasma could be used as beam steering elements within the FLAPS™ technology. However, what Phase I failed to unveil was twofold:

> Excessive plasma absorption when used as a reflective element.

> Low plasma conductivity due to low plasma electron density.

These findings were later identified in the first stage of the Phase II period. When the expected results were not produced, further investigation (both theoretical and experimental) revealed the previously mentioned problems. As a result, plasma cannot be used as a reflective element in the proposed environment.

Although plasma cannot be the reflective medium, it was discovered that plasma could be used in a slightly different configuration to produce the sought after dynamically steerable latching array antenna. The revised design makes use of the plasma dielectric perturbation as opposed to relying on the conductivity of the plasma. With this revised antenna design concept, the major advantages of the original premise are maintained, and are as follows:

> Concept revolves around plasma.

> Plasma is the active element of the electronic scan antenna.

> The latching property of the antenna array, due to the plasma hysteresis.

> Considerable cost savings over conventional phased array systems.

Following this enlightenment, it was decided to build an in-house chamber in order to speed up the data acquisition as well as to enable full control (over the "controllable" parameters of plasma) of the plasma properties. This turned out to be the

key factor in successfully producing the plasma phase shifter element.   Throughout the plasma phased-array antenna research major stumbling blocks were overcome; namely:

> Viability of plasma within a stripline circuit.

> Optimum stripline configuration, including plasma firing mechanism.

> Produce and demonstrate a one-bit plasma phase shifter.

> Generating an environment promoting the plasma hysteresis.

The research progression is presented in the following sections in detail.

2.0 INITIAL RESEARCH OF PHASE II

The premise of this SBIR was to develop a Low-Cost Phased-Array antenna by merging two technologies, the plasma and Malibu Research FLAPS™ (FLAt Parabolic Surface) phased surface technology. Plasma enables a latching addressing scheme, thus reducing the complexity and cost of the drivers. The FLAPS™ technology transforms a flat dipole surface in parabolic reflector. By merging both technologies, the focal point of the flat dipole surface can be dynamically scanned. The results of the SBIR Phase I (Contract #N00039-96-C-0010) demonstrated 60 degree beam-scanning with a discrete plasma-element mini-array antenna. These initial results confirmed the vision of producing a dynamic FLAPS™ electronic scan antenna.

The initial research of Phase II consisted of identifying possible design candidates, building the test sample on glass substrates and conducting preliminary tests.

2.1 PLASMA ELEMENT CANDIDATES

Three plasma element candidates were identified; they consist of the continuous dipole, the quantized dipole and the dipole bits, see **Figure 2.1-1**. The pros and cons of each candidate are presented in **Table 2.1-1**. At the time, the best candidate was the quantized dipole since it would require less plasma and would be easier to bench test.
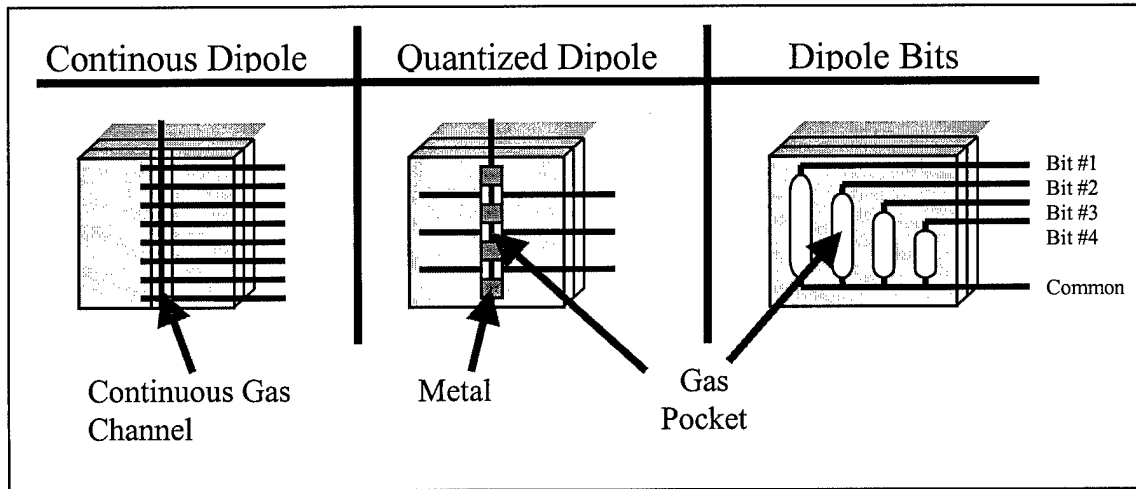
FIGURE 2.1-1 PLASMA ELEMENT CANDIDATES

TABLE 2.1-1 CANDIDATES' PROS & CONS

	Continuous Dipole	**Quantized Dipole**	**Dipole Bits**
Pros	▪ Continuous dipole length control ▪ Most adaptable to multi-band operation ▪ Naturally set up for matrix drive	▪ Adaptable lengths ▪ Natural matrix addressing ▪ Less plasma needed ▪ Identifiable development procedure (easier to bench test)	▪ Electrodes all run horizontally (should solve the RF interference problem)
Cons	▪ Pixel connectivity/ uniformity unknown ▪ Maximum electrode interference ▪ Difficult development process	▪ Quantized phase states	▪ May not have high enough electron density (most of tube plasma is in the "positive column" state) ▪ Requires high voltage to excite ▪ Electrode routing issue for a large array

2.2 TESTING CONCEPT

The next step was to define a way to establish the RF properties of the elemental plasma cell. The fact is that the individual cell is too small to radiate at in open space, the results would be corrupted by the apparatus reflections. Thus, the RF test of the elements needs to be performed in an enclosed circuit, i.e. in a stripline configuration. In **Figure 2.2-1** is shown a block diagram of the test setup which consist of an RF generator, a directional coupler, a reference portion with an adjustable phase, a detector and the test sample.
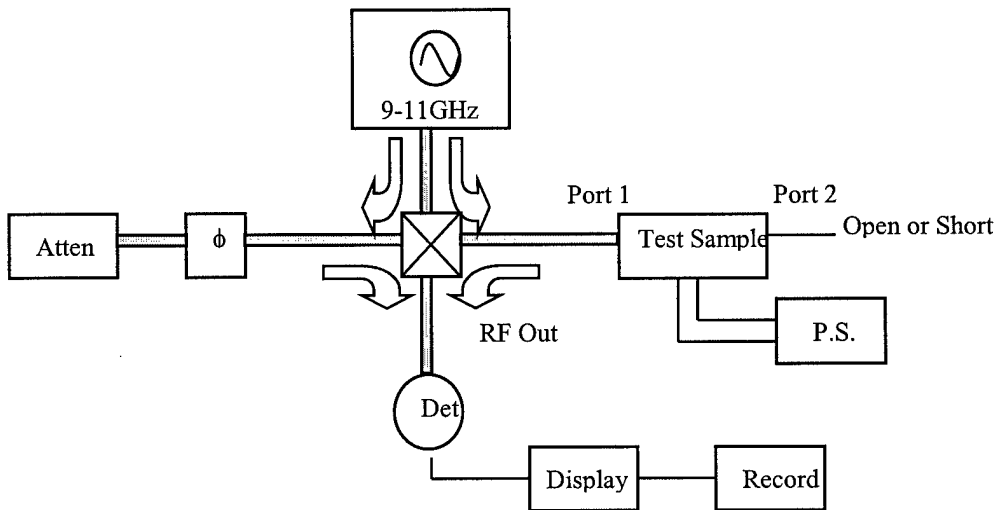
FIGURE 2.2-1 BLOCK DIAGRAM OF TEST SETUP

Two venues are chosen to produce the test samples:

- Contract out to TVI (Technical Vision Inc.) to produce samples on glass substrate.

- Build in parallel at MRA samples using Nixie Tubes.

A diagram of a test sample is shown in **Figure 2.2-2** and pictures of a test sample from

TVI, in **Figure 2.2-3**, and using Nixie Tubes, in **Figure 2.2-4**.
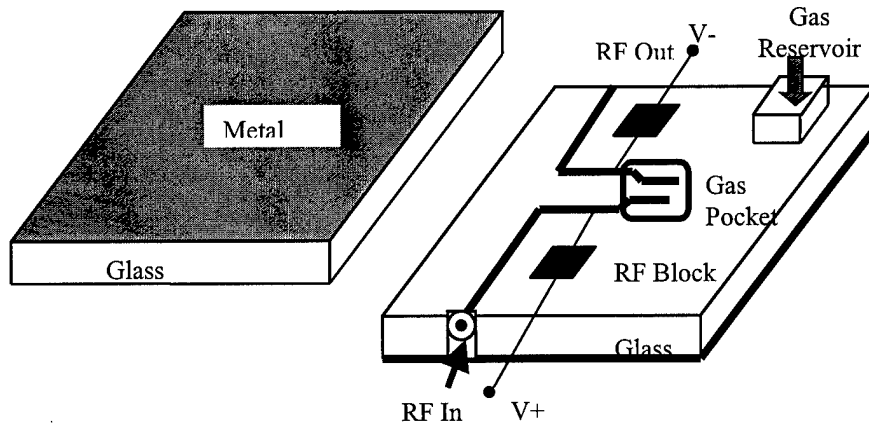
FIGURE 2.2-2 BLOCK DIAGRAM OF TEST SAMPLE
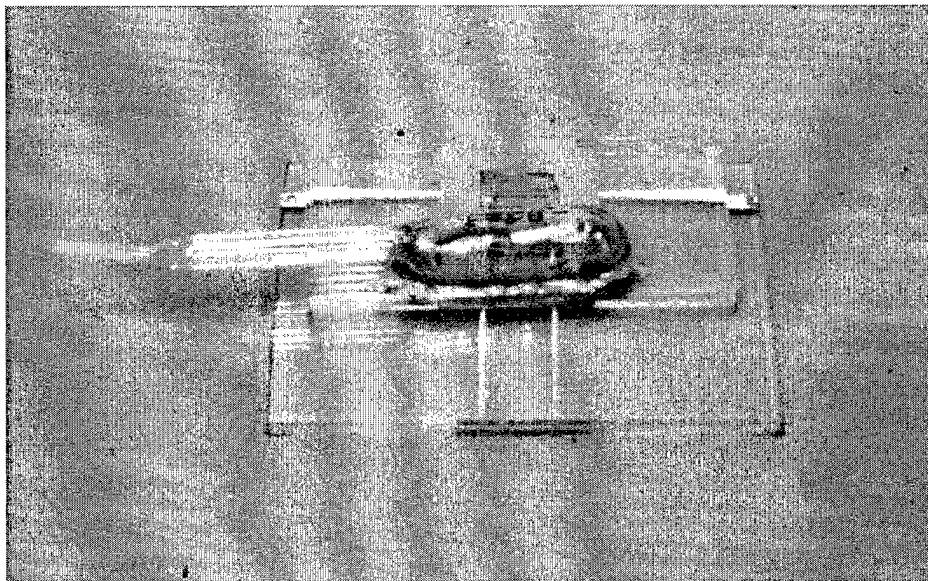
FIGURE 2.2-3 PICTURE OF TEST SAMPLE FROM TVI

2.3 THE PLASMA SWITCH CONCEPT

A stripline configuration including electrodes within a gas pocket is an excellent way of characterizing the plasma. When no plasma is present, the electrodes will act as an RF passband that will be distorted by the presence of plasma. In **Figure 2.3-1** is shown the stripline configuration. The injected RF, at Port 1, travels through the stripline and gets reflected at Port 2 (Port 2 is either short-circuited or open circuited) when no plasma is present. With the presence of plasma, part of the RF energy will be reflected or attenuated at the plasma region and part will be transmitted through. A DC bias voltage

applied to the electrodes via an RF transparent DC path (an RF block) induces plasma.

When voltage is applied to the gas immersed electrodes, some gas electrons separate

from the atoms creating an ionized region, the plasma.
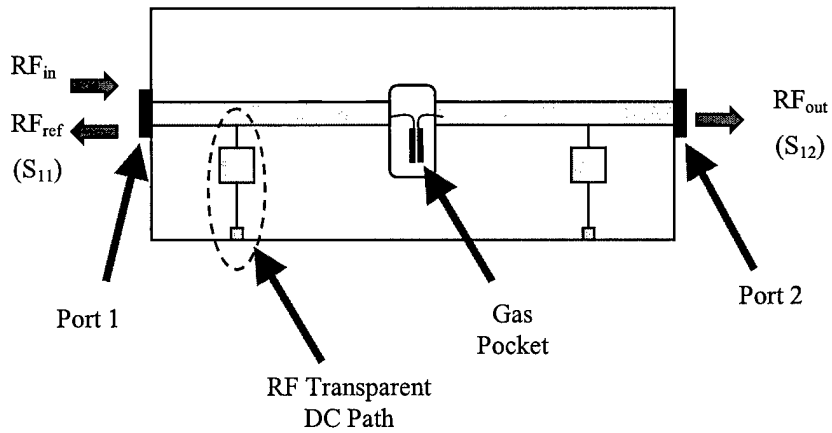
FIGURE 2.3-1 THE STRIPLINE CONFIGURATION

Shown in **Figure 2.3-2** is the equivalent DC circuit (Figure 2.3-2b) of the stripline

configuration (Figure 2.3-2a).   In Figure 2.3-2 a & b are shown the equivalent DC

representation of the electrodes to the DC current between points A & B with and without

plasma.   Without plasma, no current can flow across the electrodes due to the gap

between them; therefore, the electrodes look like an open circuit or a capacitor.   Plasma

creates a DC path to the current across the electrodes.
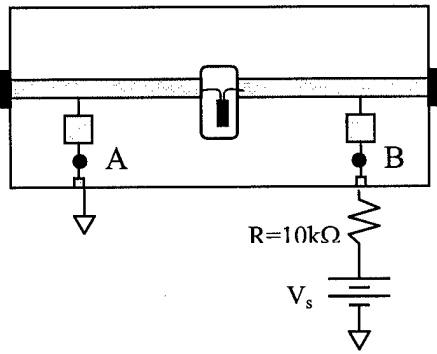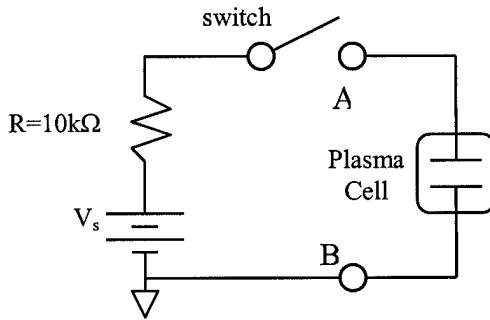
a) Stripline Configuration   b) DC Equivalent Circuit
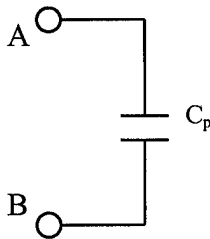
c) Electrode Representation without Plasma   d) Electrode Representation with Plasma
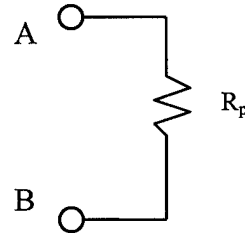
FIGURE 2.3-2 THE STRIPLINE EQUIVALENT DC CIRCUIT

In **Figure 2.3-3** is presented the equivalent RF circuit (Figure 2.3-3b) of the stripline configuration (Figure 2.3-3a). In Figure 2.3-3 a & b are shown the equivalent RF representation of the electrodes to the DC current between points A & B with and without plasma. Without plasma, RF can propagate across the electrodes within the passband of the circuit since the electrodes are tightly coupled. The presence of plasma creates a wall to the incident RF energy and thus reflects or absorbs the energy.

a) Stripline Configuration   b) RF Equivalent Circuit

c) Electrode RF Representation   d) Plasma RF Representation
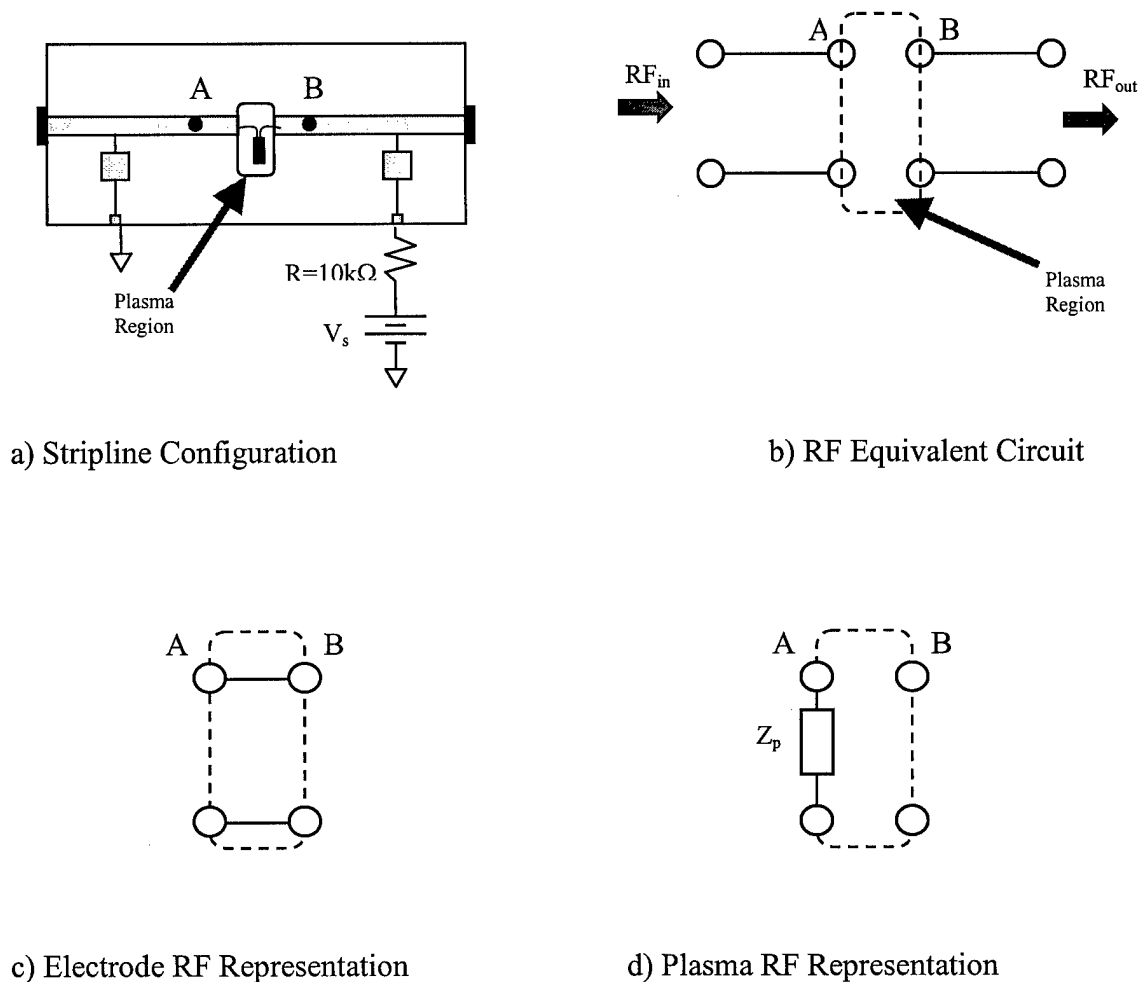
FIGURE 2.3-3 THE STRIPLINE EQUIVALENT RF CIRCUIT

2.4 PHASE II PRELIMINARY TEST RESULTS

Parallel testing was conducted using the glass substrate samples created by TVI and the Nixie Tube stripline circuits. Within the stripline circuit, the plasma behaves well. The glass substrate sample results are shown in **Figure 2.4-1**. Notice the passband of the circuit between 5.5GHz and 7GHz with a low insertion loss (<2dB). On the same plot is shown the insertion loss (S21, the ratio of the transmitted energy to the incident energy) of the circuit, with the presence of plasma, for various gas pressure. It is seen here that the efficiency of plasma to block the incident RF energy is dependent on the pressure of the gas within the electrode area. On average, the plasma blocks 10dB of the incident RF energy.

In **Figure 2.4-2** results of the Nixie Tube configuration are shown. With the Nixie Tube the passband is centered around 10.1GHz (seen on the 0vts curve). Here the efficiency of plasma to block RF energy is measured as a function of DC applied voltage to the electrodes. In this case the plasma blocks the RF energy by at least 25dB when a DC voltage of 80 is applied to the electrodes.
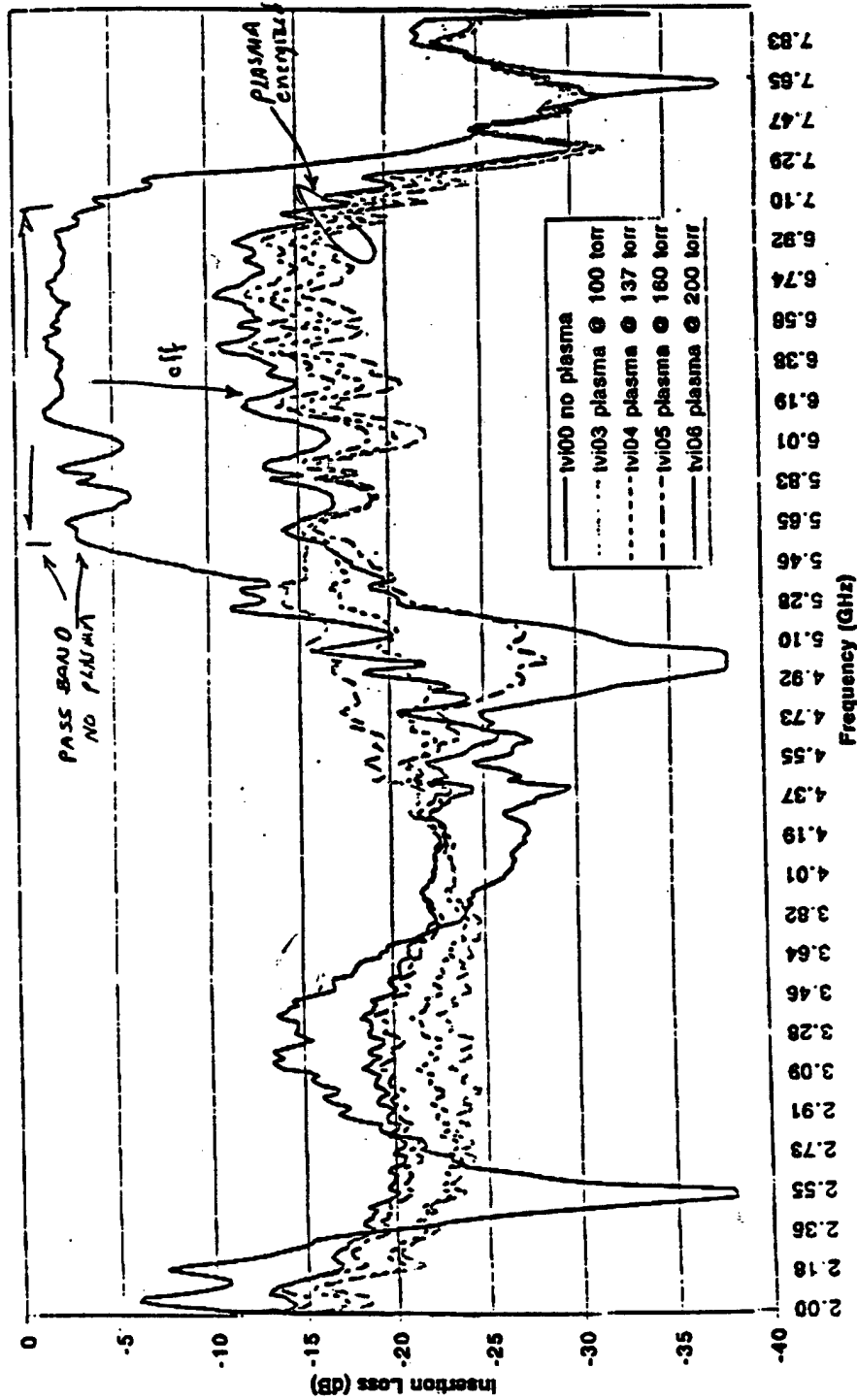
FIGURE 2.4-1 INSERTION LOSS OF GLASS SUBSTRATE AS A FUNCTION OF PRESSURE
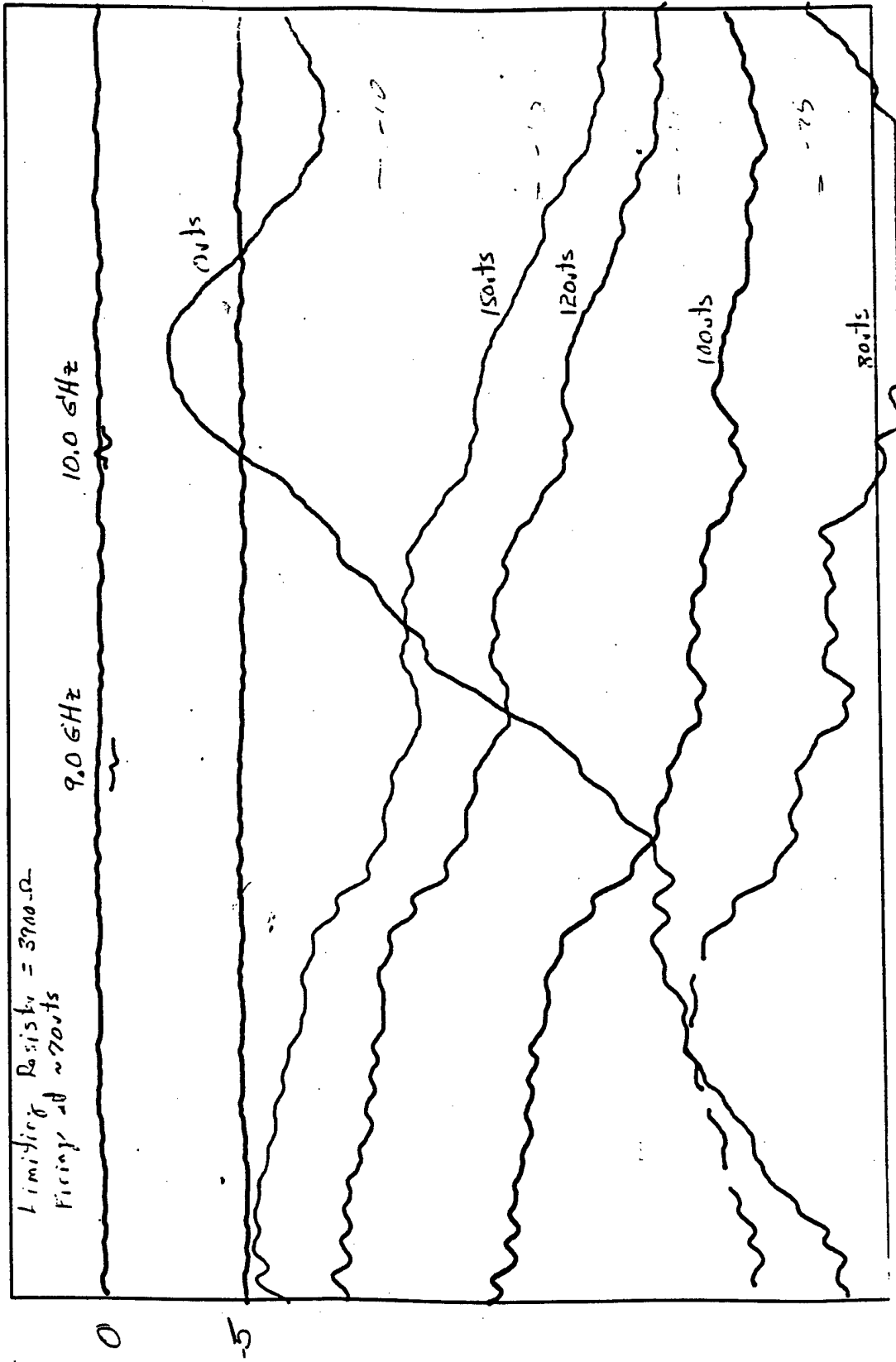
FIGURE 2.4-2 INSERTION LOSS OF NIXIE TUBE SAMPLE AS A FUNCTION OF DC VOLTAGE

2.5 INITIAL OBSERVATIONS

Initial testing demonstrated the efficiency of plasma to block the incident RF energy. Furthermore this testing showed that the Neon-Argon (NeAr) gas mixture was the better choice of all the mixture tested. The turn-around time to produce monolithic glass sample was between 2-3 weeks, which considerably reduced the progress of the research. Acceleration of sample production was necessary, as was having more control over the plasma parameters.

After the success of these preliminary tests, an initial mini-glass substrate array was manufactured and tested. The idea was to observe a beam scan of the glass substrate plasma array antenna. The mini-array was subjected to a plane wave and the reflected wave was to be measured. It turned out that the initial result did not reflect what was anticipated. Most of the energy went through the array; there was minimal reflected energy. It was realized that creating a virtual wire out of plasma seemed to be problematic. The observed plasma phenomenon also demonstrated that it could create a phase shift in the stripline test circuit.

To better understand the plasma phenomenon, Dr Paul Bellan, a plasma physicist from CalTech, was included in the team as a consultant.

3.0 THEORETICAL PLASMA ANALYSIS

Presented in this section is a plasma theoretical analysis focusing on the importance of the collision frequency, electron density and skin-depth to the conductivity of plasma. The original concept of the gas-discharging plasma displays was to use the monochromatic display as the reflecting surface, where dipole elements of modulable length would be created dynamically via the display's plasma pixels. As will be demonstrated, the plasma conductivity is very low therefore the efficiency of using plasma as a dipole is considerably reduced.

3.1 DERIVING THE SKIN DEPTH EQUATIONS

To act as a dipole, the plasma reflecting properties must be in close proximity to a metal conductor. Basically when plasma is present, it has to display high conductivity to the impinging electric fields; in other words, its skin depth must be small compared to the impinging electric field wavelength. There are two kinds of skin depth, the collisional and the collisionless skin depth. In the following, the theory leading to the skin depth is derived.

The derivation starts, as do most electromagnetic derivations, from Maxwell's equation to which are coupled: Ampere's Law, Faraday's Law and Newton's electron force equation.

$$\nabla \times \mathbf{E} = -\frac{\partial \mathbf{B}}{\partial t} \tag{1}$$

$$\nabla \times \mathbf{B} = \mu_0 \mathbf{J} + \varepsilon_0 \mu_0 \frac{\partial \mathbf{E}}{\partial t} \tag{2}$$

$$m_e \frac{d\mathbf{v}}{dt} = q_e \mathbf{E} - v_e m_e \mathbf{v} \tag{3}$$

Where v_e is the collision frequency (also known as the collisional drag) on the electrons due to the collisions with the ions and neutrons, m_e is the electron mass and q_e is the electron charge. In this plasma application, the collisions with neutrons are the main contributors to the collisional drag since the plasma is weakly ionized. In the frequency domain, equation (3) can be re-written as

$$\mathbf{v} = \frac{q_e \mathbf{E}}{-i\omega m_e + v_e m_e}$$

$$= \frac{q_e \mathbf{E}}{-i\omega m_e \left(1 + i v_e / \omega\right)} \tag{4}$$

From equation (4) are defined the collisional and collisionless regions as:

Collisional   => $v_e/\omega \gg 1$

Collisionless => $v_e/\omega \ll 1$

Thus in the collisionless regime, the electron velocity is effectively independent of the collision frequency v_e.

Using the definition of both regimes, the skin depth of the plasma can be derived by defining first the propagation constant k via the corresponding wave equation. Along the way the plasma frequency will be defined.

Taking the curl of equation (1) (Faraday's Law) one obtains:

$$\nabla \times \nabla \times \mathbf{E} = -\frac{\partial}{\partial t}\left(\nabla \times \mathbf{B}\right) \qquad (5)$$

which, after using vector identities and assuming that the wave is transverse, becomes

$$\nabla^2 \mathbf{E} = \mu_0 \frac{\partial \mathbf{J}}{\partial t} + \varepsilon_0 \mu_0 \frac{\partial^2 \mathbf{E}}{\partial t^2}$$
$$= -i\omega\mu_0 \mathbf{J} - \omega^2 \mu_0 \varepsilon_0 \mathbf{E} \qquad (6)$$

The current $\mathbf{J}$, is mainly propagated by the electrons, and thus is given as

$$\mathbf{J} = n_e q_e \mathbf{v} \qquad (7)$$

where n_e is the electron density. Replacing equation (7) into Newton's electron force equation, (4), one can derive the plasma frequency (an important parameter in the plasma world).

$$\mathbf{J} = \frac{n_e q_e^2 \mathbf{E}}{-i\omega m_e \left(1 + iv_e / \omega\right)}$$
$$= \varepsilon_0 \left\{ \frac{n_e q_e^2 \mathbf{E}}{-i\omega m_e \varepsilon_0 \left(1 + iv_e / \omega\right)} \right\} \qquad (8)$$

from which the plasma frequency is defined as:

$$\omega_{pe}^2 = \frac{n_e q_e^2}{\varepsilon_0 m_e} \qquad (9)$$

Substituting equation (9) into (8) and the result in the wave equation, (6), the following is obtained:

$$\nabla^2 \mathbf{E} = \left\{ \frac{\omega_{pe}^2}{\left(1 + i v_e / \omega\right)} - \omega^2 \right\} \mu_0 \varepsilon_0 \mathbf{E} \tag{10}$$

The solution to the wave equation is then given as

$$\left\{ \frac{\omega_{pe}^2}{\left(1 + i v_e / \omega\right)} - \omega^2 + k^2 c^2 \right\} \mathbf{E} = 0 \tag{11}$$

where $c^2 = 1/(\varepsilon_0 \mu_0)$, is the speed of light. From (11) is obtained the so-called wave dispersion relation:

$$\omega^2 = \frac{\omega_{pe}^2}{\left(1 + i v_e / \omega\right)} + k^2 c^2 \tag{12}$$

In this application, the plasma is assumed to have a sufficiently high density such that the left-hand term in the dispersion relation can be ignored.

$$\omega^2 << \frac{\omega_{pe}^2}{\left(1 + i v_e / \omega\right)}$$

Thus,

$$k^2 = -\frac{\omega_{pe}^2}{\left(1 + i v_e / \omega\right) \cdot c^2} \tag{13}$$

Note that the smallest k value between both regimes will dominate. Now let's derive the skin depth for both regimes.

3.1.1 The Collisionless Regime

The collisionless regime was defined as

$$v_e/\omega \ll 1$$

Thus, equation (13) becomes

$$k^2 = -\frac{\omega_{pe}^2}{c^2} \qquad (14)$$

Which means that the wave will be evanescent, thus exponentially decaying at a rate of $e^{(-x\omega_{pe}/c)}$. The skin depth is defined as the distance for the electric field to decay by a factor of e^{-1}. Therefore,

$$\partial_{collisionless} = \frac{c}{\omega_{pe}} = \frac{5x10^5}{\sqrt{n}} \text{cm} \qquad (15)$$

where n is the density per cm cube. In the collisionless regime the skin depth is independent of the frequency.

3.1.2 The Collisional Regime

The collisional regime is defined as $v_e/\omega \gg 1$, thus equation (13) becomes

$$k^2 = -\frac{\omega_{pe}^2 \cdot \omega}{iv_e \cdot c^2} \qquad (16)$$

$$= i\frac{\mu_0 \cdot n_e \cdot q_e^2 \omega}{m_e \cdot v_e}$$

In the collisional regime, equation (8) can be expressed in terms of the electrical resistivity as

$$\mathbf{J} = \frac{n_e q_e^2 \mathbf{E}}{v_e \cdot m_e}$$

$$= \frac{1}{\eta} \mathbf{E} \qquad (17)$$

From which equation (15) may be expressed in terms of the electric resistivity, η, as

$$k^2 = -\frac{\omega_{pe}^2 \cdot \omega}{i v_e \cdot c^2}$$

$$= i \frac{\mu_0 \omega}{\eta} \qquad (18)$$

The wave will have an evanescent mode exponentially decaying at the rate defined by the real part in the exponential term solving to the wave equation. The exponential term is:

$$\exp(ikx) = \exp(i\sqrt{i\mu_0\omega/\eta} \cdot x \qquad (19)$$

Thus, the collisional skin depth is

$$\partial_{collisional} = \sqrt{\frac{2\eta}{\mu_0\omega}} \qquad (20)$$

3.2 PREDICTING THE PLASMA SKIN DEPTH

As mentioned earlier, the plasma reflecting properties must be fairly close to a metal conductor to act as a dipole. In other words, the skin depth presented by the plasma to the impinging field has to be as close as possible to the skin depth of a metal. To grasp the implication of this statement a comparison between the skin depth of metal, copper, and plasma is presented.

3.2.1 Skin Depth of Copper

The copper's parameters are:

- $n_e = 10^{23}$ cm^{-3}

- $\eta = 1.8 \times 10^{-8}$ Ω/m

Therefore at 9.0GHz the copper's skin depths for both regimes are:

⇒   Collisionless

$$\partial_{collisionless} = \frac{5 \times 10^5}{\sqrt{10^{23}}} cm = 1.6 \times 10^{-6} cm$$

⇒   Collisional

$$\partial_{collisional} = \frac{1.8 \times 10^{-8} \Omega/m}{\sqrt{4 \times 10^{-6} \pi^2 \cdot 9 \times 10^9}} = 2.25 \times 10^{-7} m = 2.25 \times 10^{-5} cm$$

The effective skin depth of copper is 2.25x10^{-5}cm (since it's the largest of both, remember that the dominant regime is the one that "produces" the smallest k which is inversely proportional to the skin depth).

3.2.2 Skin Depth of Plasma

The plasma density will be in the range of $n_e = 10^{12}$ cm^{-3}

$\Rightarrow$ Collisionless

$$\partial_{collisionless} = \frac{5 \times 10^5}{\sqrt{10^{12}}} cm = 0.5cm$$

Even without calculating the collisional skin depth, it is seen from the plasma collisionless skin depth that the copper's skin depth is in the order of 20,000 times smaller than that of the plasma, see **Table 3.2.2-1**.   Therefore, plasma cannot be considered as an equivalent to metal by no means.

It is conclusive that plasma will not act as a dipole. It is not a good passive reflector (plasma does not act as a metal conductor to an impinging field). However, as will be demonstrated in the following section, plasma can be used as a good RF block/reflector within a circuit.

TABLE 3.2.2-1 SKIN DEPTH OF COPPER VS PLASMA @ 9GHZ

	n_e (cm^{-3})	$\eta(\Omega/m)$	Collisional	Collisionless
Copper	1.0E23	1.8E-8	2.25E-5 cm	1.6E-6 cm
Plasma	1.0E12			0.5 cm

3.3 THEORETICAL ANALYSIS OUTCOME

Theoretical analysis demonstrated that plasma conductivity is very low and thus, renders the initial concept of using plasma as a dynamic dipole non-realistic. Although plasma cannot be used as a pure dipole, in the initial research leg of Phase II it was seen that plasma could be used in a stripline configuration as an RF wall, some sort of a switch with hysteresis.

Following these results, a revised antenna design concept was brought forward. While the design was modified, the major advantages of the original premise were maintained. These are:

- Concept revolves around plasma.

- Plasma is the active element of the plasma phased-array antenna.

- Plasma hysteresis enables a latching configuration.

- Considerable cost savings over conventional phased-array systems.

In order to continue the research at an accelerated pace, an in-house test chamber needed to be built. This would allow us to have full control over the major plasma parameters. Furthermore, new test samples were designed in order to increase throughput.

4.0 IN-HOUSE TEST CHAMBER

As mentioned in the previous section, an in-house vacuum test chamber would reveal itself to be very beneficial. The major reasons for building such a system are as follows:

- The subcontractor's sample turn around was too slow.

- Needed to increase throughput of experiments.

- To have full control over the plasma key parameters.

- Decrease the cost of producing test samples.

In this section is presented the fully assembled test setup including some photos of the arrangement as seen in **Figure 4.0-1**.
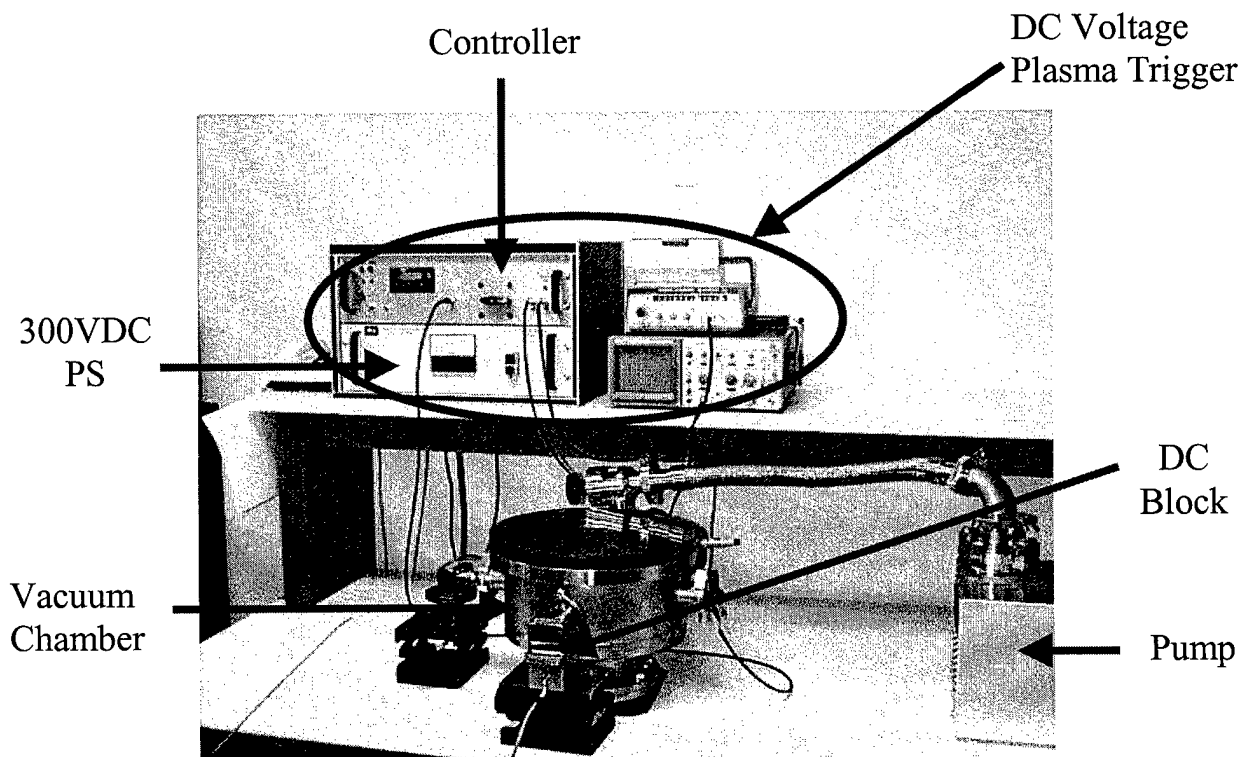
FIGURE 4.0-1 IN-HOUSE VACUUM TEST CHAMBER

In **Figure 4.0-2** is a photo of a stripline test sample in the vacuum chamber with the top portion lifted and the plasma firing between the electrodes.
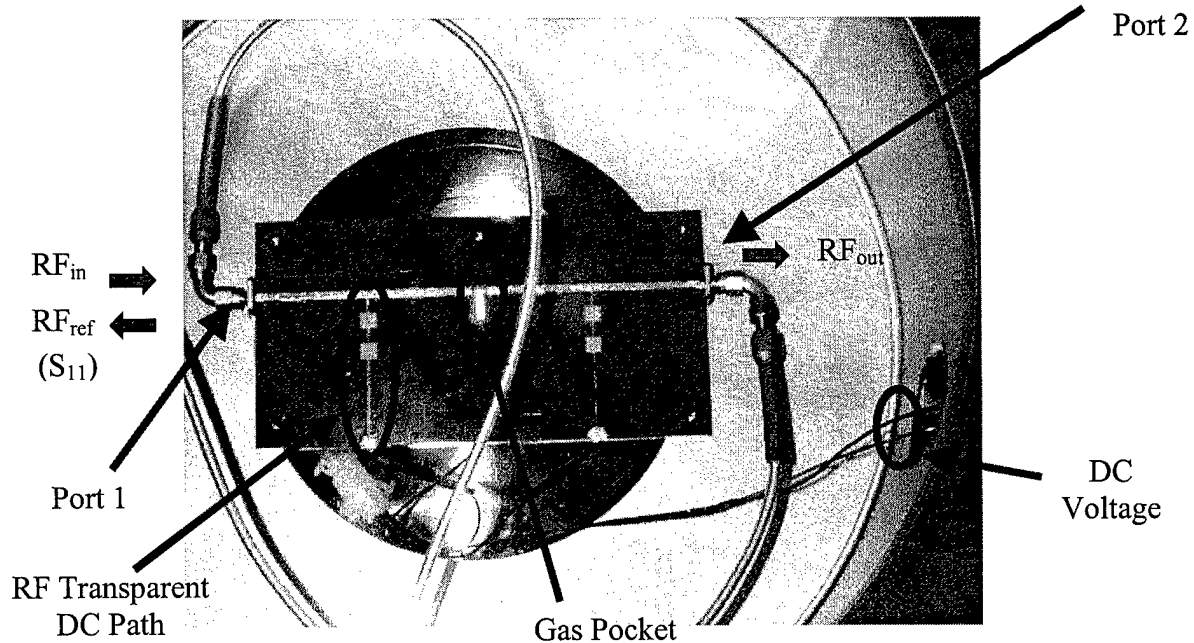
FIGURE 4.0-2 TEST SAMPLE WITH PLASMA FIRED

4.1 THE STRIPLINE TEST SAMPLES

The stripline test samples are conventional stripline technology, copper transmission line etched over a dielectric medium, in which a pocket is machined out and electrodes are introduced. The stripline test samples are inserted into the vacuum chamber in which air is pumped out and replaced by a pure gas. The stripline is a simple 50Ω transmission line surrounded by a duroid medium ($\varepsilon_r = 2.2$) and slotted in the middle where an air gap is machined. To each end of the transmission line are then soldered electrodes extending well into the air gap. The DC plasma triggering/sustaining voltage is applied to the electrodes via four quarter-wavelength impedance mismatch between the

DC power supply and the transmission lines, two per transmission line. The impedance mismatch renders the DC path invisible to the RF within the stripline. A typical stripline test sample described above is shown in **Figure 4.0-2** with the top portion lifted and the plasma firing between the electrodes.

The plasma is characterized by taking insertion loss measurements of the stripline with and without its presence while varying the sensitive parameters. **Figure 4.1-1** shows how the insertion loss is measured (P_{in} & P_{out} are the input and output power respectively).

$RF_{in} \longrightarrow$ $\longrightarrow RF_{out}$

$IL = 10 \log (P_{out}/P_{in})$
$IL = 0 \text{ dB} \quad ; \text{ for } P_{out} = P_{in}$
$\quad\quad = -3 \text{ dB} ; \text{ for } P_{out} = P_{in}/2$
$IL_{ideal} \quad -20dB \text{ in presence of plasma}$
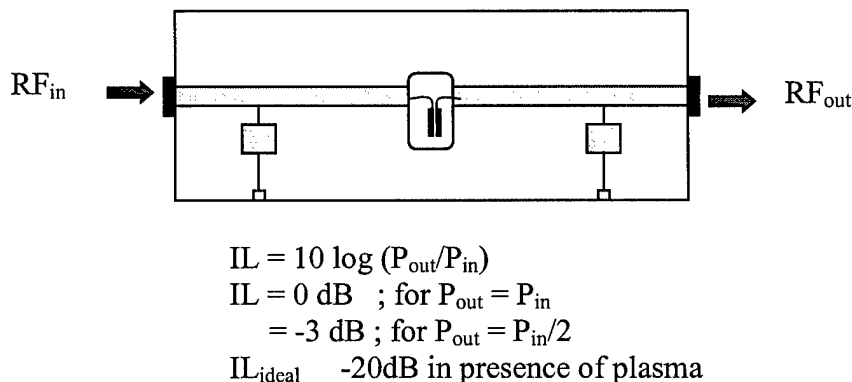
FIGURE 4.1-1 INSERTION LOSS OF THE TEST SAMPLE

4.2 INITIAL CHARACTERIZATION OF THE PLASMA

The result of having an in-house vacuum test chamber was to substantially increase the throughput of the measurements. It was easier and faster to change the sensitive variables on-the-fly. These parameters include the gas pressure; DC applied voltage and current limiting resistor. With one test sample a slew of data was now possible due to the availability of such a test chamber. In **Figure 4.2-1 a-c** is shown the

insertion loss of a test sample under full investigation. One parameter is held constant while the other two are scanned. Looking at Figure 4.2-1c one notices the so-called "sweet spot" near 30 Torrs with maximum insertion loss with the case of a current limiting resistor of 11kΩ. These results enabled a better understanding of the RF interaction with plasma.

Insertion Loss @ 9.0GHz
as a function of P & V
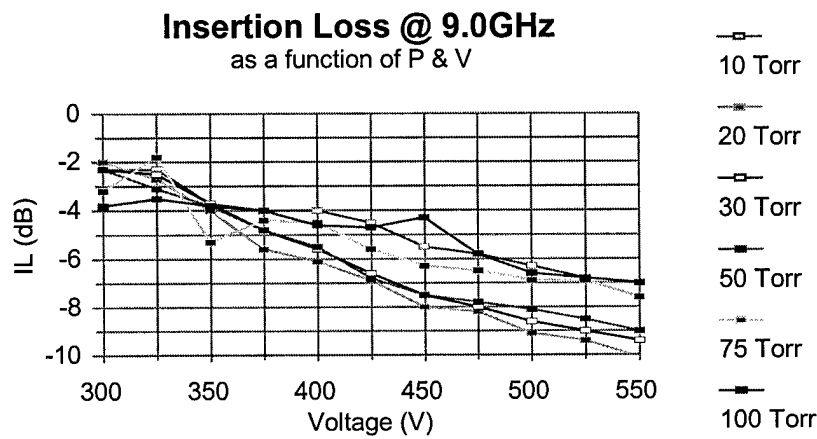
FIGURE 4.2-1A SAMPLE INSERTION LOSS AS A FUNCTION OF PRESSURE & VOLTAGE

Insertion Loss @ 9.0 GHz
as a function of R & V
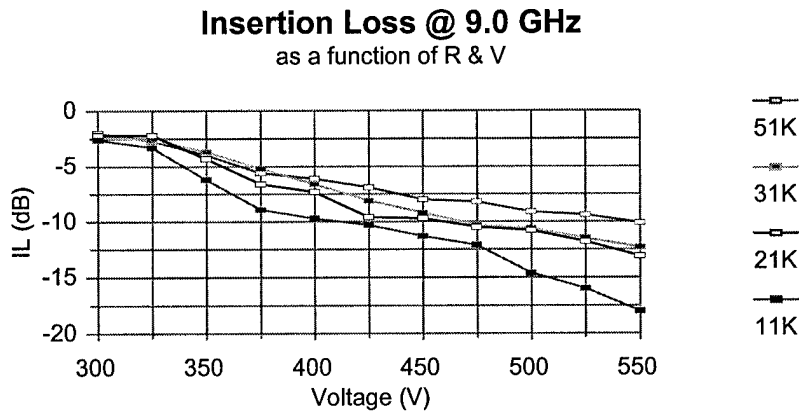
FIGURE 4.2-1B SAMPLE INSERTION LOSS AS A FUNCTION OF VOLTAGE & RESISTOR

Insertion Loss @ 9.0GHz & 500V
as a function of R & P
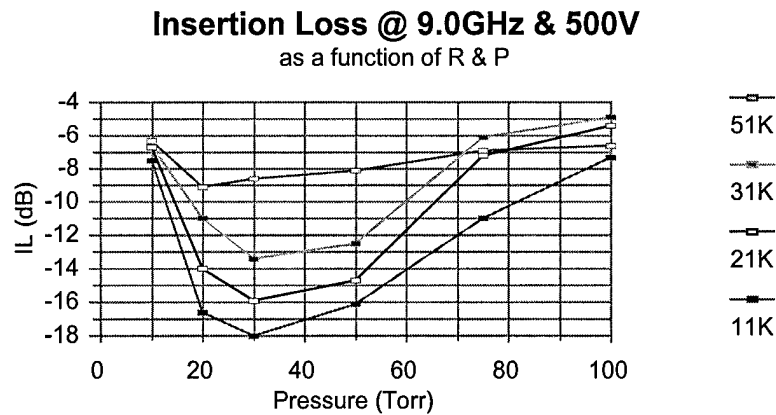
FIGURE 4.2-1C SAMPLE INSERTION LOSS AS A FUNCTION OF RESISTOR & PRESSURE

4.3 TEST CONFIGURATION SAMPLES

A slew of test samples was generated in order to determine the most efficient stripline design. Efficient in the following sense:

- define the optimum firing method (that which yields the highest RF insertion loss);

- determine the simpler manufacturing method yielding adequate RF insertion loss.

The major configurations tested were:

- Electrode-to-electrode

    Consists of inserting a gap in the middle portion of the stripline and coupling the RF energy from one side of the stripline to the other via two electrodes soldered on each end of the stripline, see **Figure 4.3-1a.**

- **Electrode-to-stripline**

  An electrode is inserted between the stripline and the ground plane in order to disrupt the RF energy, shown in **Figure 4.3-1b.**

- **Stripline-to-ground**

  Consists of soldering a piece of copper to the stripline, see **Figure 4.3-1c**.

- **Stripline-to-stripline**

  In terms of manufacturing cost, this configuration would be the least expensive. The coupling transmission lines are printed on each of the stripline plates and inserted between the plates is a thin dielectric plate with gas pocket where the stripline couples, see **Figure 4.3-1d**.

Out of the different samples tested the electrode-to-electrode configuration yielded the best results. Previously, only the insertion loss was measured. As a result we had to ask: Is the plasma acting as an RF wall or an RF absorber?
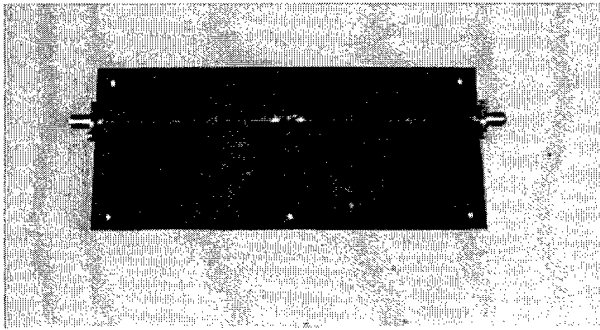
A) Electrode-to-Electrode
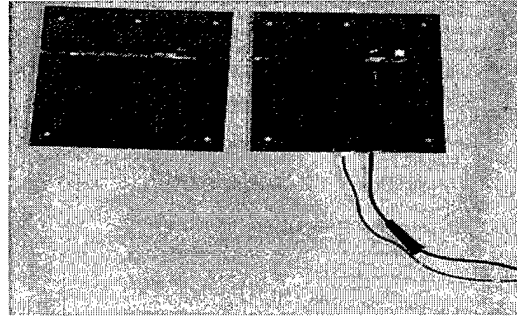
B) Electrode-to-Stripline
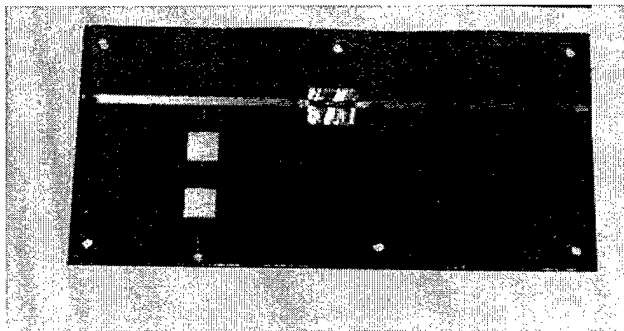
c) Stripline-to-Ground
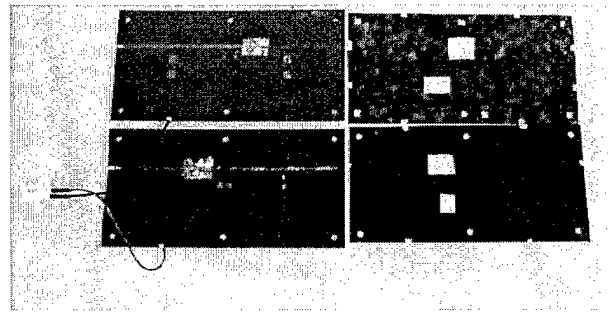
d) Stripline -to-Stripline

FIGURE 4.3-1 TEST CONFIGURATION SAMPLES

5.0 PLASMA, RF ABSORBER OR RF WALL

An interesting observation with regard to plasma is that, from the initially gathered data, it seems the plasma is a RF absorber. If such was the case, then the plasma cannot be used as a phase shifting element. As will be seen, the plasma seemed to act as an RF absorber due to the fact that the stripline was not matched to the electrodes. By inserting tuning stubs near the electrodes on the transmission line, the plasma then reflects most of the energy back to the source.

For plasma to present a wall (an open circuit) to the RF, the electrodes must have a considerable air gap between them. Furthermore, the circuit must be very well tuned using series inductance in conjunction with the capacitance presented by the electrodes. With this combination, the plasma will present an RF wall to the impinging energy.

Figure 5.0-1 shows the single transmission line stripline configuration that yielded very good results, demonstrating the possibility of using plasma as an RF blocking element. The relevant dimensions of the stripline are given below:

$$L_1 = 0.048'' \quad ; \quad w_1 = 0.192'' \quad : \quad L_s = 0.087''$$

$$L_e = 0.189'' \quad ; \quad w_e = 0.09'' \quad ; \quad w_{TL} = 0.055''$$

The stripline is etched on a duroid substrate with a relative dielectric constant of 2.25 and a thickness of 31mils.
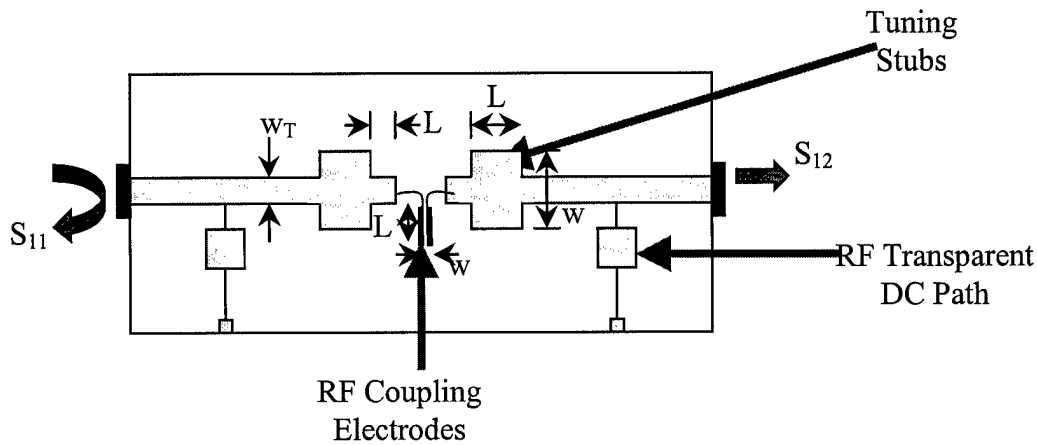
FIGURE 5.0-1 SINGLE TRANSMISSION LINE STRIPLINE

The first set of data shows the reflected and transmitted energy, S_{11} & S_{12} respectively, with and without the presence of plasma (see **Figures 5.0-2** and **Figures 5.0-3**). Figure 5.0-2 presents the data of the stripline without plasma. Notice the passband, 8.75GHz to 9.0GHz, of the stripline seen in the S_{21} measurement (S_{21} & S_{12} are identical measurements since the circuit is symmetrical) and the low level of the reflected energy, S_{11}. In Figure 5.0-3 is presented the reflected and transmitted energy with the presence of plasma (at a NeAr pressure of 15 Torr, with an applied voltage of 350V and a limiting resistor of 20kΩ). Here we conclude, from both measurements, that the plasma within this circuit acts as an RF wall since the reflected RF energy goes from –29.12dB to -1.48dB when the plasma is fired and consequently the transmitted energy (the insertion loss due to the plasma) is attenuated by 10.4dB.

The conclusion then is that plasma can be used within a stripline circuit as a phase shifting element.
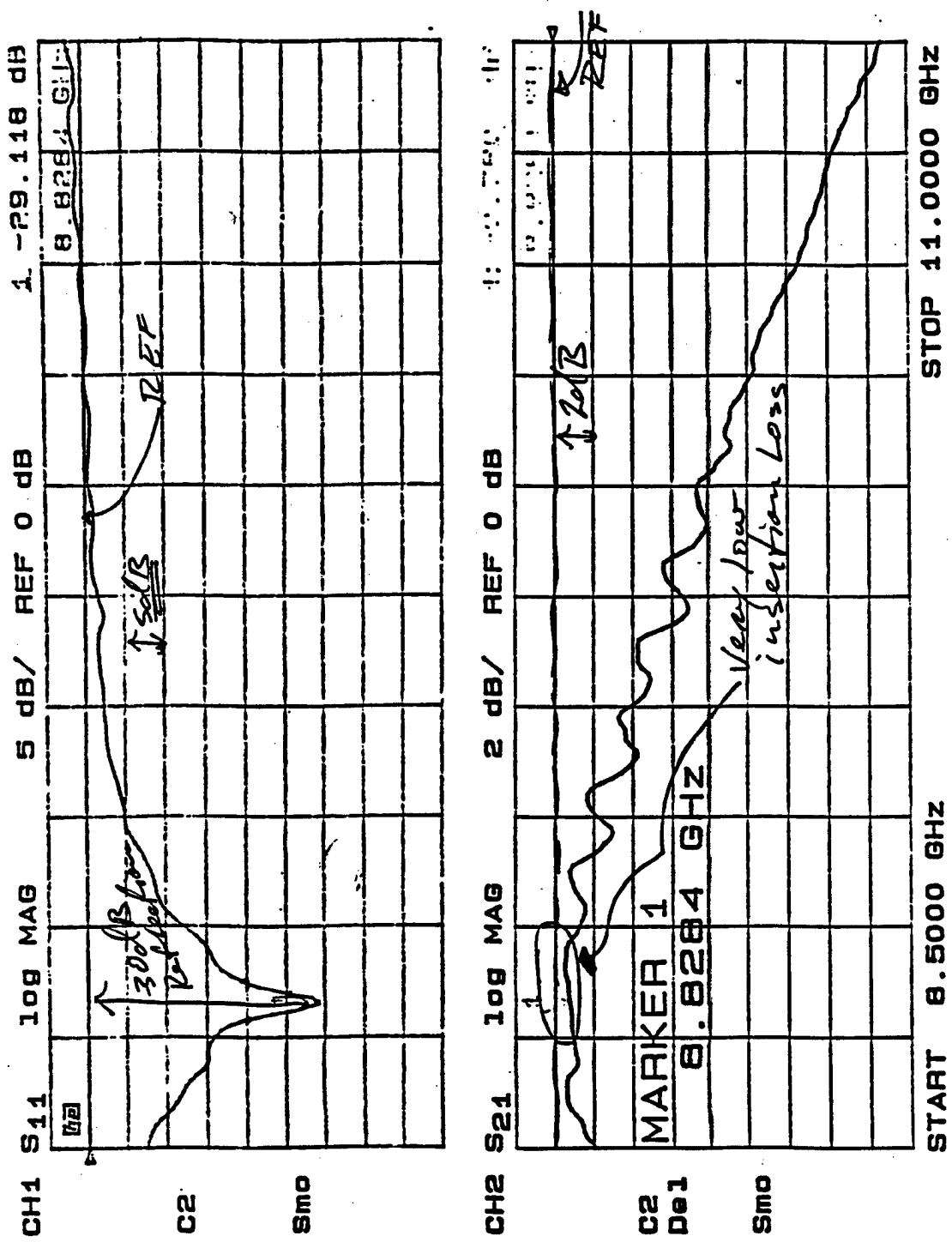
FIGURE 5.0-2 SINGLE TL STRIPLINE SIGNATURE, NO PLASMA
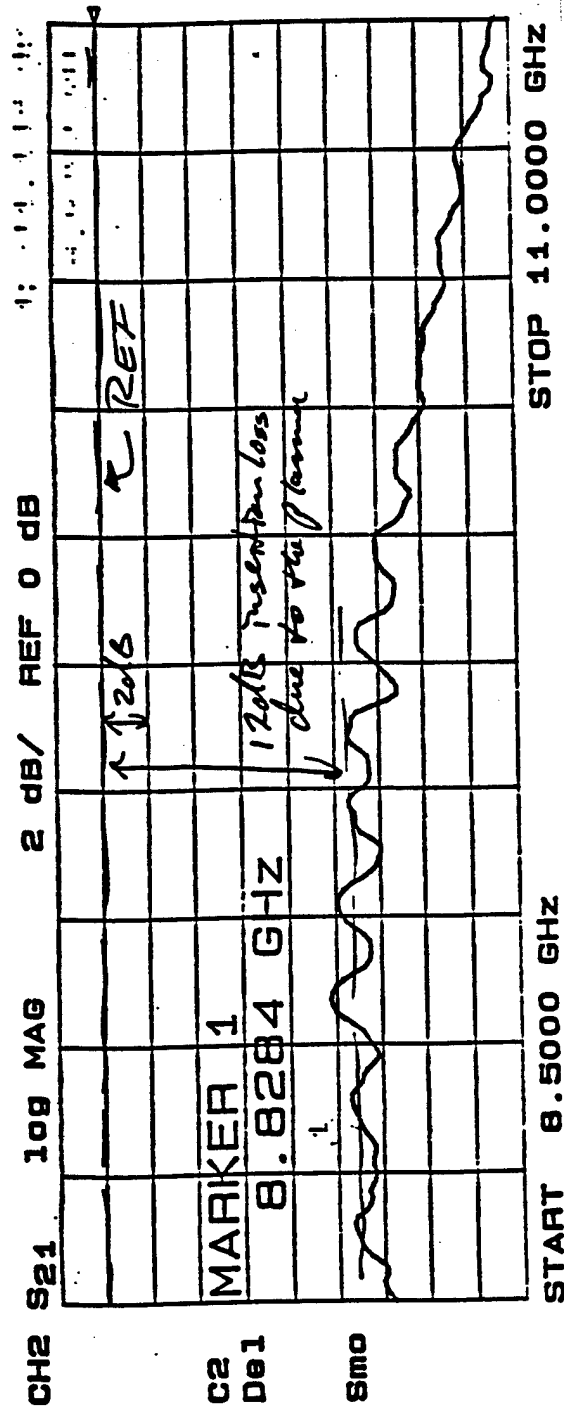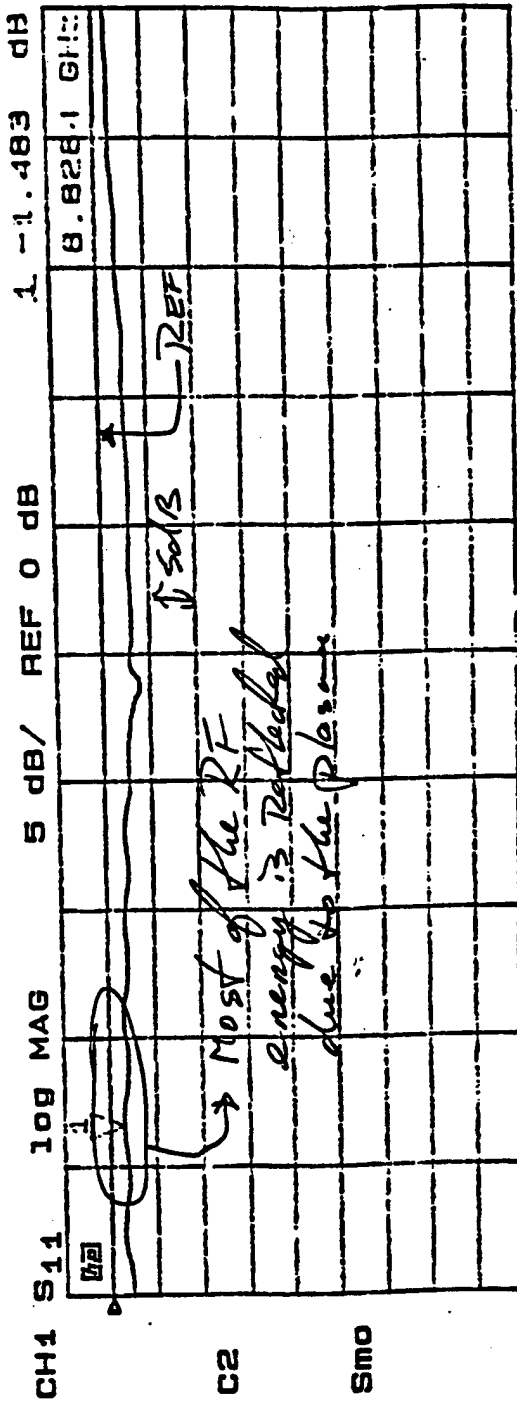
FIGURE 5.0-3 SINGLE TL STRIPLINE SIGNATURE AT 15TORR, 20kΩ & 400VDC

6.0 PLASMA HYSTERESIS

6.1 HYSTERESIS IMPORTANCE

The importance of the plasma hysteresis is that it enables a latching configuration thus generating considerable cost savings over conventional phased array systems. The properties presented by the plasma microwave phase shifter are the reason for such savings, these are:

1. The basic device can ultimately be fabricated as a printed circuit, requiring no semiconductor or ferrite components as in current devices. This property alone offers a tremendous savings in array costs.

2. The device, because of the plasma hysteresis, can be configured in a "latching" configuration. That is, the device can be set to a phase state and it will stay at that state until reset. This would be accomplished using a simple holding voltage that would be applied to all plasma elements in the array. In theory (if time permits) a single driver could be used to scan the entire array; the more drivers employed the faster the scan. This is in contrast to a conventional phase shifter, where a driver is associated with each array element.

3. The device is reciprocal and operates equally well on transmit and receive.

6.1.1 Hysteresis in the Plasma Phase Shifter

The advantages of a plasma phase shifter device over a conventional pin diode device stems from its hysteresis property. The fact that plasma can remain excited with a driving voltage lower than the initial firing voltage allows the complexity of the driving circuitry to be substantially simplified. In a pin diode phased array antenna, the number of drivers required for N by M elements is NxM drivers; that is one driver per pin diode element. Thus for an array of 100 by 100 elements, 10,000 drivers are required. In a plasma phase shifter device individual element settings can be accomplished in a row-column addressing fashion due to the plasma latching capability, see **Figure 6.1.1-1**. (This addressing scheme is used in plasma displays, i.e. computer laptops). Therefore typically N+M drivers are required, that is 200 drivers are required for an array of 100 by 100 elements. This is a substantial reduction in driver requirement over that of a conventional approach by a factor of 50.
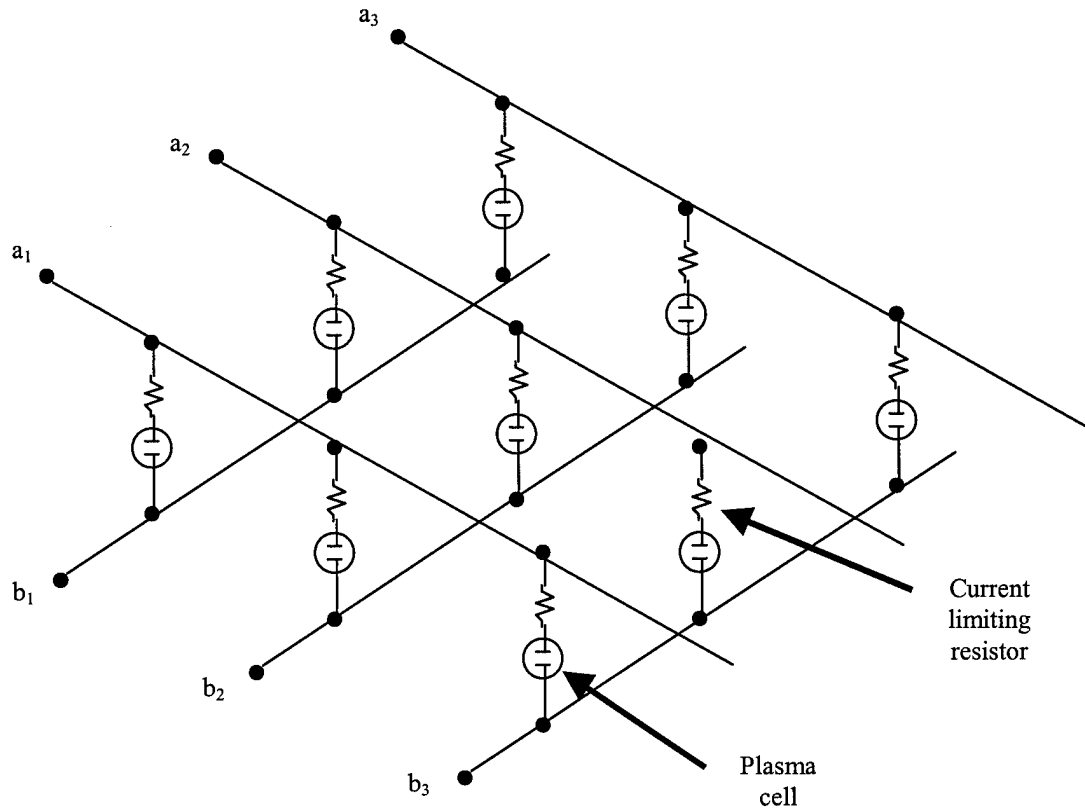
FIGURE 6.1.1-1 ROW-COLUMN ADDRESSING OF THE PLASMA PHASE SHIFTING DEVICE

6.1.2 Plasma Hysteresis Generates Cost Saving

The cost savings of a plasma scanning array can best be illustrated by the following example. Consider a two-dimensional phased array scanning antenna operating at 5.4 GHz. The example antenna has nominal dimensions of 42 inches by 42 inches. If the array was to scan over a sector of ±45deg. in azimuth and ±45deg. in elevation, it would require approximately 1000 radiating elements (N=31 rows by M=31 columns). Each element would be fed by a phase shifter. The following table compares the cost of fabrication using a conventional ferrite phase shifter approach and that using the plasma device.

Conventional Ferrite Phased Shifter Approach

Typical ferrite phase shifters at C-band cost around $150/pc for modest volume production. The price is equally divided between the ferrite device and driver.

Cost: Ferrite Phase Shifter Scanning Array

	Each	(NxM) Number	Total
Ferrite Phase Shifter	$150	1000	$150,000
Drivers	$150	1000	150,000
Support Structure			10,000
Integration & Test			15,000
		Total:	**$325,000**

Plasma Phase Shifter Element Approach

In the final configuration the phase shifting device would be a simple multilayer printed circuit.

Cost: Plasma Phase Shifter

	Each	Number	Total
Plasma Electrode Printed Circuit		1000 ϕ's	$2,000
Drivers	$150	62 (N+M)	9,300
Support Structure			10,000
Integration & Test			15,000
		Total:	**$36,000**

As can be seen with this simple example, the cost of the phased array can become relatively inexpensive when compared to the conventional approach. The plasma hysteresis plays an important role in this proposed antenna, without hysteresis, the system cannot be used as a latching device.

6.2 PLASMA HYSTERESIS MEASUREMENTS

6.2.1 Initial Plasma Hysteresis Measurements

The hysteresis phenomenon of the Nixie Tube and of the stripline test sample was measured, as reported in **MRA P354-05**. The Nixie Tube was used as a baseline for future hysteresis analysis. **Figure 6.2.1-1** plots the plasma drawn current in mA as a function of the applied DC voltage where the arrows depict the direction of the applied voltage (increasing or decreasing). It is seen that the Nixie Tube plasma did not present any hysteresis properties at voltages beyond the plasma turn-on point, 75V. The phenomenon came into action when decreasing the applied voltage below the turn-on point. As the applied voltage decreases, the plasma current slowly diminishes to zero at which point the effective plasma ceases to exist.

Nixie Tube Hysteresis
with 51KOhms
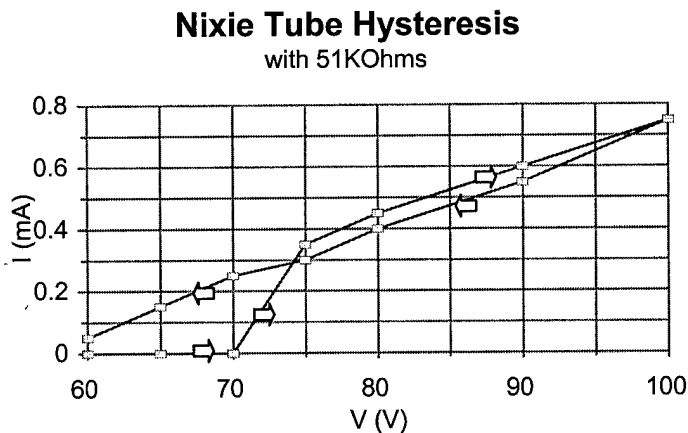
FIGURE 6.2.1-1 NIXIE TUBE PLASMA HYSTERESIS PHENOMENA

The stripline plasma current displayed similar properties as the Nixie Tube plasma current. **Figure 6.2.1-2** plots the plasma current as a function of the applied voltage. As for the plasma in the Nixie Tube, in the stripline configuration it yielded a somewhat

linear relation between the applied voltage and the drawn current beyond the turn-on point. The hysteresis property of the plasma in the stripline was observed when decreasing the applied voltage below the turn-on point (315V) once the plasma has fired.

Sample Hysteresis
P=20Torr, R=51K
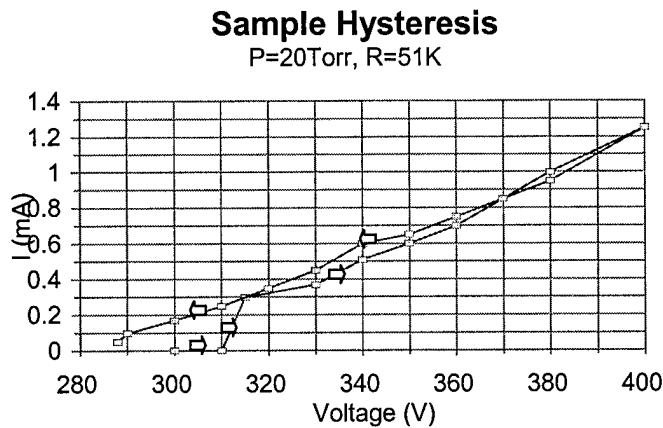
FIGURE 6.2.1-2 STRIPLINE PLASMA HYSTERESIS PHENOMENA

The hysteresis defines a required property of the RF switch, namely that the insertion loss due to the plasma must be in the order of 10 to 20 dB within the hysteresis region. The initial hysteresis measurements proved that plasma does in fact display a hysteresis property. However, the hysteresis curve is not quite the ideal situation. For one thing, the hysteresis span is fairly short (25V) and its starting position coincides with the plasma turn-on voltage position. Further investigation of the hysteresis phenomenon was definitely necessary.

6.2.2 Plasma Hysteresis Research

An extensive literature search was conducted to gather as much information on the hysteresis phenomenon as possible. As it turns out, the gas composition plays an important role in the hysteresis signature of the generated plasma.

In Zhan's paper [1], the authors compare the hysteresis presented by plasma generated in pure hydrogen, H_2, to one generated in a methane-hydrogen, CH_4-H_2, mixture. **Figure 6.2.2-1** shows the hysteresis of plasma in a pure hydrogen gas at a pressure of 300 Pa (approximately 2Torr) and, in **Figure 6.2.2-2**, the hysteresis of plasma in a methane-hydrogen mixture at a neutral gas pressure of 2500Pa (about 20Torr). It was very exciting to see such results since the pure hydrogen results mimic the hysteresis curve that was observed at Malibu Research using a Neon-Argon (NeAr) gas mixture. Other results that confirm the hysteresis signature of plasma in the NeAr gas mixture are the results presented in Merlino's paper [2]. Merlino et al, were the first to talk about the negative derivative resistance of plasma thus explaining the hysteresis phenomenon of plasma. Furthermore, Merlino presented the hysteresis signature of plasma in a pure Argon gas. Their observations match very well with what was observed in stripline configuration, see **Figure 6.2.2-3**. Notice in Figure 6.2.2-3 the narrow region of hysteresis as well as the fact that hysteresis comes into play at voltages below the plasma turn-on point. Merlino further investigates the hysteresis phenomenon of plasma in pure Argon gas surrounded by a magnetic field strength in another paper [3], see **Figure 6.2.2-4**. Notice here the beautiful plasma hysteresis signature. Unfortunately, it is not feasible to introduce a magnetic field in the stripline configuration.
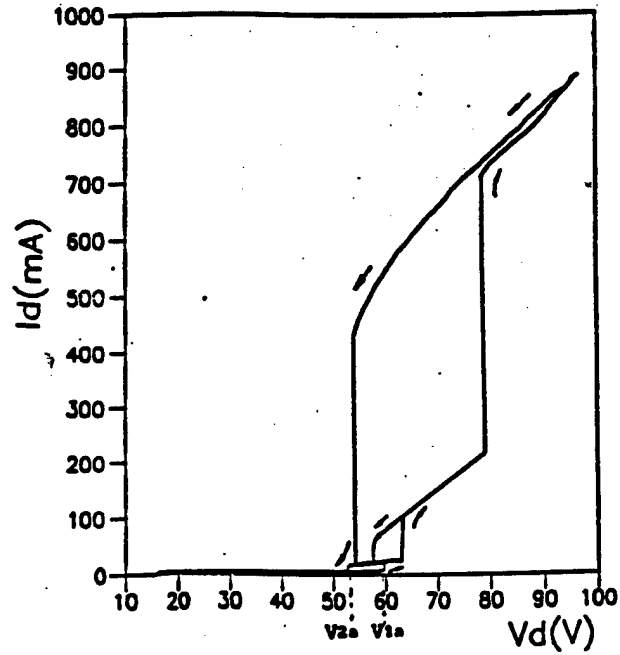
FIGURE 6.2.2-1 ZHAN : PLASMA HYSTERESIS IN PURE HYDROGEN, P= 300 PA
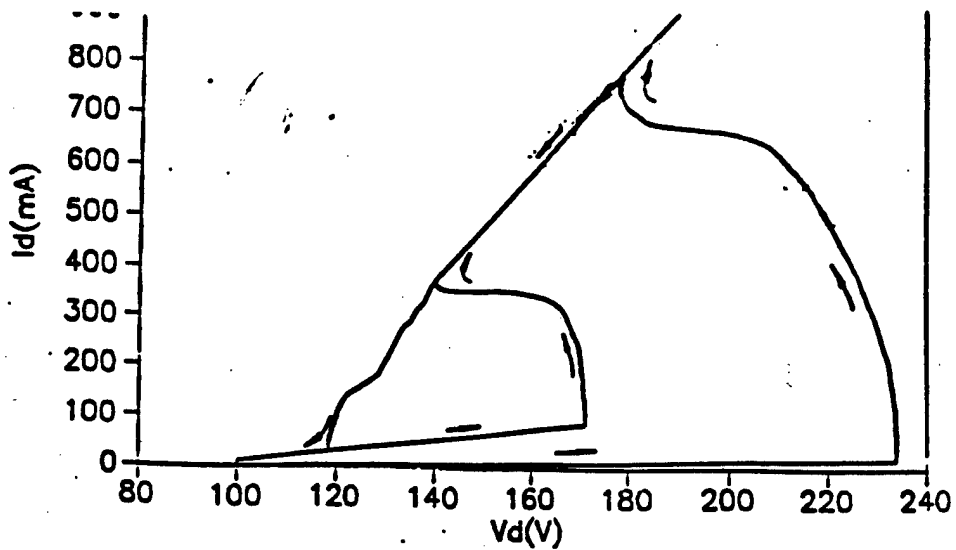
FIGURE 6.2.2-2 ZHAN : PLASMA HYSTERESIS IN CH_4-H_2, P= 2500 PA
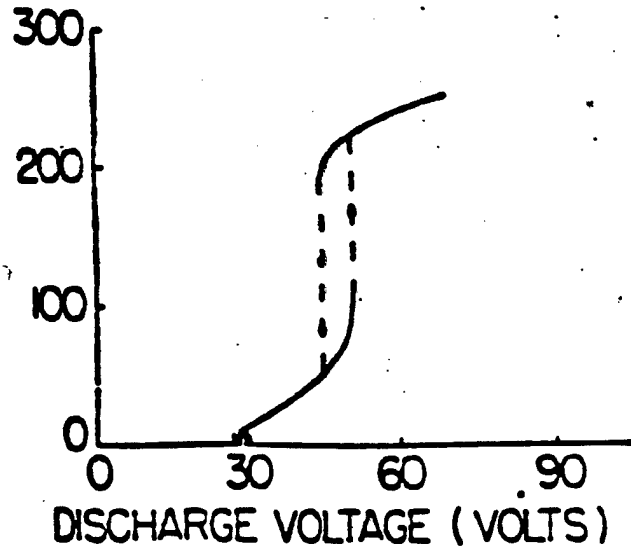
FIGURE 6.2.2-3 MERLINO : PLASMA HYSTERESIS IN PURE ARGON, P= 1mTORR
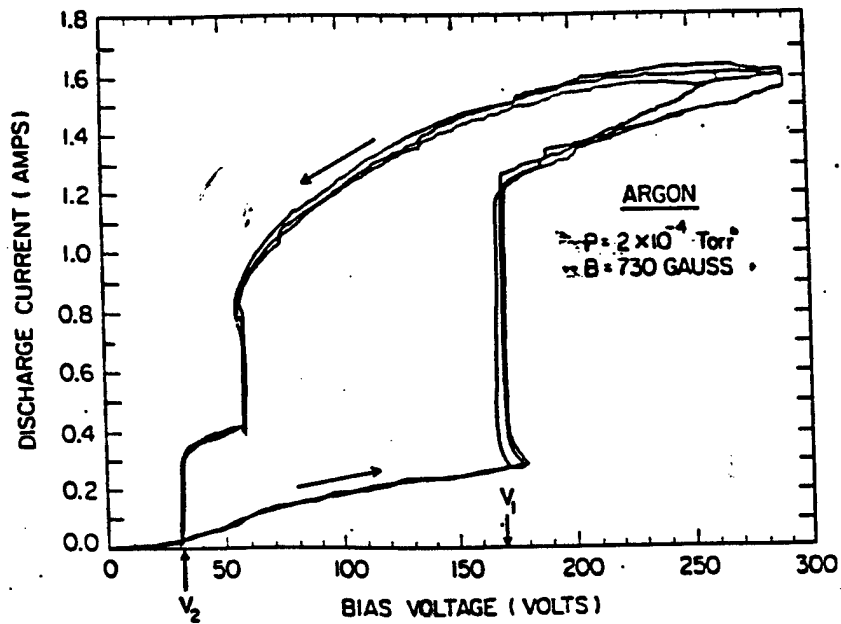
FIGURE 6.2.2-4 MERLINO : PLASMA HYSTERESIS IN PURE ARGON, P= 0.2mTORR, H=730GAUSS

In defining the appropriate gas mixture/purity, the regime under which this application is to work needs to be determined. The regime sought after is the non-collisional regime in which the ions and electrons are relatively free to travel within the plasma with minimal interaction. In the book by Yuri P. Raizer, "Gas Discharge Physics", a few curves are plotted depicting the number of collisions per cm for various gases, see **Figure 6.2.2-5**. As seen in these curves, Helium, He, and Xenon, Xe are two extremes of the different gases shown. Research purity level samples of these two gases were tested.
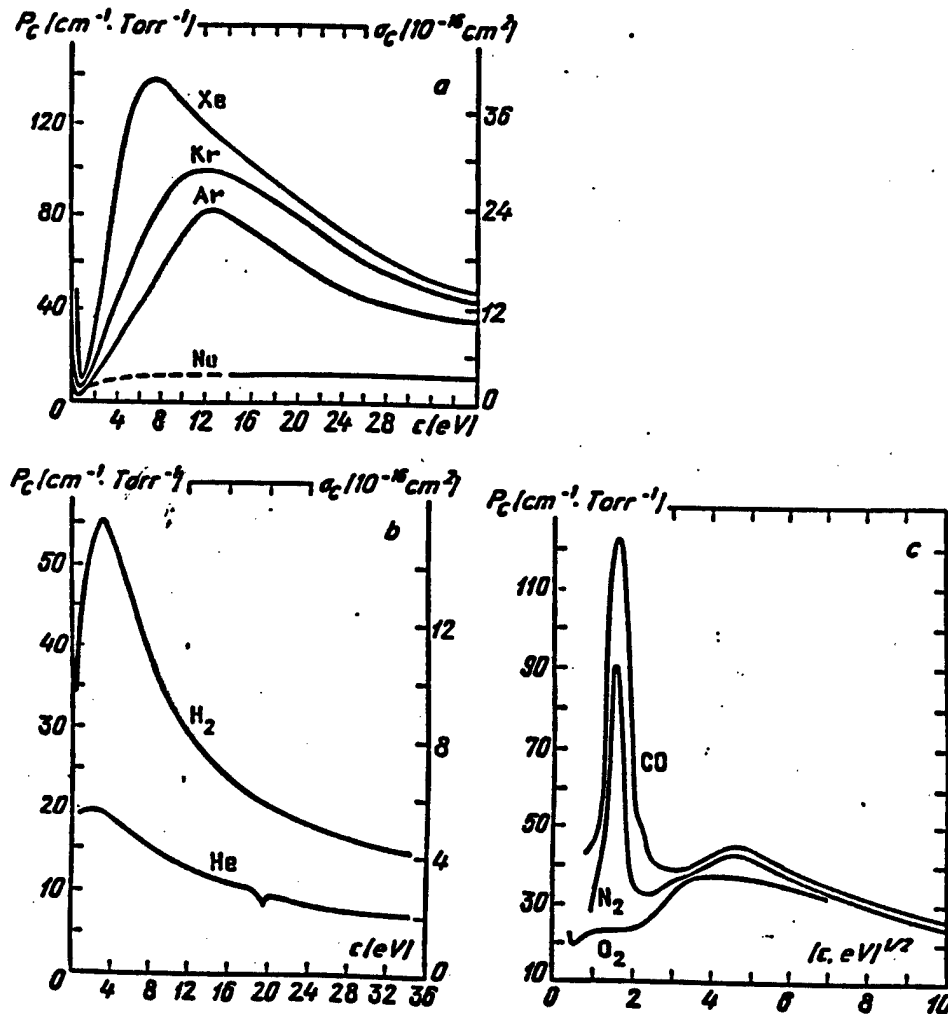
FIGURE 6.2.2-5 PROBABILITIES OF ELECTRON ELASTIC COLLISIONS @ P=1TORR & T=0°C

Also, throughout the literature, many different metals are used for the electrodes. The investigation process consisted of testing various gas mixtures as well as various electrode metal coatings, i.e. Gold, Zinc, Nickel, Rhodium, Silver, Tantalum, as well as Tungsten wires.

6.2.3 Plasma Hysteresis Investigation

6.2.3.1 Hysteresis: Plated Electrodes

The plasma is generated by separating electrons from the molecules/atoms of the gas surrounding the charged anode. Of course, the interaction between the gas and the anode's molecules has a potential to be a major influence in the generation of the plasma and thus, the hysteresis phenomenon of the plasma. The effect of introducing various electrode metals was investigated. The idea was to observe and hopefully determine the best combination of gas-to-electrode combination yielding a near ideal plasma hysteresis response; ideal refers to the plasma phased antenna array application.

Four different metal types of wire plated electrodes were acquired: Gold, Silver, Rhodium and Nickel Sulfurate. The electrodes were inserted in the stripline test circuit as shown in **Figure 6.2.3.1-1**. For this analysis the hysteresis is measured in terms of the current flowing through the plasma region. The plasma current measurement is a good indication of the plasma signature since the RF return loss of the circuit is directly related to the plasma current. The aim was to determine the plasma turn-on voltage and thereafter monitor the hysteresis of the plasma as the voltage is decreased.
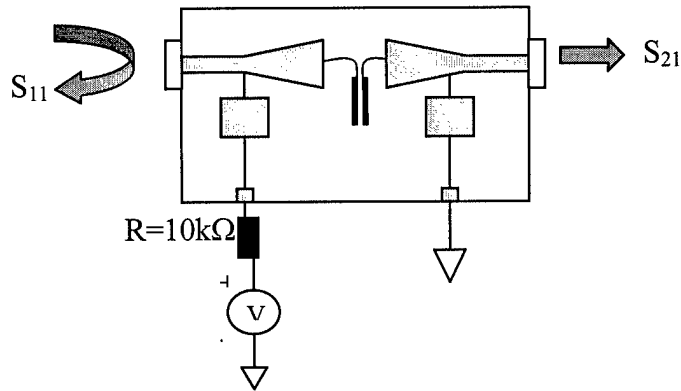
FIGURE 6.2.3.1-1 PLASMA HYSTERESIS MEASUREMENTS IN THE TEST STRIPLINE CIRCUIT

Shown in **Table 6.2.3.1-1** is the result of the data gathered on the various plated electrodes. The Gold plated electrode produced the widest span, between the turn-on and turn-off voltages (170 volts), with a fairly flat current response (60 volts below the turn-on position, the current reduced by only 25%). This result is very encouraging as Gold produced the widest plasma hysteresis span so far encountered. The Silver didn't produce much of a hysteresis (40 volts only) and with minimum induced current (the plasma resistance is fairly high). The Rhodium generated erratic plasma, with non-reproducible phenomenon. Furthermore, the Rhodium required a very high voltage potential to initiate the plasma formation. The Nickel generated a somewhat wide hysteresis (70 Volts), but nothing extraordinary.

Table 6.2.3.1-1 Plated Electrodes Results

Metal	Gold	Silver	Rhodium	Nickel
$V_{turn-on}$ (V)	460	300	490	315
$I(V_{turn-on})$ (mA)	8.3	1.5	9-20	4.6
$I(V_{turn-on}-60V)$ (mA)	6.5	0	NA	1.4
$V_{turn-off}$ (V)	290	260	NA	245

In **Figure 6.2.3.1-2** is shown the plasma hysteresis, in terms of plasma current, for the various metals (excluding the Rhodium for lack of reproducible data). As seen in the previous table and in Figure 6.2.3.1-2, Gold plated electrodes seem to be the best type of electrodes encountered thus far. Unfortunately, the plasma didn't seem to affect the incident RF. The best results were as follows:

➢ Reflected loss (S11) comes up to a mere –9dB.

➢ Insertion loss (S21) goes down from –1.08dB to only –5.47dB.

These results are not what one would expect from the measured plasma currents. They are very deceiving when compared to the plasma effect while using the Nixie tube electrodes (see report **MRA P354-05**).

Hysteresis of Plated Electrodes
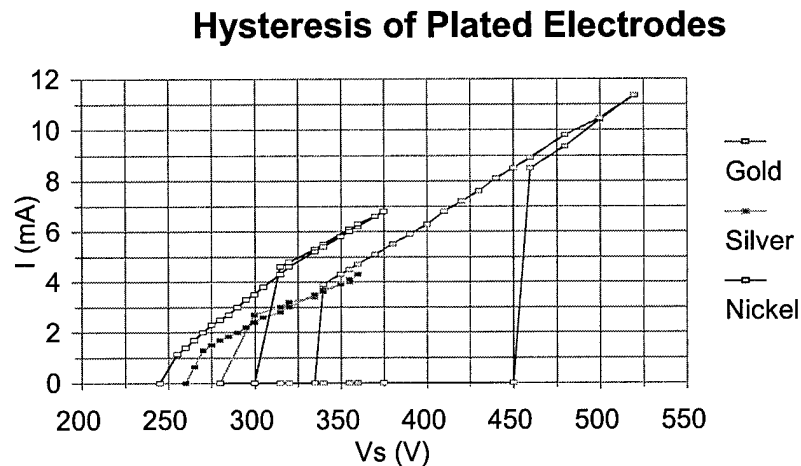
Figure 6.2.3.1-2 Plasma Hysteresis Effect on RF Incident Energy

6.2.3.2 Hysteresis: Gases

Different types of pure gases were tested. First, the hysteresis curve of the NeAr (Neon-Argon) gas is shown in **Figure 6.2.3.2-1**. The NeAr gas has been the preferred gas thus far. The gas pressure was set at 30Torr and a current limiting resistor of 10kΩ was inserted between the DC source and the electrodes. The hysteresis of the Neon-Argon gas is fairly wide and flat; the effective plasma sustain region would be around the 240 volts, 60 volts below the turn-on position.

When the Xenon was fired, nothing much happened in terms of efficient plasma wall, therefore the hysteresis curve in terms of RF was not measured.

Microstrip Hysteresis
P=30Torr, R=10k, @ 9.13GHz
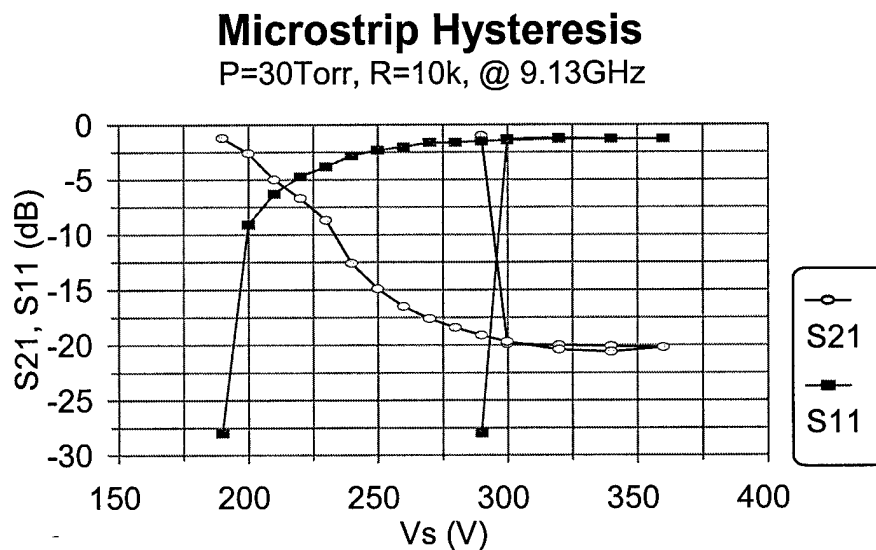
FIGURE 6.2.3.2-1 NE-AR HYSTERESIS SIGNATURE @ P=20TORR & R=10KΩ

The Helium on the other hand produced a very flat and wide hysteresis, see **Figure 6.2.3.2-2**. For Helium to create efficient plasma RF wall, its pressure was set at 60Torr and a 20kΩ current limiting resistor was inserted between the DC source and the

electrodes.   The effective plasma sustain region would be around 375 volts; that's 120

volts below the turn-on position!   This wider efficient hysteresis span allows for better

latching property. Helium was the preferred gas.

Hysteresis @ 9.6GHz
Helium @ 60Torrs (20KOhms)
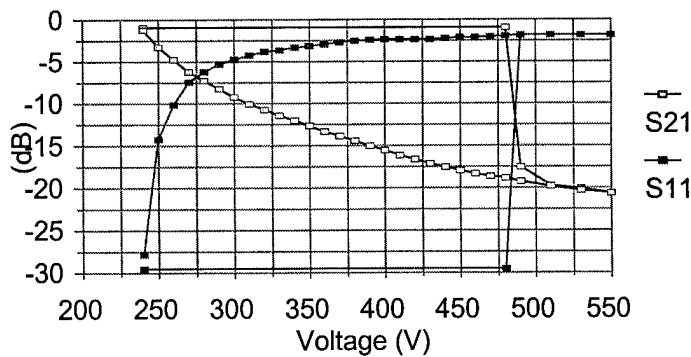
FIGURE 6.2.3.2-2 HELIUM HYSTERESIS SIGNATURE @ P=60TORR & R=20KΩ

7.0 THE PLASMA PHASE SHIFTER ELEMENT

The plasma phase shifting device consists of two parallel stripline circuits; each segmented by coupling electrodes (where the plasma will fire) and a rat-race (ring hybrid). The reason for using a hybrid is to isolate the input port from the output port. The full system will include a power-distributing element from which the source RF energy will be divided and distributed, with equal phase front, to the phase shifting devices. The energy will then be phase shifted by the plasma stripline circuit before exiting the hybrid where it will be directed toward radiating dipole elements (see **Figure 7.0-1** for a block diagram of the system's RF portion). The hybrid is presented in the next section.
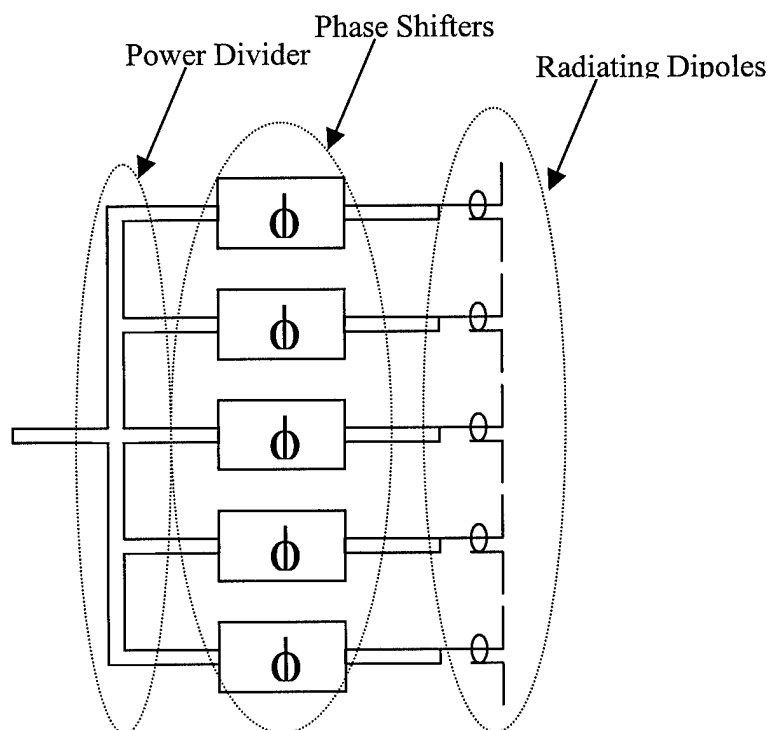
FIGURE 7.0-1 BLOCK DIAGRAM OF THE SYSTEM RF PORTION

7.1 THE RAT-RACE

The rat-race, also known as a ring hybrid, is generally used as a power divider. It has high isolation between input & output ports (In & Out shown in **Figure 7.1-1**) and is easily etched on a stripline configuration. The rat-race can be used as an isolation device, a power divider, or in this case a phase shifter.

The rat-race is frequency dependent with an operating bandwidth of approximately 10%. The distance between the ports are as follows (refer **to Figure 7.1-2**):

> Port 1 to Port 3 => $\lambda/4$ (CCW) & $5\lambda/4$ (CW, Clock Wise)

> Port 1 to Port 4 => $3\lambda/4$ (CCW & CW)

> Port 1 to Port 2 => $2\lambda/4$ (CCW) & λ (CW)

A) The rat-race as a power divider:

*The input energy, Pin, is equally divided at Port 1, half the power will circulate CW (P_{1A}) and half CCW (P_{1B}). At Port 3 the phase of P_{1A} with respect to P_{1B} is in phase ($\lambda/4$ via CCW and $5\lambda/4$ via CW), therefore the energy adds up and is transferred to Port 3. The same occurs at Port 4; the phase of P_{1A} is coincident with the phase of P_{1B} ($3\lambda/4$ via CCW and $3\lambda/4$ via CW). On the other hand at Port 4 the phases of P_{1A} and P_{1B} are 180° ($\lambda/2$) out of phase. Therefore if Port 3 & 4 are terminated with a matching load, the input energy will be equally distributed to Ports 3 & 4 with minimal energy reflected back to Port 1.*

B) The rat-race as a phase shifter:

As stated in the power divider application the rate-race directs half the input energy to Port 3 and half to Port 4. If Ports 3 & 4 are open circuited, such that the energy that goes out of these ports is reflected back to the rat-race, and the transmission line length of Port 4 is 180° ($\lambda/2$) longer than that of Port 3, then

the sum of the input energy is added and directed at Port 2. By including a device in both branches attached to Port 3 & 4, variable phase shifts can be introduced to the input energy.
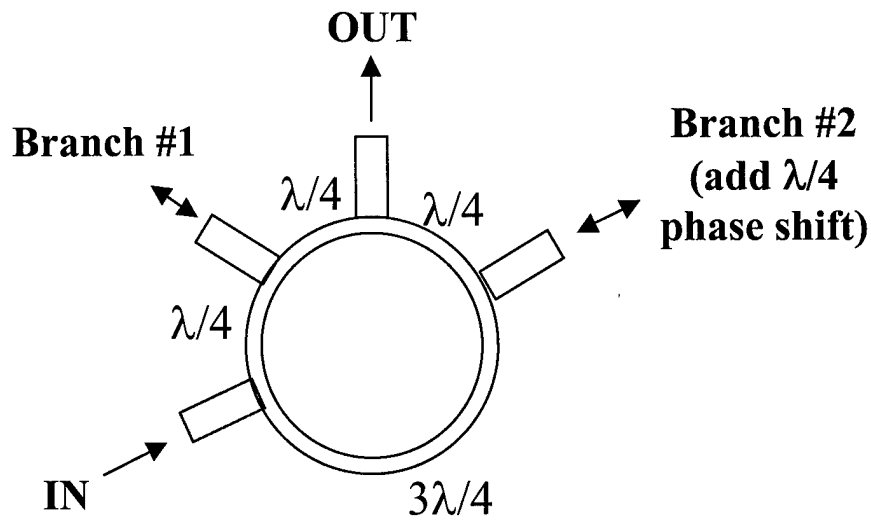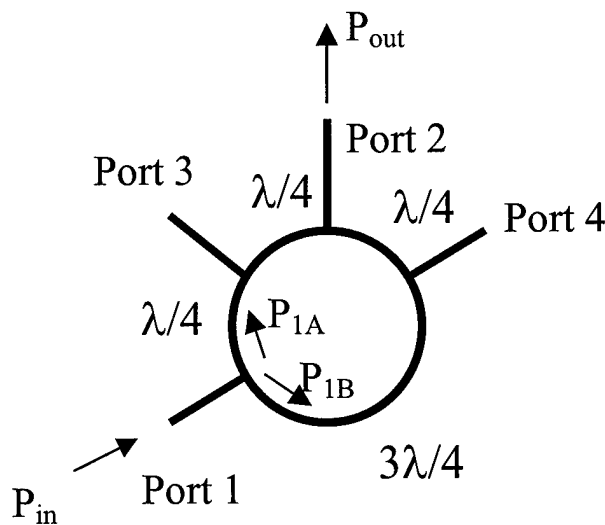

FIGURE 7.1-1 BRANCH LINES OF THE RAT-RACE

FIGURE 7.1-2 RAT-RACE ROUTING OF INPUT POWER

7.2 THE PLASMA PHASE SHIFTER

This section investigates the basic plasma phase shifting (PPS) element. In order to reduce the complexity of the system and to properly address the plasma efficiency as a phase shifting element, a commercial hybrid was used instead of the rat-race (ring hybrid). The available commercial hybrid had an operating region between 4GHz and 6GHz; thus a circuit was designed and tuned at the center frequency of 4.7GHz.

The plasma phase shifter test sample consisted of a Narda hybrid connected to the stripline, which is composed of two identical and parallel circuits. The stripline circuits include RF transparent DC path, tuning elements, transmission lines and plasma regions. The actual configuration is shown in **Figure 7.2-1** with the following dimensions:

$$L_l = 0.230” \quad ; \quad w_l = 0.35” \quad ; \quad L_s = 0.151”$$

$$L_a = 1.1485” \quad ; \quad L_b = 2.618” \quad ; \quad w_{TL} = 0.090”$$

The stripline is etched on a duroid substrate with a relative dielectric constant of 2.25. Therefore, at an operating frequency of 4.722 GHz (an available hybrid was chosen for this proof of principle, the one on hand was a Narda with an operating frequency of around 4.5 GHz), the wavelength of the RF energy is:

$$\lambda_\varepsilon = c_0/(f*sqrt(\varepsilon_r))$$

$$= 3.0E08m/s \, / \, (4.722E09*sqrt(2.25))$$

$$= 4.235cm = 1.67”$$

The aim of the analysis is to show that the system can track the phase difference due to the plasma as well as the transmission line length. The length of L_b will be slowly reduced in steps of about $\lambda_\varepsilon/10$, that is around 80 degrees (2*360/10) of phase difference between steps. In doing so the transmitted power should reflect the phase difference

induced by shortening the RF path. If the plasma is in fact a good RF wall, then the phase of the transmitted RF energy should be independent of the TL length L_b.
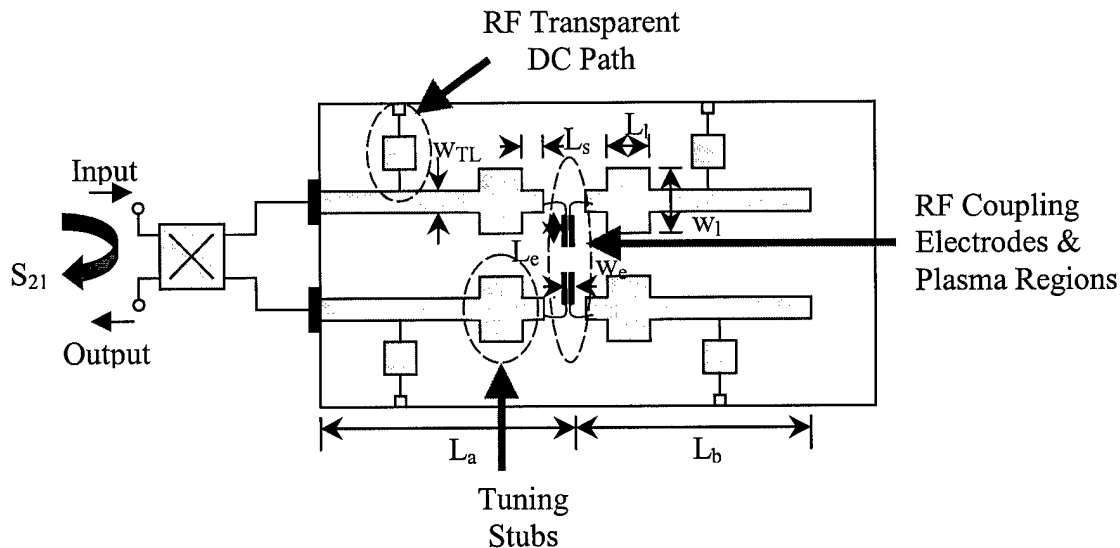
Figure 7.2-1 Plasma Phase Shifter Element

Figure 7.2-2a shows the magnitude and phase signature of the plasma phase shifter element with L_b equal to 2.618"; S_{21} is the transmitted energy from the input port to the output port of the hybrid referenced to the input level. This is the reference data to which the phase information will be compared. Note the relatively low insertion loss, around 4dB, presented by the plasma phase shifter element (the circuit was grossly tuned).

The circuit was immersed in Neon-Argon (NeAr) gas at a pressure of 14Torrs (ambient pressure is 760Torrs) and DC voltage was applied to the electrodes in the "plasma region" which created the plasma. **Figure 7.2-2b** shows the signature of the transmitted energy while the plasma is energized. There are two important observations to make here; first, the transmitted power level is practically unaffected by the plasma (which is very good) and secondly, the phase response of the transmitted energy is drastically altered.

FIGURE 7.2-2A MAGNITUDE & PHASE OF CIRCUIT, L_B = 2.618", NO PLASMA

FIGURE 7.2-2B MAGNITUDE & PHASE OF CIRCUIT, L_B = 2.618", 15TORR, 20KΩ, 400VDC

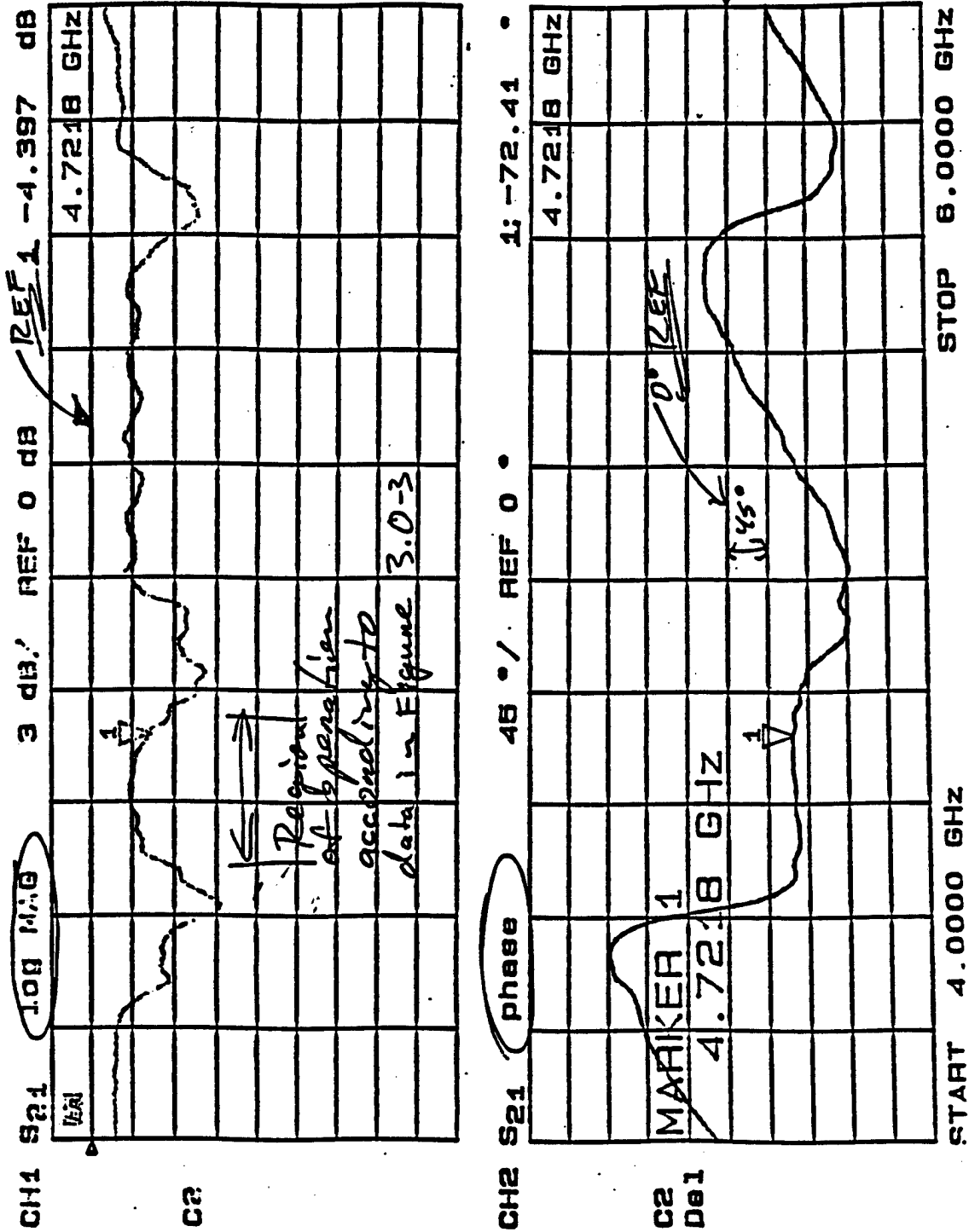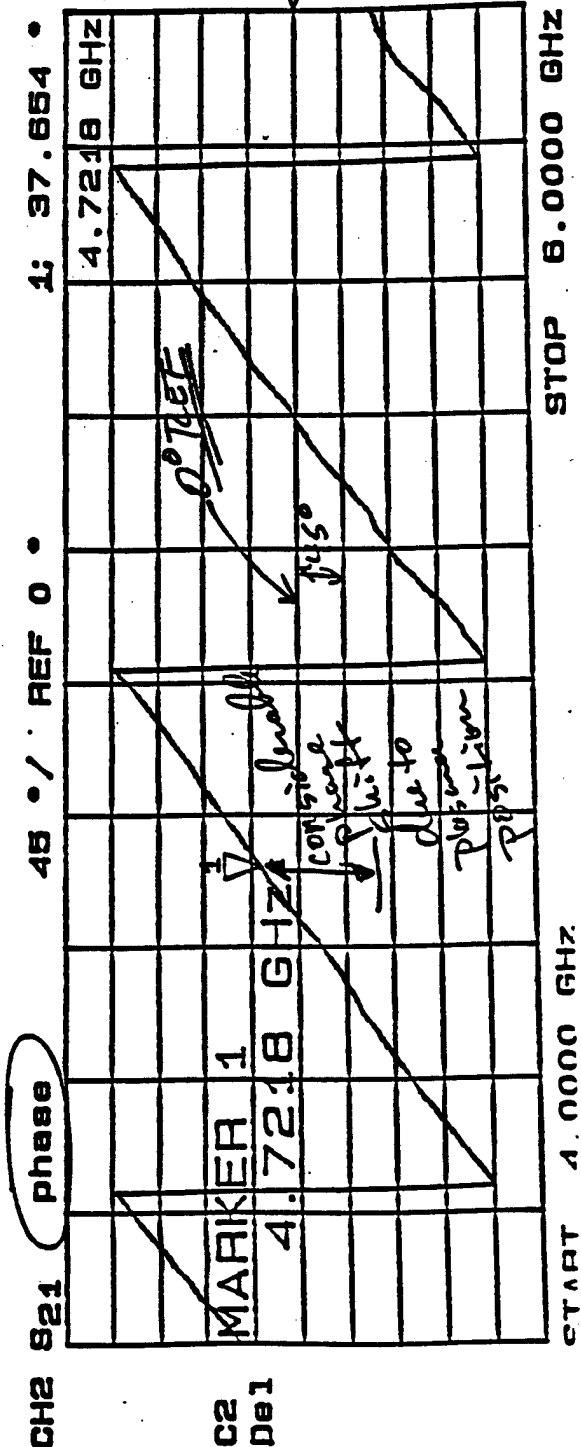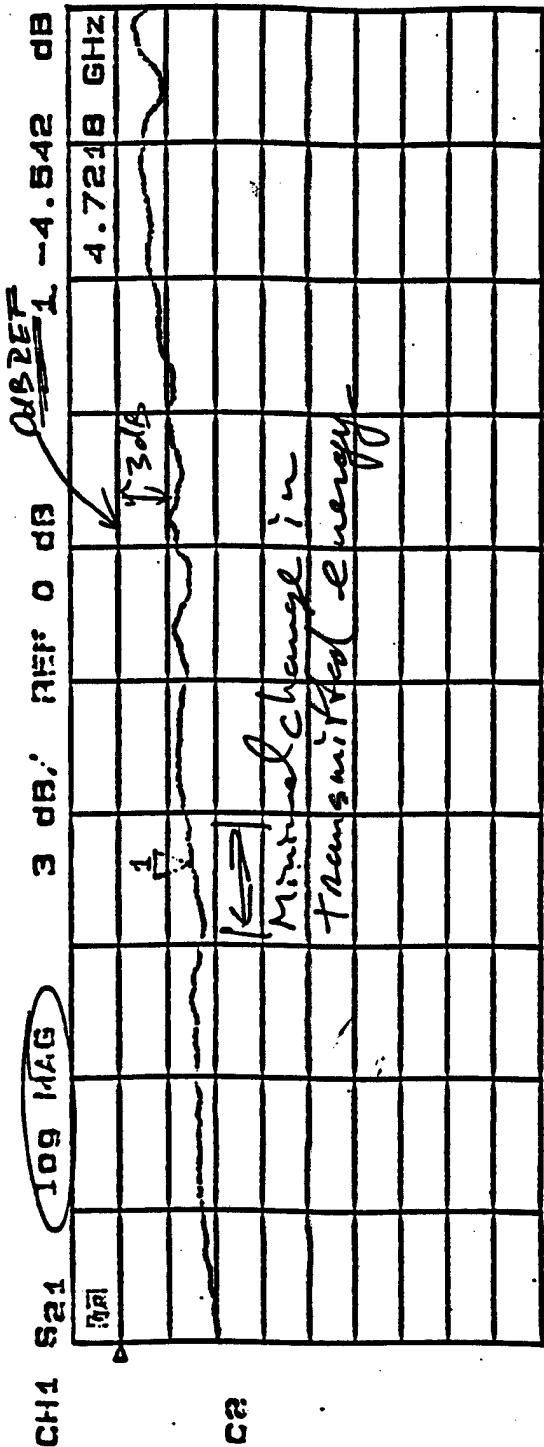In **Table 7.2-1** is shown the effect of modifying the TL length. As can be seen, the phase difference actually tracks the TL length L_b when the plasma is not energized. Furthermore the phase of the transmitted energy, ϕ_{Plasma}, is in fact independent of the TL length while the plasma is energized. Much data was gathered and normalized to the above baseline data.

TABLE 7.2-1 PLASMA PHASE SHIFTER ELEMENT INVESTIGATION

L_b (inches)	ΔL_b (λ_ε)	$\phi_{NoPlasma}$ (deg.)	ϕ_{Plasma} (deg.)	$\Delta\phi_{Theory}$ (deg.)	$\Delta\phi_{Meas.}$ (deg.)	Plasma Insertion Loss (dB)
2.618	0	−72.41	37.65	0	0	0.15
2.538	0.096	−15.37	51.24	34.6	43.5	0.786
2.478	0.168	15.87	41.51	60.5	82	-0.054
2.437	0.218	51.77	37.68	78	124	0.615
2.358	0.311	93.69	36.75	112	167	-0.058
2.300	0.381	145.25	38.12	137	217	0.168
2.232	0.462	179.22	43.84	167	245	-0.549
2.127	0.588	212.09	46.44	212	275	-1.415

The data is presented in a graphic format in **Figures 7.2-3** through **7.2-5**. In the first graph is plotted the normalized differential phase of the circuit; the phase differential is between the state of plasma OFF and ON. The differential phase is normalized to the phase difference of the longest TL length; that is for L_b equal to 2.618". For example, the measured phase difference for an L_b of 2.618" is 110.06 degrees, which is normalized to 0 degrees, therefore the normalized phase difference for an L_b of 2.538" is 43.45 degrees {that is 110.06 (51.24 - -15.37)}. The theoretical normalized phase difference is calculated as ΔL_b * 360 degrees (ΔL_b is expressed in terms of the wavelength in the dielectric medium). In Figure 7.2-3, note the linearity of the measured normalized phase difference and also the fact that it follows closely the theory. The important result here is

that the measured phase difference is linear and thus any phase shift can be accomplished

with the plasma phase shifter element.

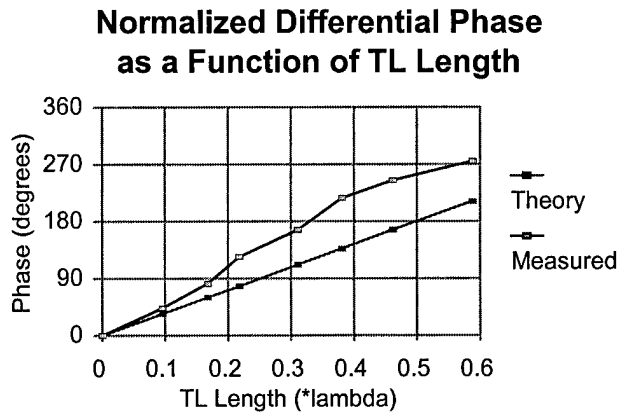**Normalized Differential Phase
as a Function of TL Length**

FIGURE 7.2-3 THE NORMALIZED DIFFERENTIAL PHASE

In **Figure 7.2-4** is presented the measured phase of the RF at the output of the

plasma phase shifter element, relative to the input phase, as a function ΔL_b. This data

shows the efficiency and consistency of the plasma to create an effective RF plasma wall.

When the plasma is excited, the output RF phase is effectively constant regardless of the

length of the TL beyond the plasma region. Furthermore, without the presence of

plasma, the output RF phase displays a constant slope with respect to the TL length.

Another important parameter to consider is the loss presented by the plasma to the

transmitted RF energy. Ideally, when the plasma is energized, the level of the transmitted

energy should be unaltered, only the phase should change. **Figure 7.2-5** shows the

transmitted loss due to the plasma. Notice that the loss oscillated around 0dB, not

exceeding 1dB on average. Also, since the electrodes in the plasma region were grossly

tuned, the plasma wall actually reflected with better efficiency than in the case without
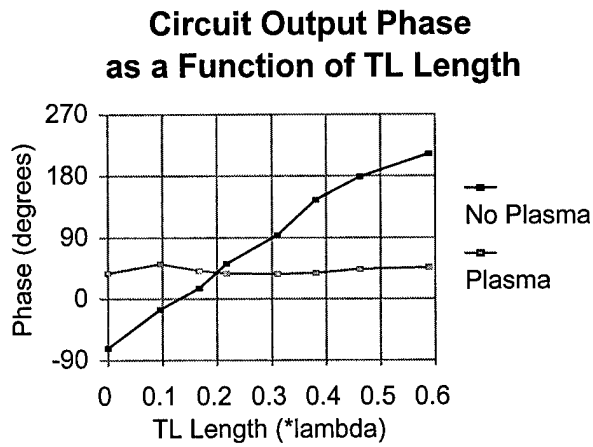
plasma.

Circuit Output Phase
as a Function of TL Length

FIGURE 7.2-4 THE PLASMA PHASE SHIFTER ELEMENT OUTPUT PHASE
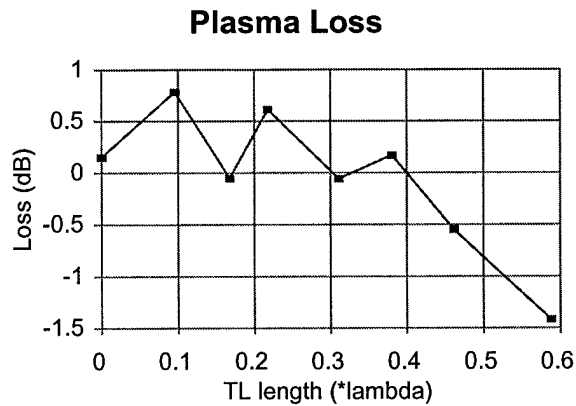
Plasma Loss

FIGURE 7.2-5 THE PLASMA PHASE SHIFTER ELEMENT INSERTION LOSS

7.3 THE INTEGRATED PPS USING NIXIE TUBE ELECTRODES

It was shown in the previous section that the plasma could effectively be used in conjunction with a commercial off-the-shelf hybrid to produce a phase shifter. The next step consisted of integrating the rat-race and the plasma phase shifter (PPS) within the same circuit. Nixie Tube electrodes are used within the plasma region as they have been used throughout, these along with the RF and DC connectors are the only external elements to the PPS element.

7.3.1 Integrated One-Bit PPS Using Nixie Tube Electrodes

In the previous Section the on-bit plasma phase shifter elements were shown to be very stable and predictable using a commercial off-the-shelf hybrid (rat-race). Having demonstrated the functionality of the breadboard circuit, a fully integrated circuit was designed and tested. Shown in **Figure 7.3.1-1** is the integrated one-bit phase shifter including the rat-race and the plasma region. The board shown is tuned at 9.6GHz and measures 2.5" x 6". To the left is the RF input connector and to the right the RF output connector along with the plasma DC exciters. Shown directly above the circuit is the stripline duroid cover followed by the top ground plane. This particular circuit is a one-bit phase shifter phased to 0° (no plasma) and around 90° (with plasma) phase.
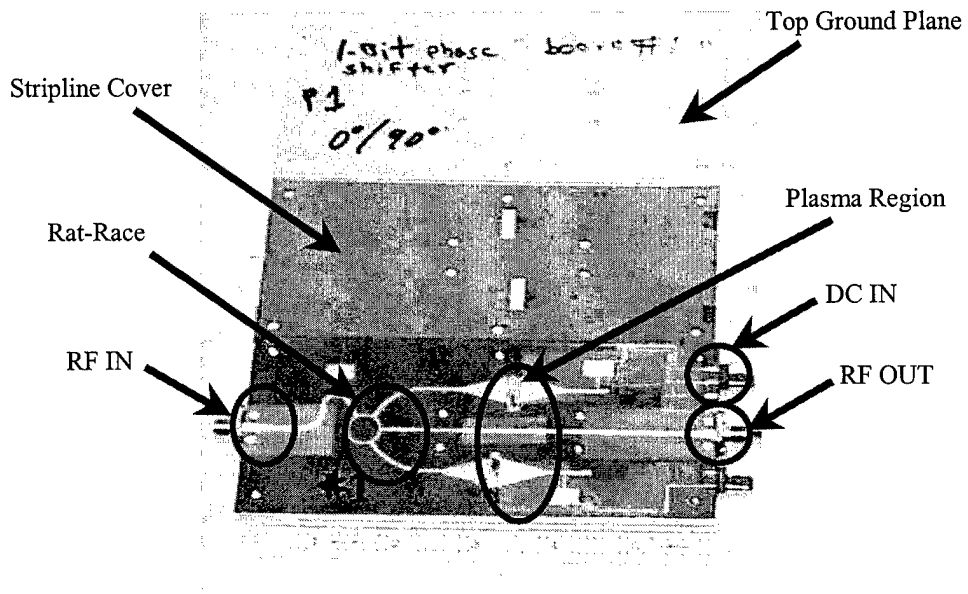
FIGURE 7.3.1-1 INTEGRATED ONE-BIT PHASE SHIFTER

A picture of the board is shown in **Figure 7.3.1-2** along with the tabulated results, which are also shown in **Figure 7.3.1-3a & b**. Figure 7.3.1-3a shows the energy level of the RF energy at the output of the phase shifter along with the relative phase. Without the presence of plasma, the RF energy level at the output of the circuit is –2.6dB with a relative phase of –177°. When the plasma is fired, the energy level at the output is basically the same, -2.8dB, but the relative phase shifted to –97°; that is an 80° phase shift between the two states (see Figure 7.3.1-3b). **Very good phase results with effectively no incurred energy loss between the two phase states (-2.6dB compared to –2.8dB with plasma).**

	No Plasma	With Plasma
Magnitude	$|S_{21}| = -2.6\text{dB}$	$|S_{21}| = -2.8\text{dB}$
Phase	$\angle S_{21} = -177°$	$\angle S_{21} = -97°$

RF IN →

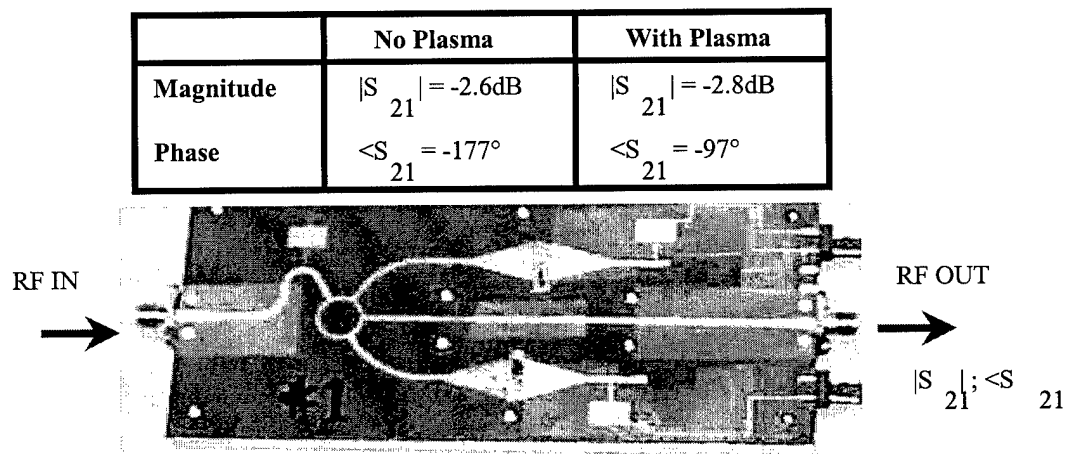RF OUT →

$|S_{21}|; \angle S_{21}$
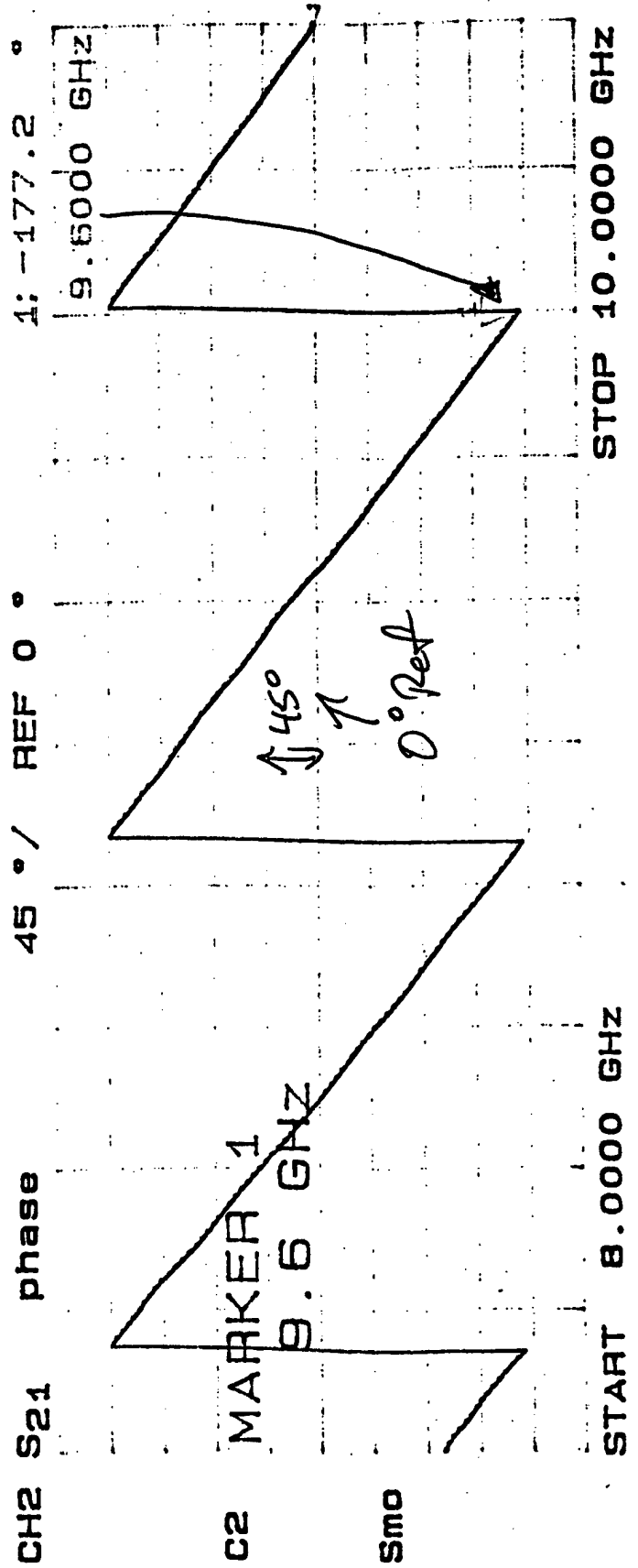

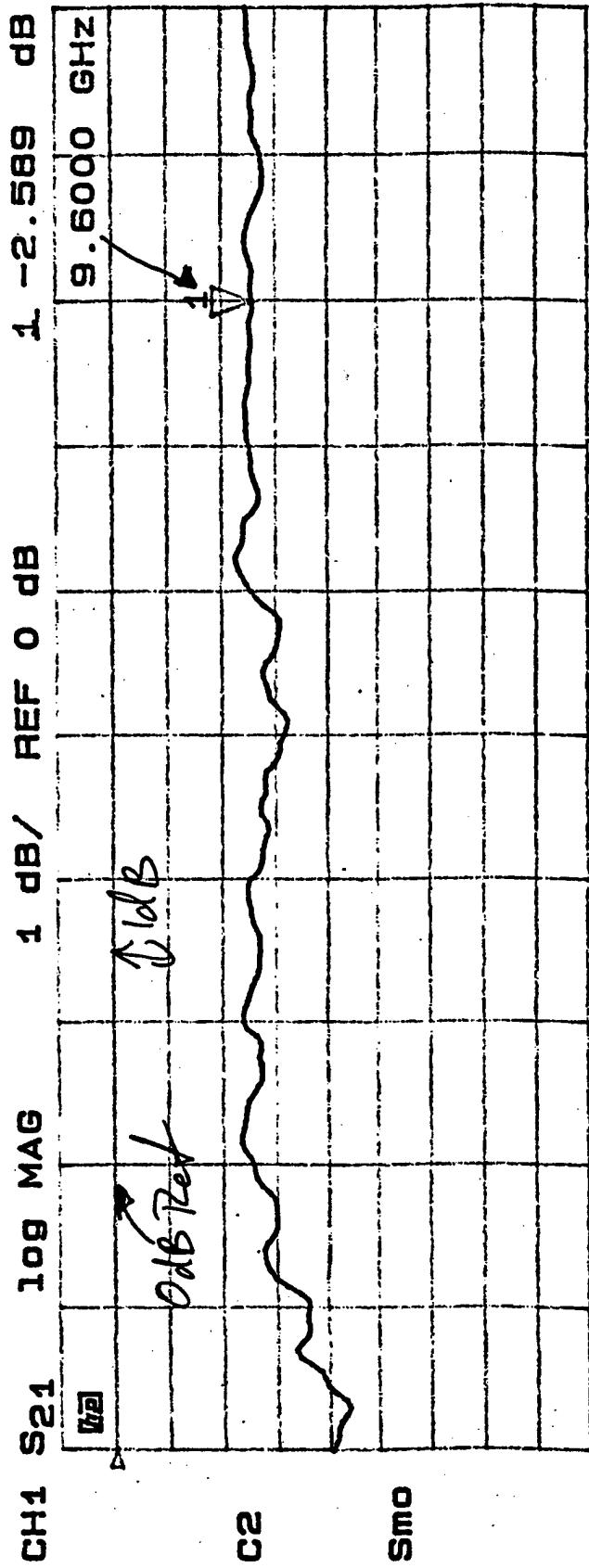FIGURE 7.3.1-2 ONE-BIT PHASE SHIFTER WITH MEASURED VARIABLES

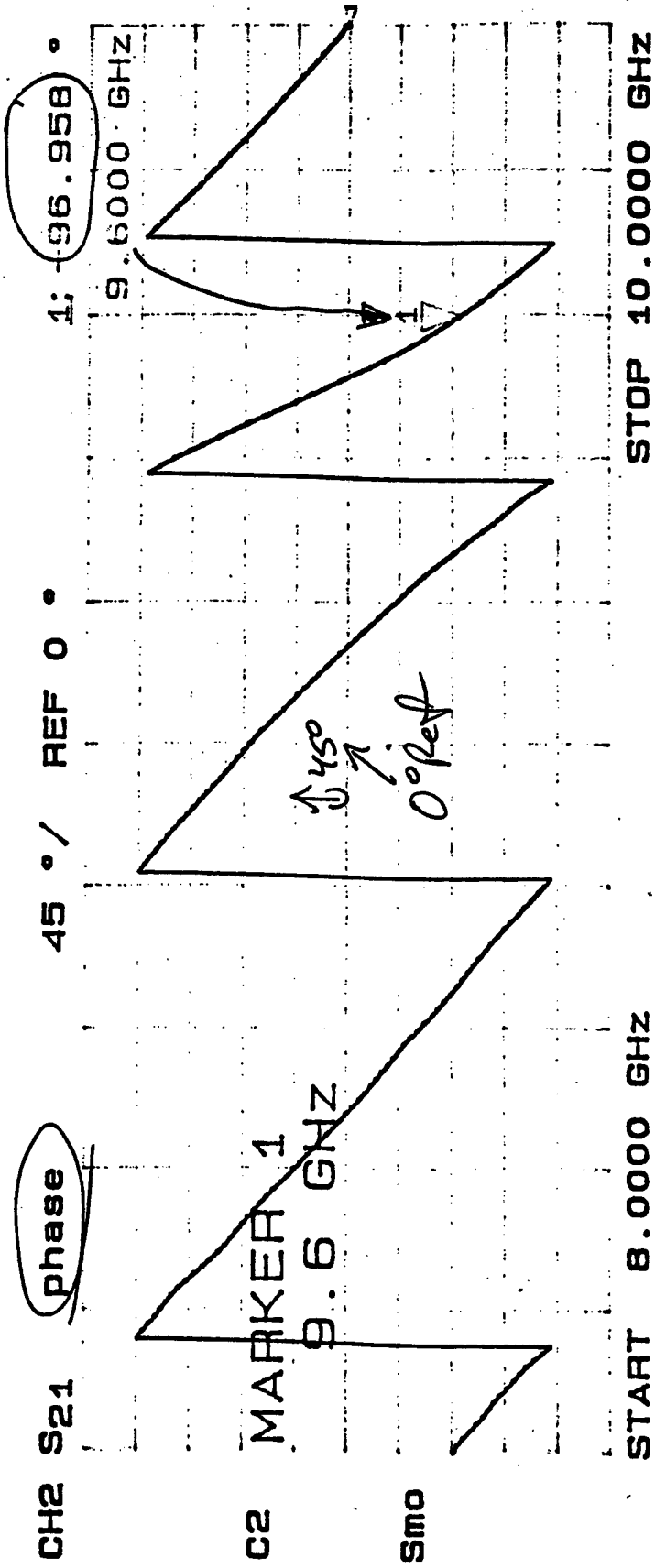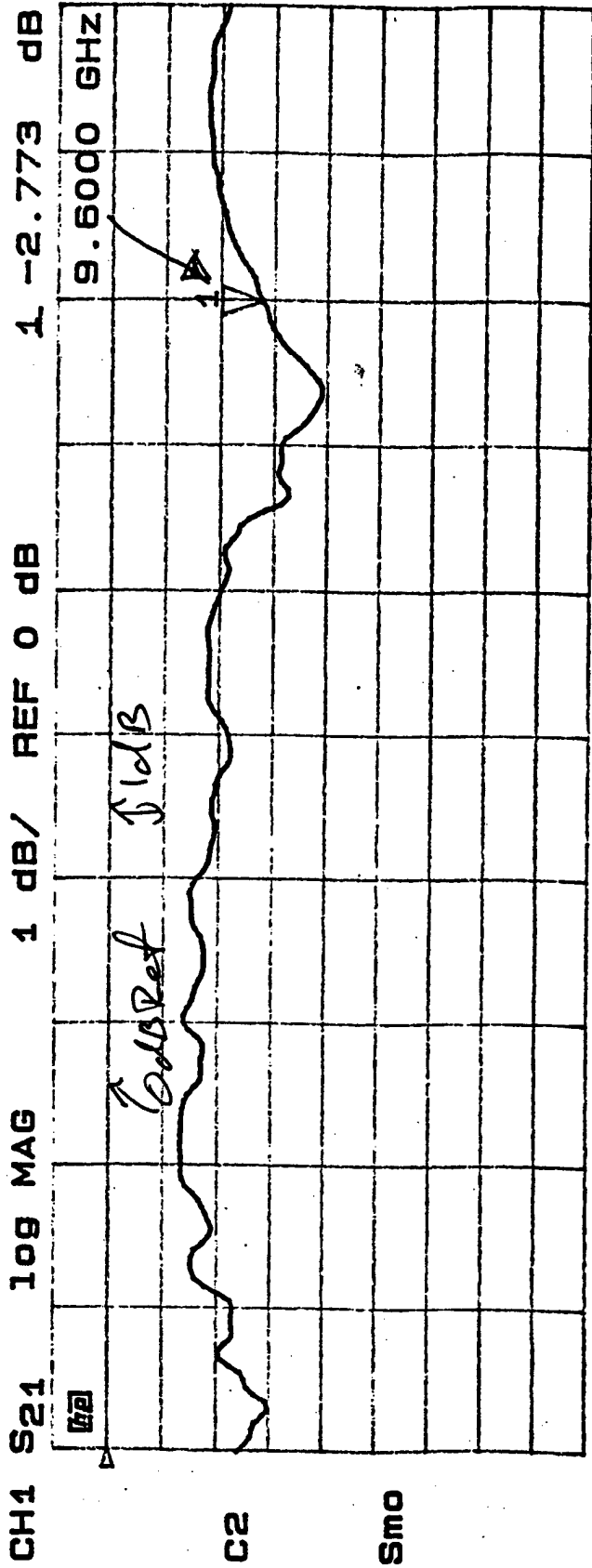FIGURE 7.3.1-3A ONE-BIT PLASMA PHASE SHIFTER, NO PLASMA (0° PHASE STATE)

FIGURE 7.3.1-3B ONE-BIT PLASMA PHASE SHIFTER, PLASMA FIRED (80° PHASE STATE)

7.3.2 Two Cascaded One-Bit PPS Using Nixie Tube Electrodes

Two one-bit phase shifters were cascaded to verify the two-bit phase shifter process. The output of the board presented in the previous section was connected to the input of a similar board, which had a 180° phase shift between the two states. Having two boards back to back with different phase states produces a two-bit phase shifting element scanning the 360° range, with the following possible phase states:

- 0° (no plasma on either board)

- 90° (plasma on 1st board, none on second)

- 180° (plasma on 2nd board, none on first)

- 270° (plasma on 1st board, plasma on 2nd board)

Figure 7.3.2-1 shows the two one-bit phase shifters, the one on the left being the same board presented in the previous section. **Figure 7.3.2-2** shows the two boards in the vacuum chamber with interconnections, and **Figure 7.3.2-3** is a picture of the boards taken over the plotted results (the plotted results can be seen in the Report **MRA P354-13 Figures 4.1-4a** through **4.1-4d**). The tabulated results, **Table 7.3.2-1**, show the four states of this two cascaded one-bit phase shifter. Notice the relative phase progression, from 0° to 80° to 176° to the last state, 258°. This is very close to the sought after 0°, 90°, 180°, 270° phase states which are easily achieved by fine-tuning the circuits.

Table 7.3.2-1 Two Cascaded One-Bit Phase Shifter: The Four States.

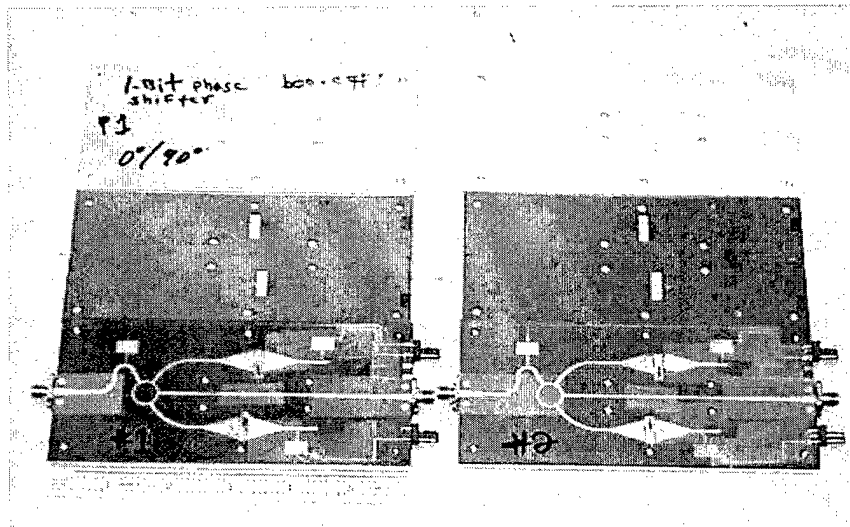| Board State (No Plasma > OFF Plasma Fired > ON)		Shown in Figure	Magnitude of Output RF (in dB)	Phase of Output RF (in Degrees)	
Board #1	Board #2			Measured	Relative
OFF	OFF	7.3.2-4a	-6.6dB	52°	0°
ON	OFF	7.3.2-4b	-8.9dB	-32°	80°
OFF	ON	7.3.2-4c	-6.4dB	-124°	176°
ON	ON	7.3.2-4d	-7.7dB	154°	258°

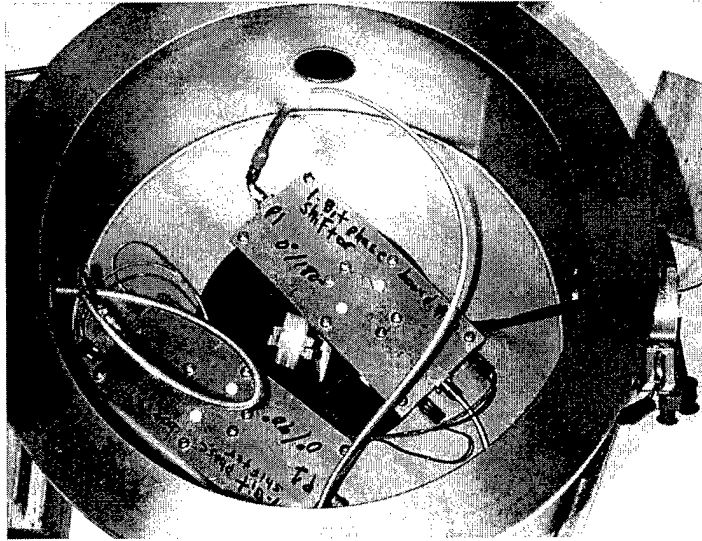FIGURE 7.3.2-1 CASCADED TWO ONE-BIT PHASE SHIFTER

FIGURE 7.3.2-2 CASCADED TWO ONE-BIT PHASE SHIFTER IN THE VACUUM CHAMBER.
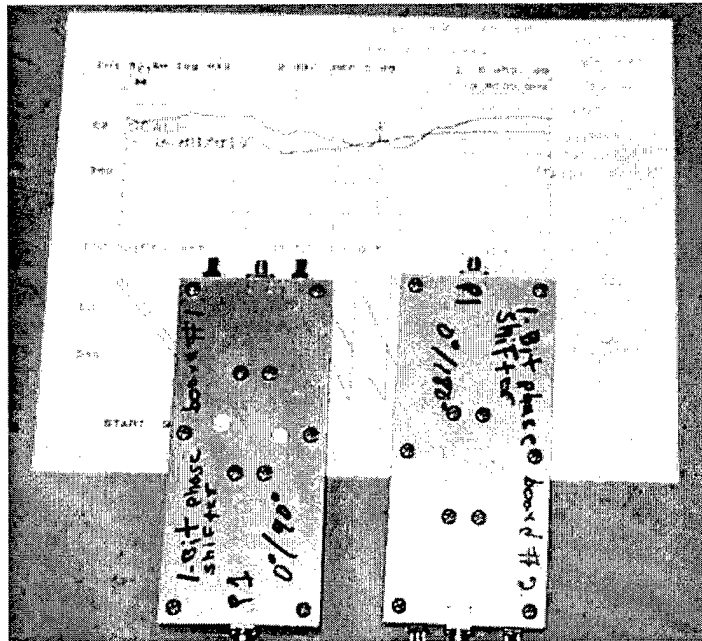

FIGURE 7.3.2-3 CASCADED TWO ONE-BIT PHASE SHIFTER WITH RESULTS.

7.3.3 Integrated Two-Bit PPS Using Nixie Tube Electrodes

In the previous section, a two-cascaded one-bit phase shifter was proven to work as required. The net result was to effectively produce a two-bit plasma phase shifter with the following phase states: 0°, 90°, 180° & 270°. The next step was to fully integrate, in one board, the two-bit phase shifter. **Figure 4.2-1** shows this integrated board.

Soldered-on Electrodes
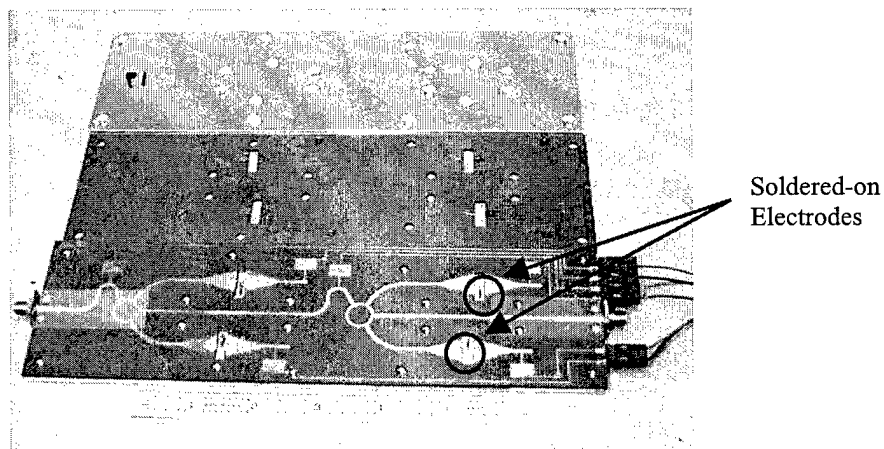
FIGURE 4.2-1 FULLY INTEGRATED TWO-BIT PLASMA PHASE SHIFTER (NIXIE TUBE ELECTRODES)

On these boards, Nixie Tube electrodes are soldered; they act as RF coupling as well as plasma energizer (see **Figure 4.2-2**). The reason for choosing the Nixie Tube electrodes is for their longevity and plasma interaction: their metal composition is very well matched to the plasma environment. Though the Nixie Tube electrode approach was well suited for the experiments up to this point, a problem arose while integrating this two-bit plasma phase shifter. The problem with this approach is maintaining precise placement of the electrodes. At these frequencies slight electrode displacement completely de-tunes the circuits, thus making it unusable in a fully integrated circuit. In the previous circuits, tuning was not a problem since, at most, only a pair of electrodes

needed to be tuned (phased matched). Here there are four electrode coupling regions which makes tuning impossible without sectioning the board as shown in **Figure 4.2-3**. This allows for each electrode pair to be tuned individually. Although this approach was tested successfully, it renders manufacturing a tedious process not to mention added problems when reconnecting the boards. A change of perspective is required before moving on with the two-bit plasma phase shifter.
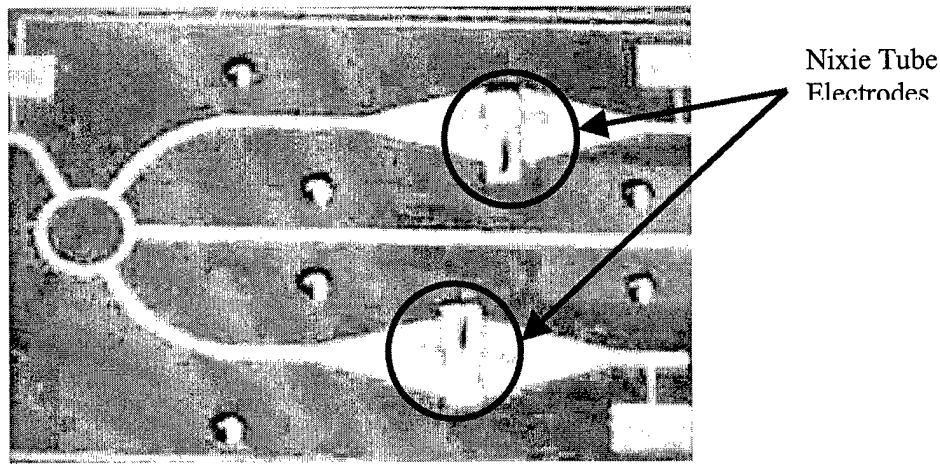

Nixie Tube
Electrodes

FIGURE 4.2-2 RF COUPLING AND PLASMA ENERGIZER VIA NIXIE TUBE ELECTRODES
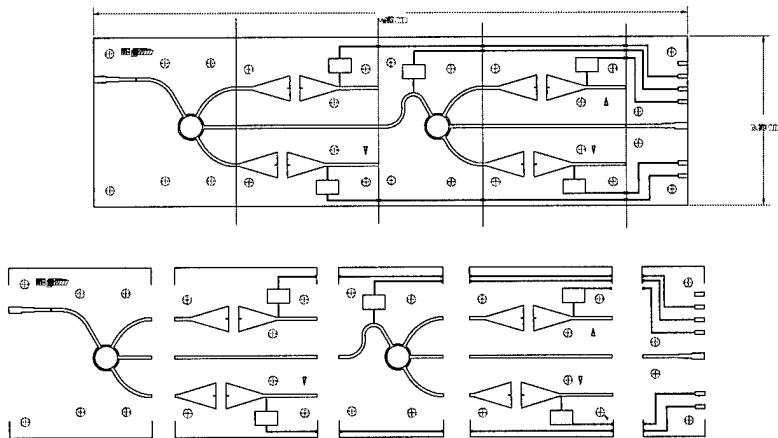

FIGURE 4.2-3 SECTIONING THE TWO-BIT PHASE SHIFTER FOR TUNING

7.4 THE FULLY INTEGRATED PPS

The Nixie Tube electrode approach created some logistic problems due to the attachment of the electrode. Since the electrodes need to be soldered onto the circuit, it makes tuning a two-bit phase shifter a challenge. Furthermore, these electrodes are not manufactured with precision; meaning, no two electrodes are identical. At these high frequencies, imperfections are manifested as unpredictable frequency response.

Consistency is required for this plasma antenna to be cost efficient and commercially viable. Repeatability with minimal effort is necessary as well as ease of assembly. Soldering electrodes is good for prototyping and for proof-of-principle concept but unacceptable for the proposed antenna application. The next approach considered was printed electrodes.

Using the previous stripline circuits; what if the electrodes were printed on both sides of a very thin duroid and then sandwiched between the stripline? Printing the electrodes onto a thin duroid substrate would enable a tight control over the electrode spacing, length, width and thickness. This process would render itself very well to high production systems with a high degree of tolerance. Is it feasible?

7.4.1 Electrodes On Thin Film Duroid

A slew of various size electrodes were printed on 10 mils duroid substrate with an identical pair of electrode printed on the opposing side of the thin film duroid. The idea was to make the printed electrode resemble a regular electrode as close as possible. Also, the electrodes were printed on both sides of the substrate to insure that the plasma will fire all around the thin film; hopefully, this will insure an equal reflection of the travelling RF on either side of the thin film (this plasma phased array element is in a stripline configuration, thus the transmission line is sandwiched between two substrates covered by a ground plane).

Shown in **Figure 7.4.1-1** are the printed electrodes on a thin film duroid sandwiched between the stripline circuit. On the bottom portion is a circuit etched from a copper covered duroid slab, the top part is a fully etched duroid slab with copper on the top side. Between these two slabs lie the printed electrodes.
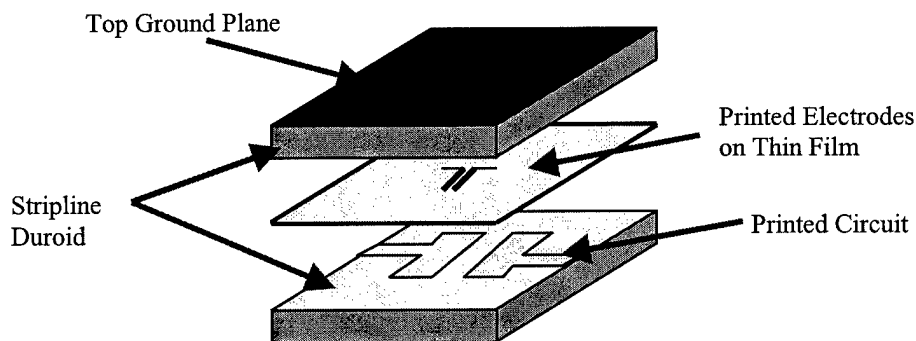

FIGURE 7.4.1-1 ELECTRODE PRINTED ON THIN FILM BETWEEN A STRIPLINE CONFIGURATION
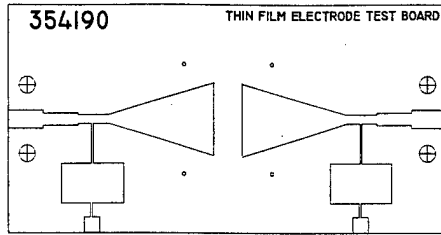
FIGURE 7.4.1-2 BOTTOM PORTION OF STRIPLINE, ETCHED CIRCUIT
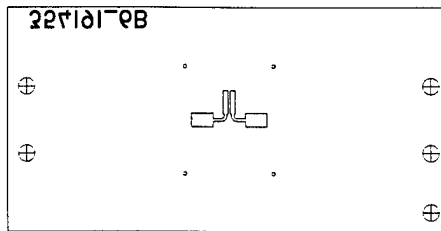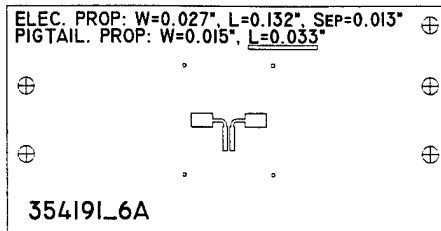
FIGURE 7.4.1-3 PRINTED ELECTRODES ON THIN FILM DUROID, VIEW FROM TOP & BOTTOM

Figures 7.4.1-2 & 7.4.1-3 show the AutoCAD drawings of the bottom portion of the stripline (including the etched circuit) and both views of the thin film duroid, top and bottom. These were assembled and tested with and without plasma. The results were very encouraging; **Figures 7.4.1-4a & 7.4.1-4b** show the insertion loss (S21, measuring the amount of energy transmitted from one end to the other of the circuit) and the reflected loss (S11, measuring the amount of reflected energy from the input) respectively.

FIGURE 7.4.1-4A S11 & S21 OF THE PRINTED CIRCUIT ELECTRODE, NO PLASMA
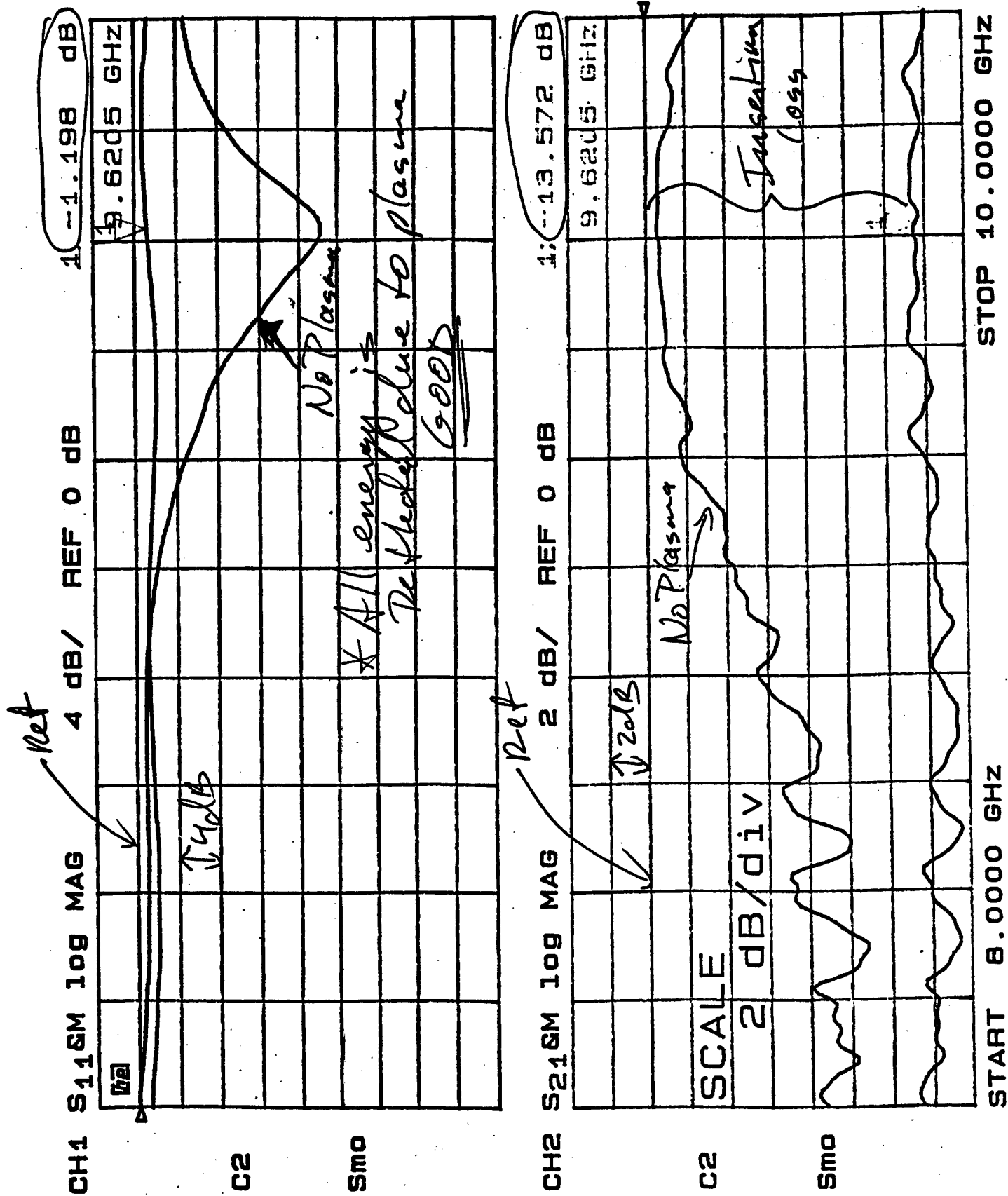
FIGURE 7.4.1-4B S11 & S21 OF THE PRINTED CIRCUIT ELECTRODE, WITH PLASMA

7.4.2 Fully Integrated Two-Bit PPS

The printed electrode concept works very well; the repeatability of the design increased considerably since practically full control over the process is achieved. The only place were there was still room for error was while soldering the tabs of the electrodes located on the top of the thin film to th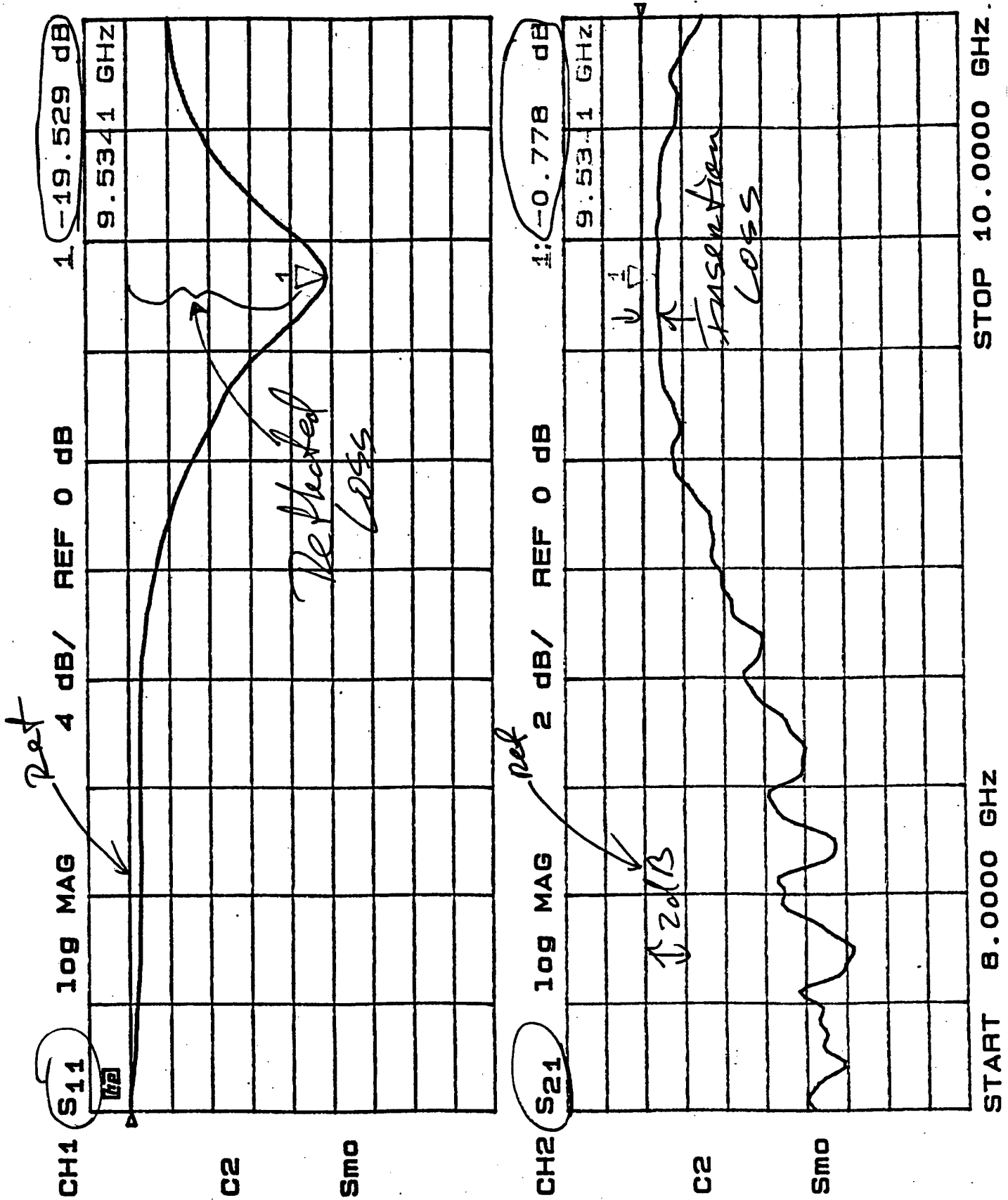e etched circuit. The solution was simple, etch the fully integrated circuit, including the electrodes, on both sides of the thin film duroid and sandwich it between two, fully etched on one side, duroid slabs (see **Figure 7.4.2-1**).
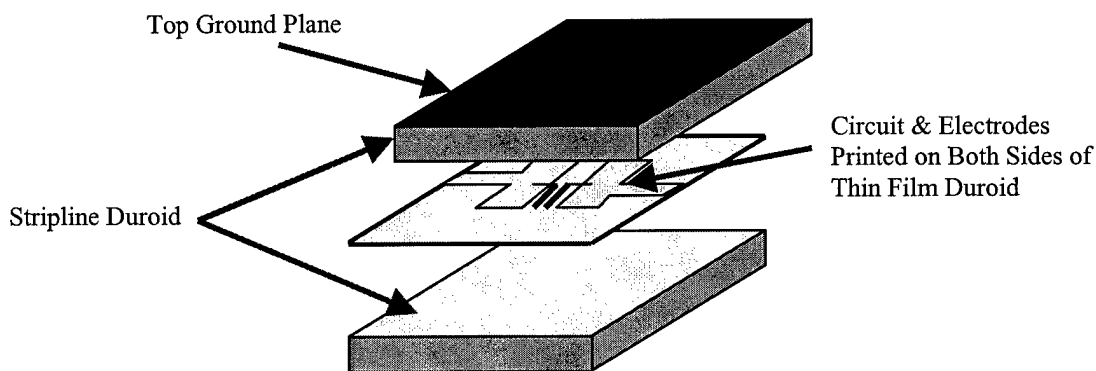
FIGURE 7.4.2-1 CIRCUIT & ELECTRODES PRINTED ON BOTH SIDES OF THIN FILM

This new approach solves all of the manufacturing problems, it makes this concept very easy to implement and also very inexpensive. A full row of phase shifters, including power splitters, electrodes & DC routers, can be etched on one single thin film duroid. **Figure 7.4.2-2** shows the AutoCAD drawing of a fully integrated two-bit plasma phase shifter (including the electrodes) and in **Figure 7.4.2-3** is the photo of the actual board with the two bits highlighted.
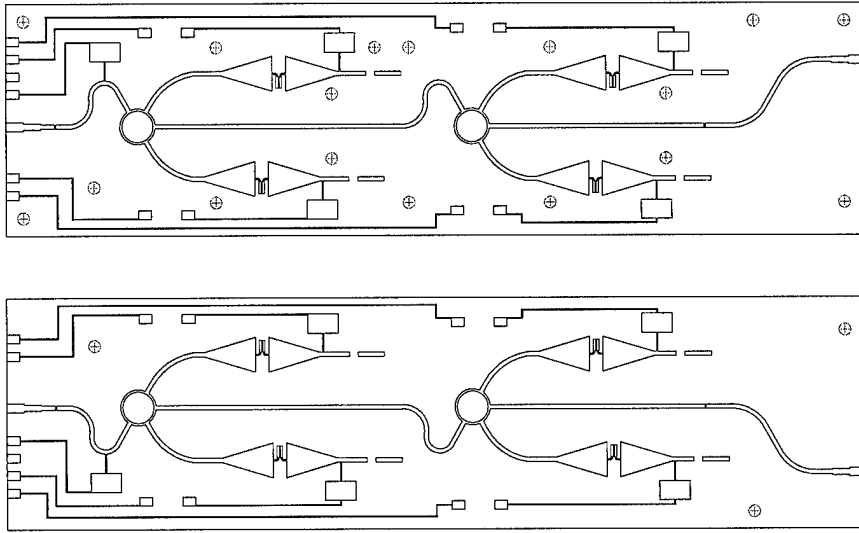
FIGURE 7.4.2-2 FULLY INTEGRATED TWO-BIT PLASMA PHASE SHIFTER ON THIN FILM, VIEW FROM TOP & BOTTOM
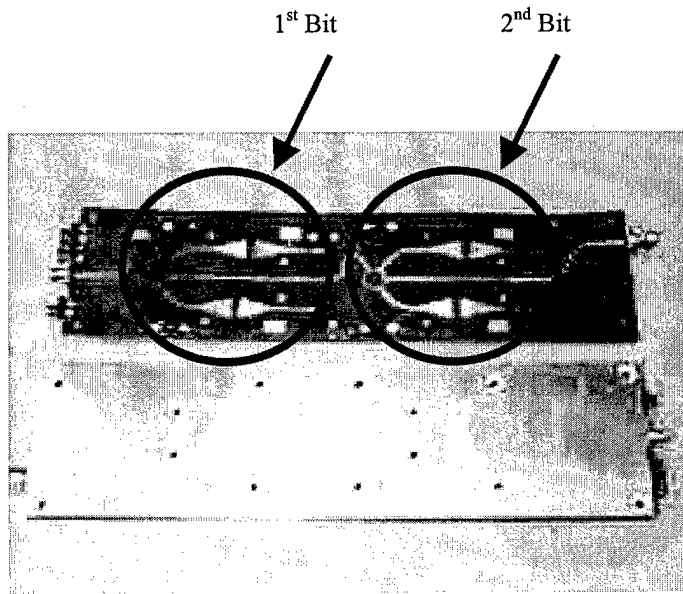
FIGURE 7.4.2-3 TWO-BIT PLASMA PHASE SHIFTER: TOP, CIRCUIT ON THIN FILM; BOTTOM, ASSEMBLED

Four different frequencies were monitored; the best results were at 9.29GHz. On board #1, the four realized phase states are:

- The 1st State … the plasma phase shifter without any plasma (87°).

- The 2nd State … plasma was applied to the first bit (176°).

- The 3rd State … the second bit was turned on (143°).

- The 4th State .. both bits are on (plasma is applied, -126°).

Effectively these represent following relative phase angle:

- The 1st State … 0°

- The 2nd State … 89°

- The 3rd State … 56°

- The 4th State .. 147°

TABLE 7.4.2-1 RELATIVE PHASE ANGLE OF TEN PLASMA PHASE SHIFTING BOARDS

Board #	No Plasma (All Bits OFF)		1st Stage Fired (1st Bit ON)		2nd Stage Fired (2nd Bit ON)		Both Stages Fired (Both Bits ON)	
	Meas.	Relative	Meas.	Relative	Meas.	Relative	Meas.	Relative
0	43°	-42°	150°	65°	105°	20°	-139°	136°
1	87°	2°	176°	91°	143°	58°	-126°	149°
2	84°	-1°	-173°	102°	144°	59°	-107°	168°
3	92°	7°	-176°	99°	142°	57°	-113°	162°
4	85°	0°	-179°	96°	142°	57°	-116°	159°
5	79°	-6°	-173°	102°	141°	56°	-109°	166°
6	74°	-11°	172°	87°	141°	56°	-120°	155°
7	47°	-38°	164°	79°	147°	62°	-118°	157°
8	40°	-45°	177°	92°	95°	10°	-121°	154°
9	96°	11°	-164°	111°	156°	71°	-100°	175°

In Table 7.4.2-1 the phase measurements of ten boards, for all four (4) states, are shown. Notice how repeatable the phase measurements are for all boards, in some cases the measured phases are within a few degrees of each other (this is very good considering that, on these boards, the line lengths on each board were adjusted after being etched).

The most compatible 8 boards are highlighted; they were used in the 1x8 plasma phased array proof-of-principle during the following progress reporting period.

The plotted results of board #1 can be seen in Report **MRA P354-13 Figures 5.2-4a** through **5.2-4d** where the insertion loss ("S21 log MAG", measuring the amount of energy transmitted from one end to the other of the circuit) and the relative phase at the output of the circuit are plotted respectively.

8.0 THE PLASMA PHASE ARRAY ANTENNA

The sections leading up to this one proved that plasma could be used as the core mechanism for producing an inexpensive RF phase switch. A two-bit plasma phase shifting (PPS) element was produced entirely using printed circuit technology. This technique of producing the PPS elements yielded very stable and repeatable measurements between different elements. The final test consists of integrating an antenna utilizing the PPS elements. A one-by-eight phased array antenna was assembled and tested at Malibu Research facilities. This section discusses the configuration, the test setup and the results of the experiment.

8.1 THE SYSTEM BLOCK DIAGRAM AND COMPONENTS

The antenna array system is shown in **Figure 8.1-1**. It consists of a PC, a power distribution unit, an RF source, a vacuum chamber with 8 plasma phase shifting elements and a radiating dipole antenna. The PC is used to control the ON/OFF state of each PPS element; this is accomplished via a serial command word that is deciphered in the power distribution unit which, in turn, routes the DC voltage to the elements in the vacuum chamber. An RF source is fed in the vacuum chamber to a 1:8 power divider; although this power divider could have been integrated in a stripline, a commercial off-the-self item was bought instead. The equi-phased RF is then fed to the eight elements from which the output is routed outside the chamber.

Figure 8.1-1 Plasma Phased Array Antenna Block Diagram

An AutoCAD drawing of the phase shifting elements as well as a photograph of two boards is shown in **Figure 8.1-2**. On the photograph, one board is shown open and one is fully assembled (the stripline thin duroid is sandwiched between two thicker layers of duroid which, in turn, is sandwiched between two aluminum ground planes). The whole assembly is screwed down tightly and some peepholes are drilled through the aluminum ground plane and the duroid to allow a free flow of the surrounding pressurized gas around the electrodes. The RF input is at the left side of the shown drawings. At the output, shown at the right in this case, is the phase shifted RF signal.
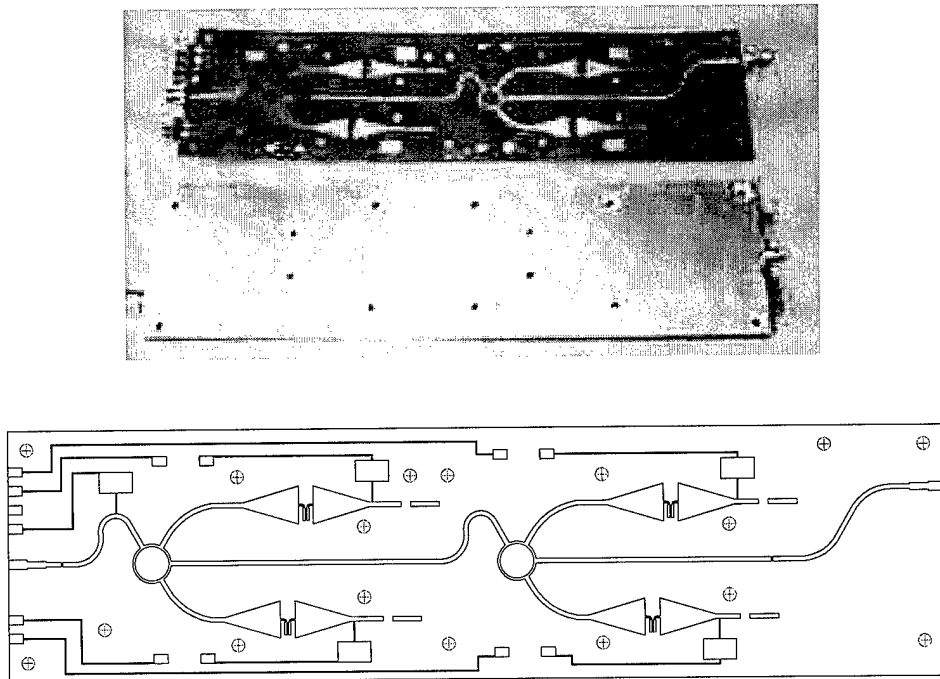

FIGURE 8.1-2 PLASMA PHASED SHIFTING ELEMENTS; PHOTO AND AUTOCAD REPRESENTATION

The PPS elements need to be surrounded by a gas at a specified pressure. In this case the gas is pure Helium and the pressure is 60 Torrs. For this demonstration a vacuum chamber was built containing the PPS elements. The AutoCAD rendering of the chamber is shown in **Figure 8.1-3**. On the left is a side view cross section of the chamber with two PPS elements and on the right side is a top view cross section showing the eight PPS elements and the 1:8 power divider at the center. **Figure 8.1-4 is the** photograph of the opened chamber showing the PPS arrangements. On the right side of the chamber is seen the pressurizing valves and on the left is mounted the radiating elements
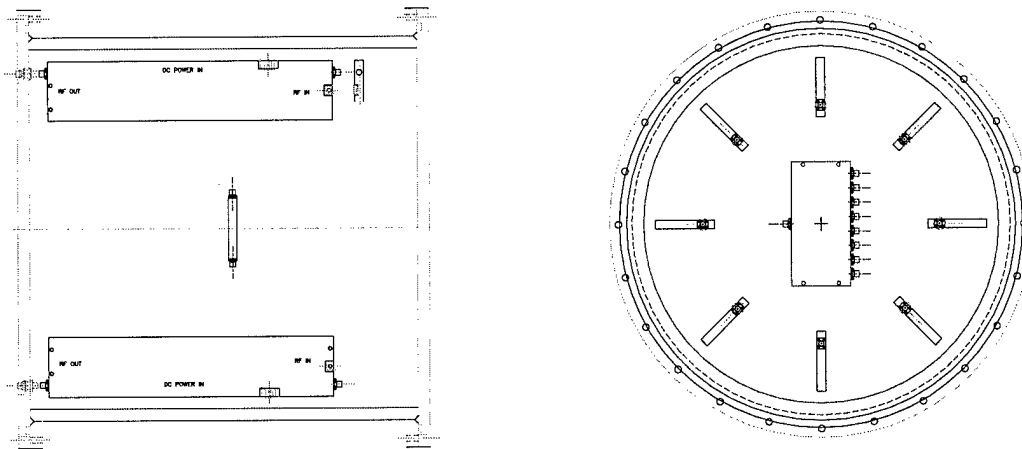

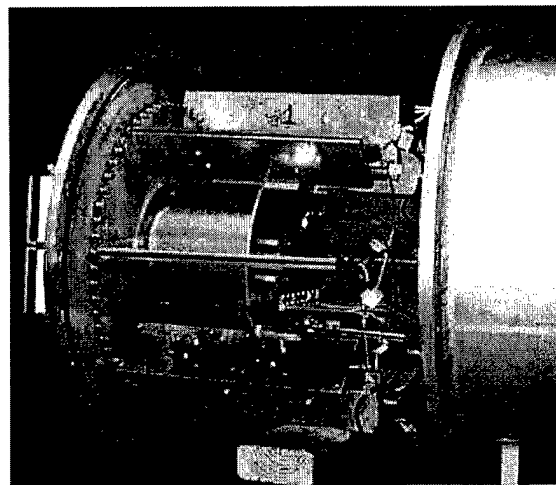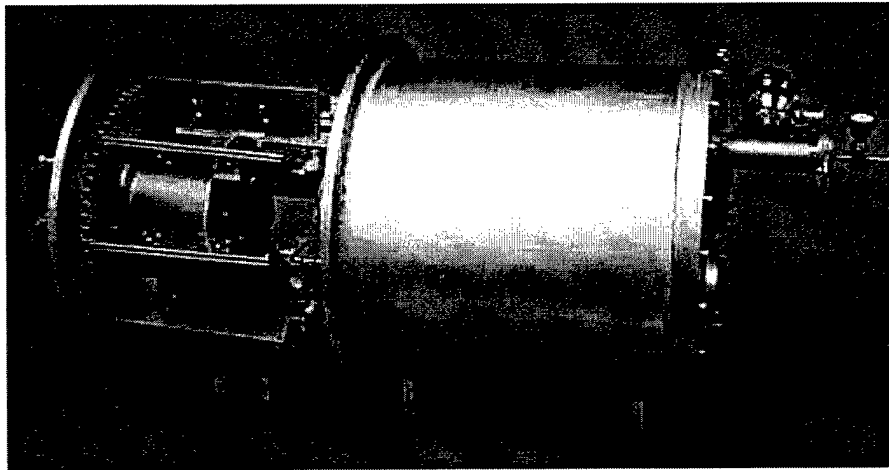FIGURE 8.1-3 THE VACUUM CHAMBER AUTOCAD LAYOUT; SIDE & TOP VIEWS

FIGURE 8.1-4 THE OPENED VACUUM CHAMBER

The radiating dipoles are shown in **Figure 8.1-5**, these are in a stripline configuration. A ground plane is fixed to the stripline just below the radiating dipoles (the fat horizontal strip at the top of the AutoCAD drawing). The radiating stripline dipole array is shown mounted on the vacuum chamber in **Figure 8.1-6**.
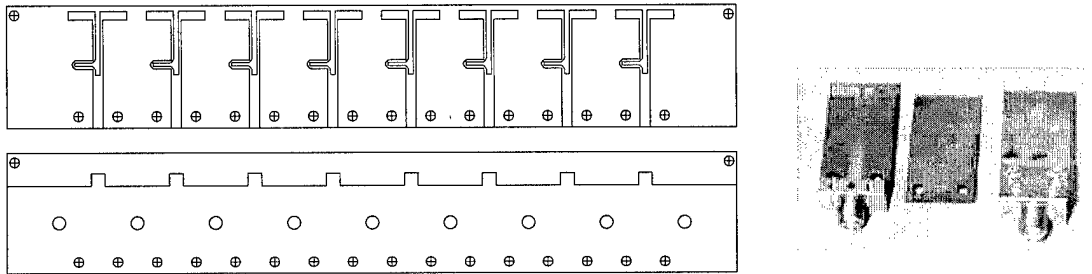

FIGURE 8.1-5 THE RADIATING STRIPLINE DIPOLE ARRAY ALONGSIDE A PHOTO OF A SINGLE DIPOLE
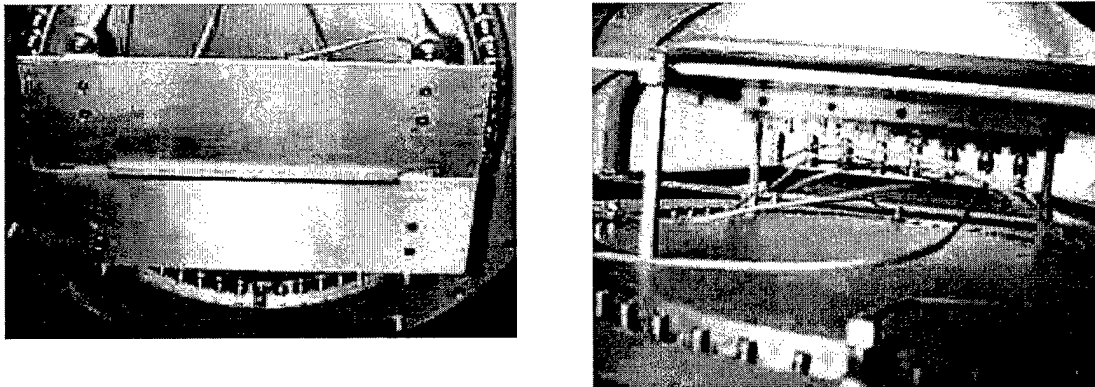

FIGURE 8.1-6 THE RADIATING DIPOLES PROTRUDING A GROUND PLANE, MOUNTED ON THE VACUUM CHAMBER (FRONT & BACK SIDE VIEWS)

8.2 THE MEASUREMENT SETUP

First the chamber needed to be pumped down and pressurized using Pure Helium to 60 Torrs. The setup is shown in **Figure 8.2-1,** the vacuum chamber is pressurized via the small chamber in order to minimize the breakdown of the in-house vacuum test chamber setup.
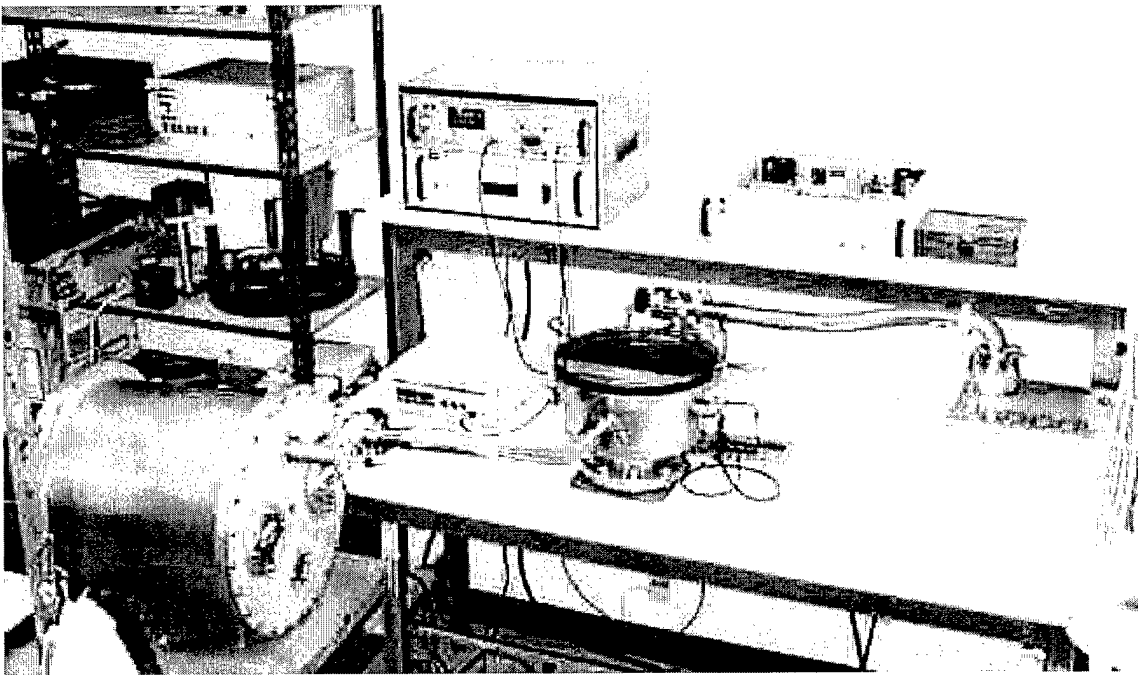

FIGURE 8.2-1 PRESSURIZING THE VACUUM CHAMBER

Next the chamber was placed in the range, on top of the rotating pedestal as shown in **Figure 8.2-2.**
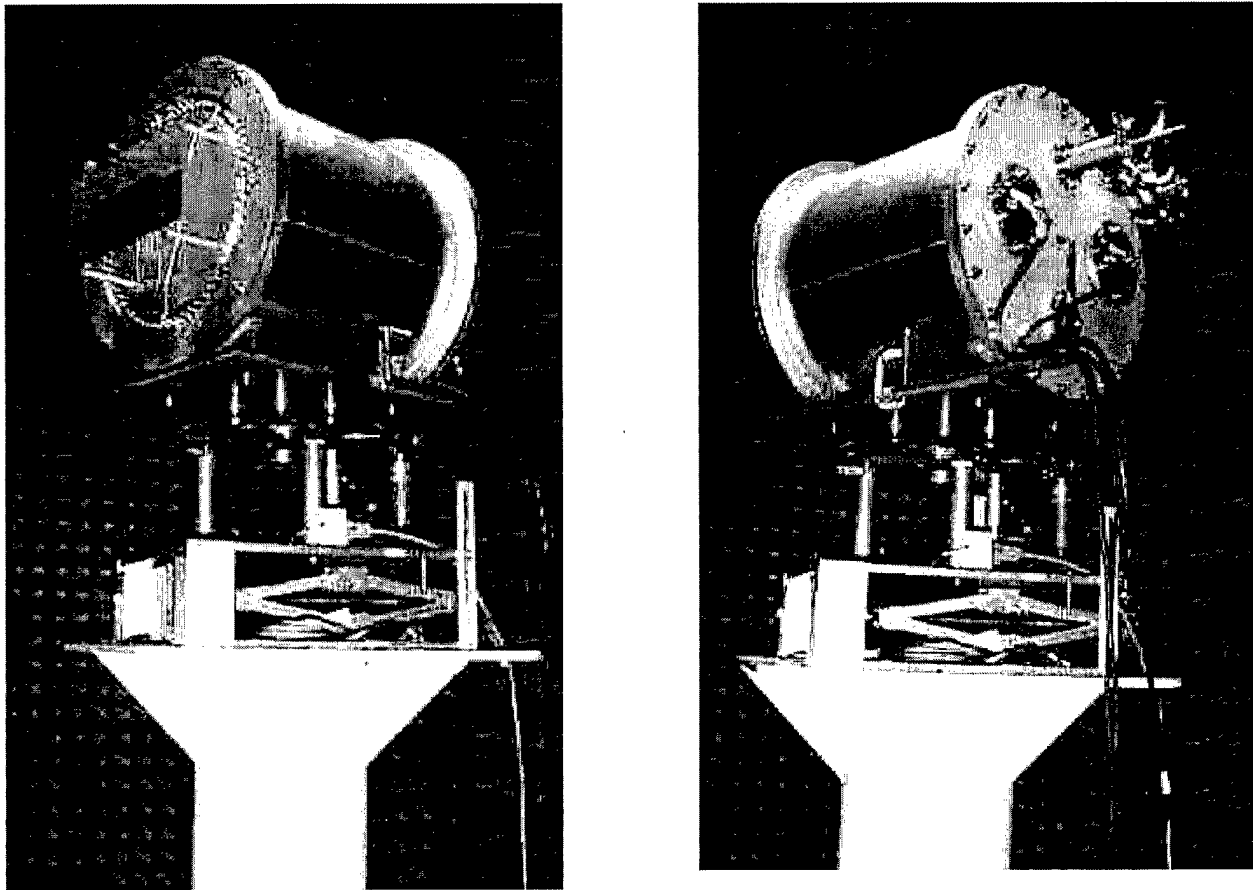
FIGURE 8.2-2 FRONT AND BACK VIEWS OF THE ANTENNA ON THE PEDESTAL

The setup is shown in **Figures 8.2-3** through **8.2-6**. The Plasma Phased-Array Antenna was radiating the RF that bounced off an 8-Foot reflector on the far end of the chamber and was received by the horn antenna. As a source, the HP network analyzer was chosen with a CW at 9.2906GHz with an output power of +15dBm. A high precision attenuator is placed between the HP and the Plasma Phased-Array Antenna for calibration purposes. Once the setup is calibrated, the attenuator was set to 1dB. The RF is directed into the chamber where a 1-to-8 power splitter distributes the energy with

equal phase front and power to the 8 plasma phase-shifter elements. The DC voltage is routed through two pressure-sealed connectors. The DC source is a 1000 Volt, 300mA, power supply. On the receiving end, the output of the horn antenna is connected to a 10dB Low-Noise Amplifier followed by a detector. The received energy is then routed to the recorder.
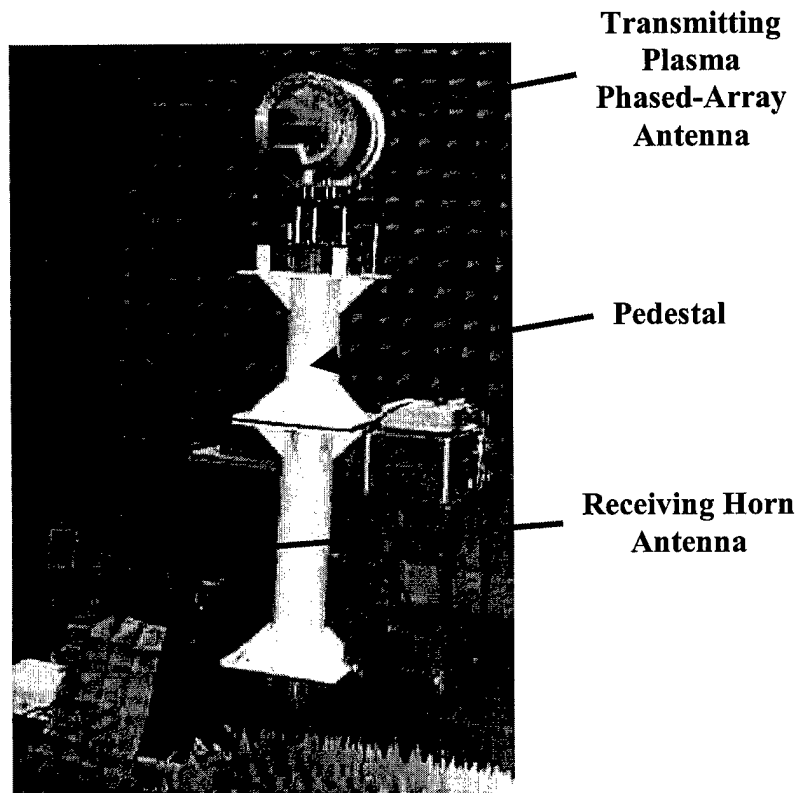

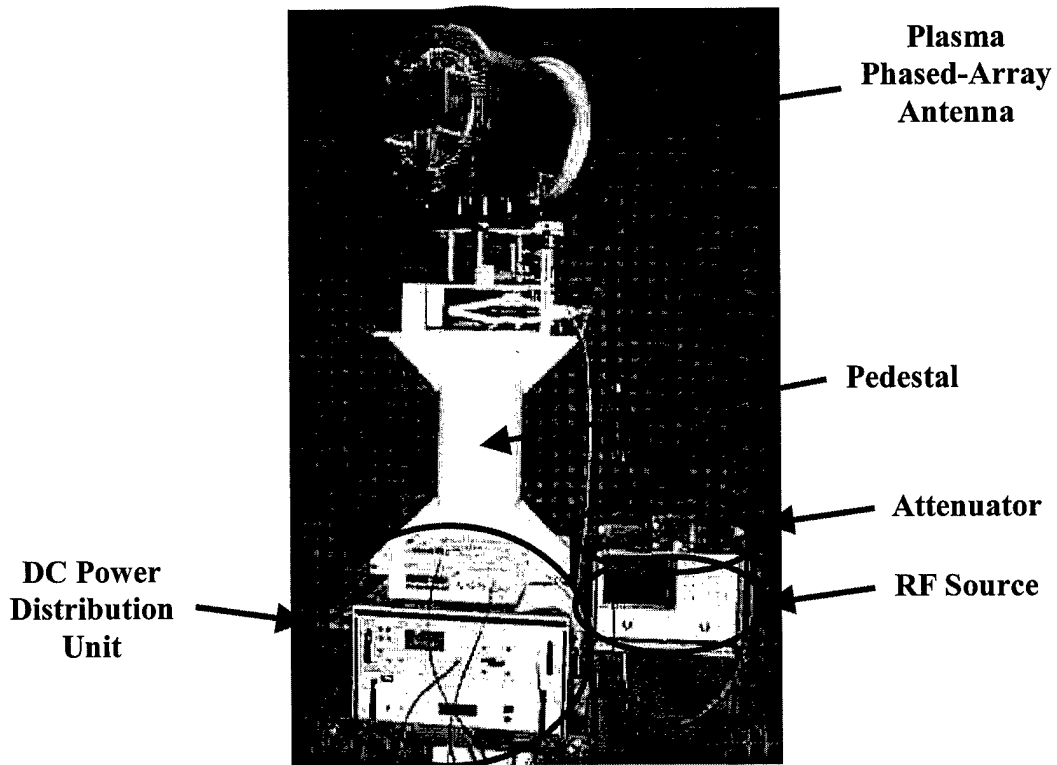FIGURE 8.2-3 THE TRANSMITTING AND RECEIVING ANTENNAS

FIGURE 8.2-4 THE PLASMA PHASED-ARRAY ANTENNA EQUIPMENT
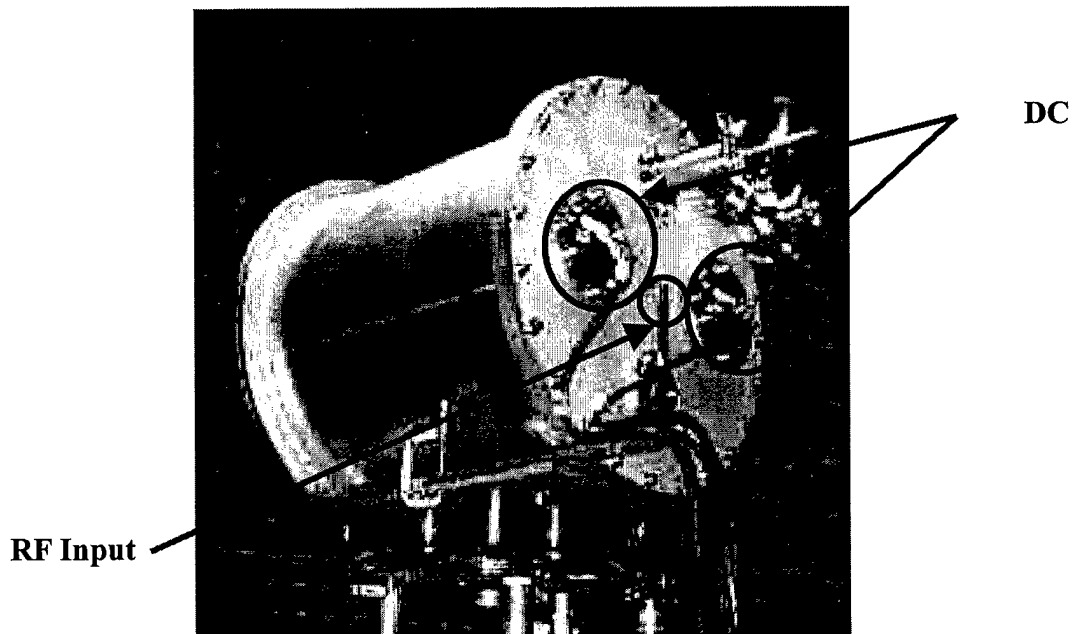
FIGURE 8.2-5 THE PLASMA PHASED-ARRAY INTER-CONNECTIONS
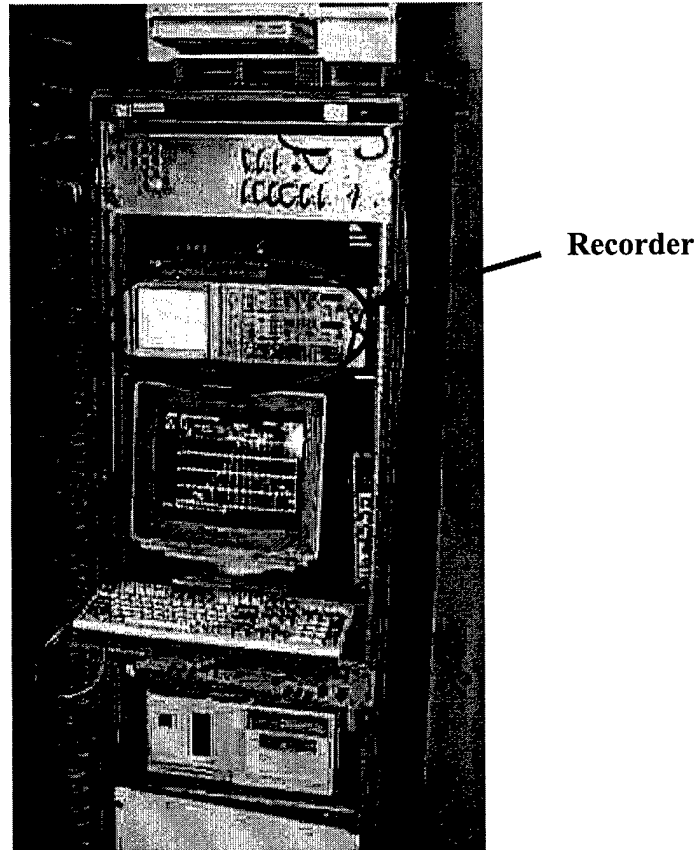
Recorder

FIGURE 8.2-6 THE RECORDING EQUIPMENT

The equipment list:

- ➤ RF Source   HP 8720c
- ➤ Variable Attenuator   HP X382A
- ➤ Amplifier   Avantek AWT-18054 8-18GHz
- ➤ Detector   0.01-12.4GHz
- ➤ Recorder   Wiltron 560A : Scalar Network Analyzer

8.3 THE PLASMA PHASED-ARRAY RESULTS

A frequency generator, used as an ON-OFF switch, was added to the setup in order to extend the life of the electrodes. The plasma needs to be pulsed so that the electrodes last longer. These electrodes are tined which increases the lifetime of the electrodes to a certain degree. The cycle used was a 10% duty cycle pulse with a cycle of approximately 1 second long pulse (the pulse is ON 75-100 ms and OFF 800-900 ms). This results in an overlapping of antenna pattern when the plasma is switched On & Off.

In **Figure 8.3-1** is a screen capture of the plasma phased-array antenna without any phase shift (plasma Off). The plot is also shown in **Figure 8.3-2**. The first sidelobe is about 12 dB down from the main beam which is very good considering that a single line array of dipoles is used.
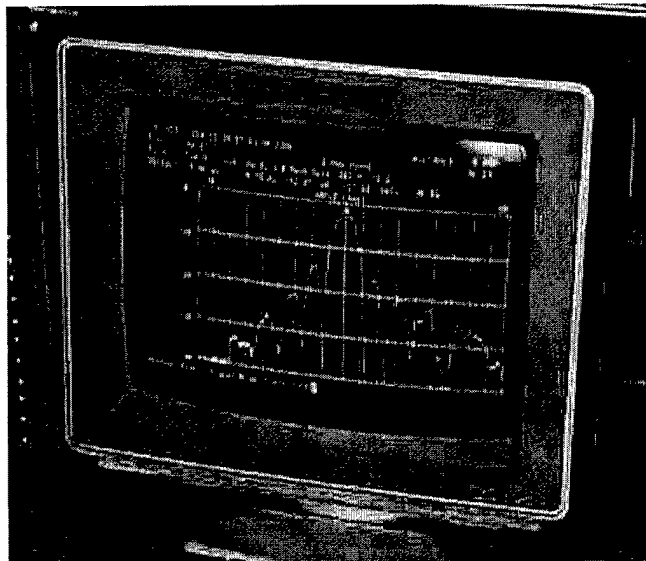

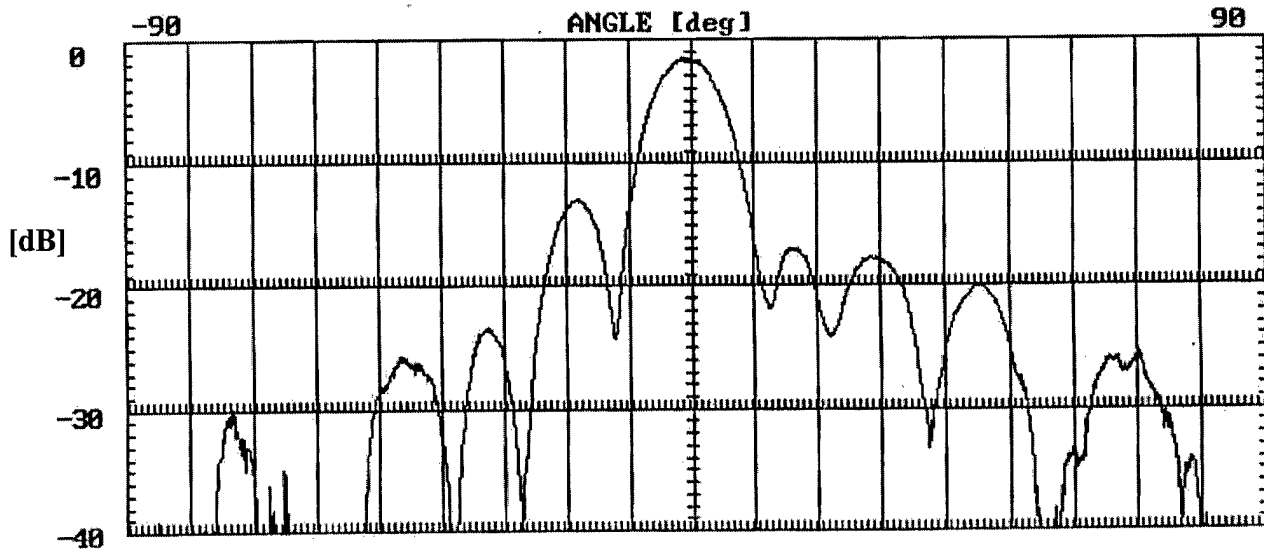FIGURE 8.3-1 SCREEN CAPTURE OF THE ANTENNA PATTERN WITHOUT PLASMA

FIGURE 8.3-2 ANTENNA PATTERN WITHOUT ANY PHASE SHIFT (NO PLASMA, F=9.209GHZ)

In **Figure 8.3-3** is the plot of the plasma phased-array antenna with an effective

phase shift of +28°. This plot tends to be confusing since the plasma is switched On &

Off by the pulse generator. The resulting antenna pattern plotted is a superposition of the

antenna with and without the phase shift (the thin vertical lines trace the antenna pattern

of the shifted case, the actual phase shifted antenna pattern was traced in red). In **Figure**

8.3-4 the antenna pattern of the phase-shifted case is hand traced and shown by itself for

clarity. In **Figure 8.3-5** is the plot of the plasma phased-array antenna with an effective

phase shift of –28° superimposed to the none phase shifted one (the thin vertical lines

traces the antenna pattern of the shifted case, the actual phase shifted antenna pattern was

traced in red). In **Figure 8.3-6** the antenna pattern of the phase-shifted case is hand

traced.

As per theory, the main beam of the scanned array (Figure 8.3-3) lost energy with respect to the non-scanned beam (Figure 8.3-2) which was, in turn, gained by the sidelobes. The further away from boresight the beam is scanned, the lower the main beam energy content will be and inversely the greater the levels of the sidelobe energy.
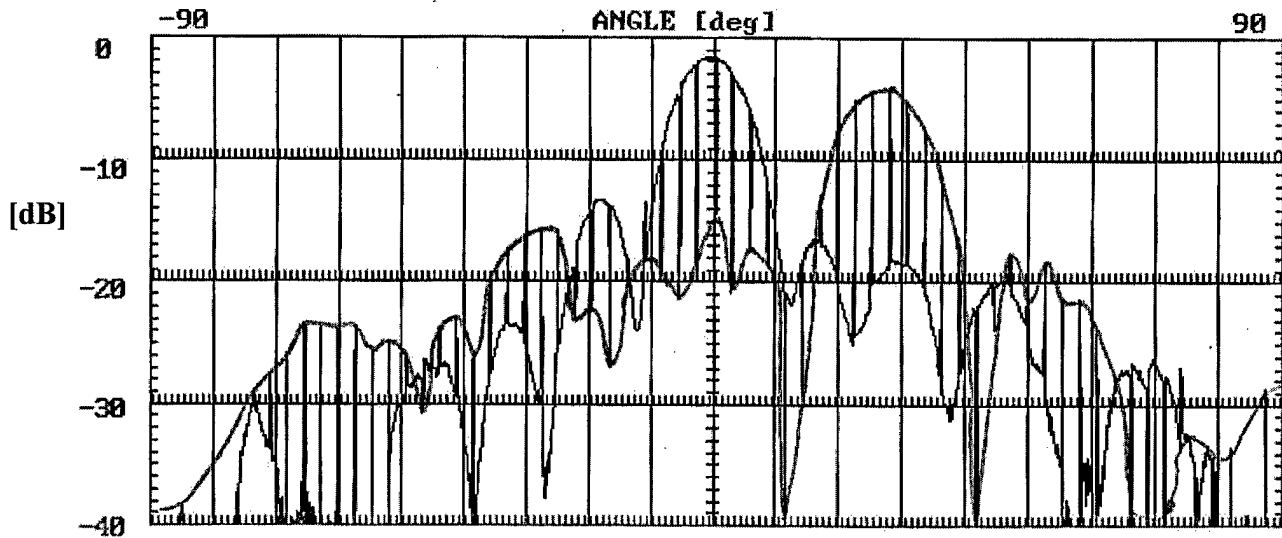

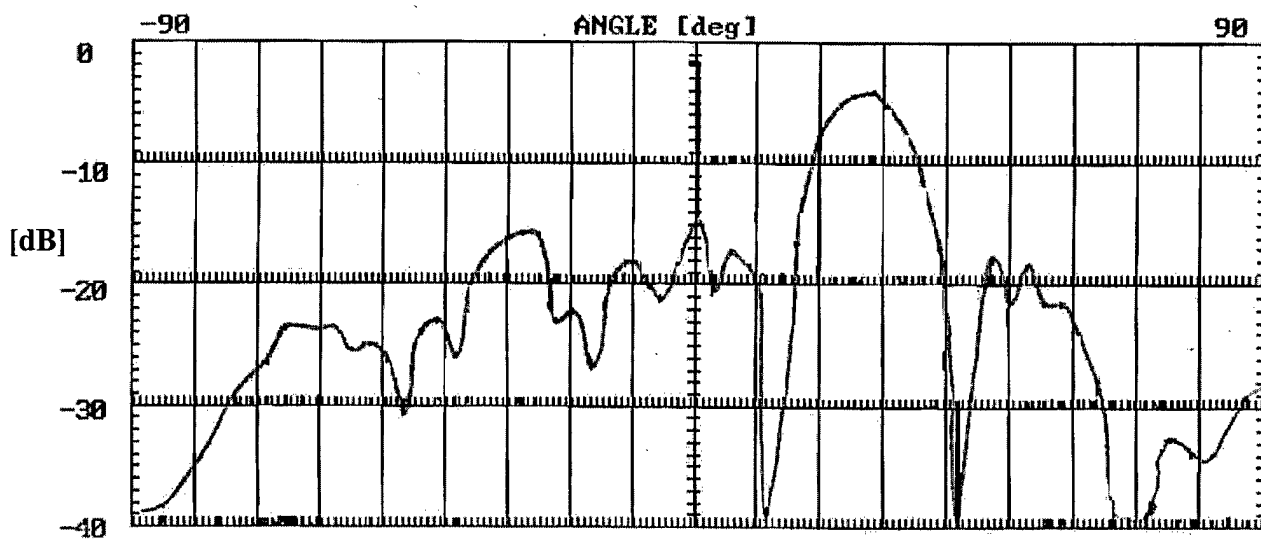FIGURE 8.3-3 ANTENNA PATTERN WITH A SWITCHING +28° PHASE SHIFT (F=9.209GHZ)

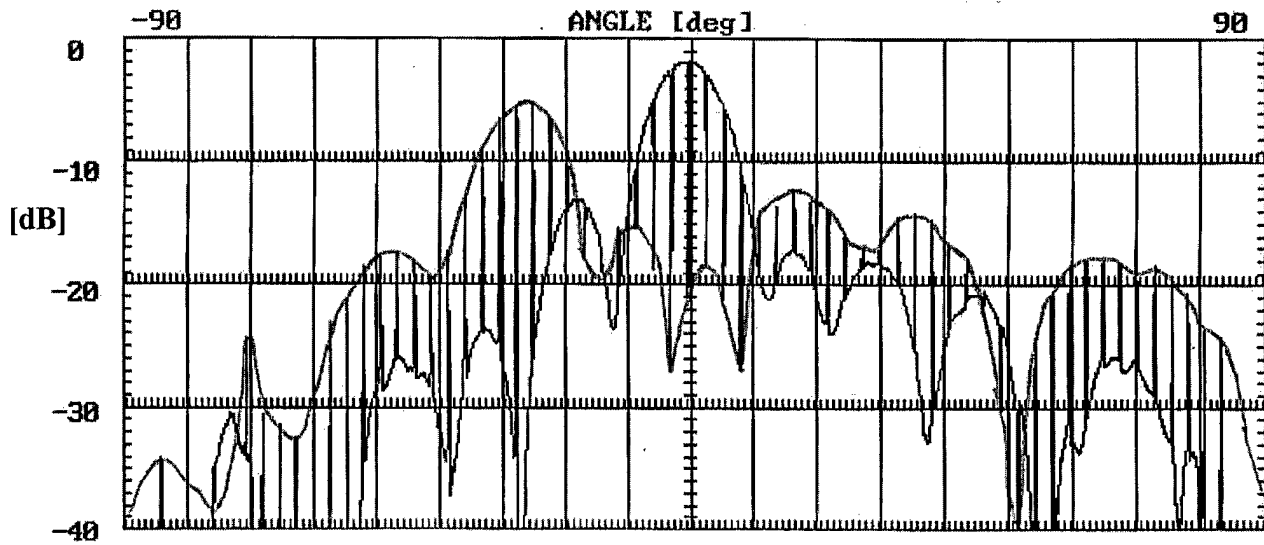FIGURE 8.3-4 ANTENNA PATTERN OF THE +28° PHASE SHIFT, HAND TRACED PLOT

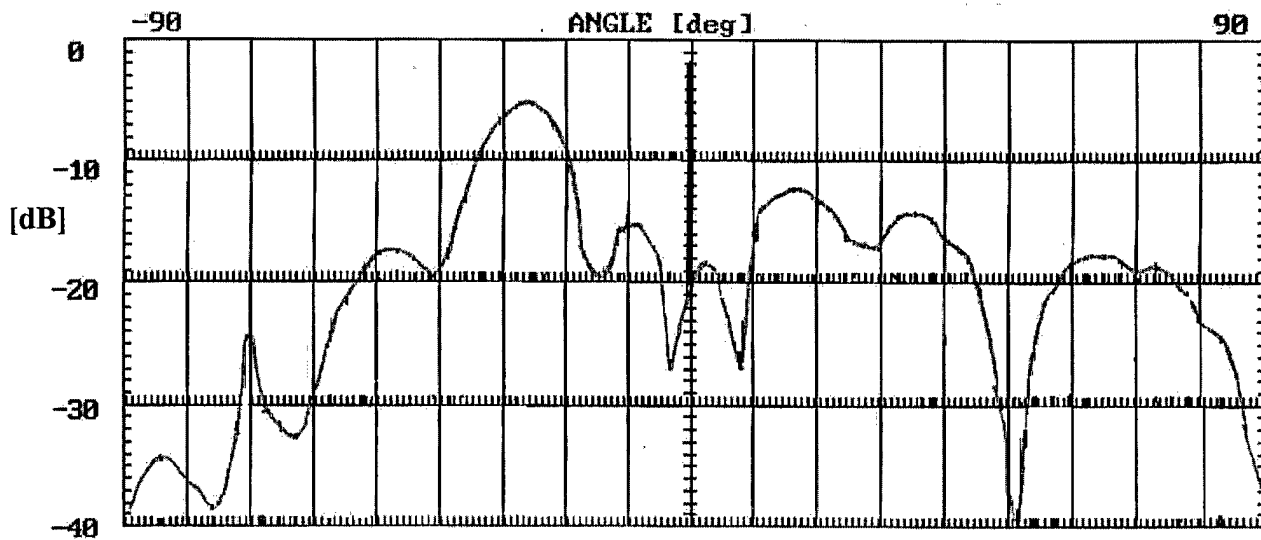FIGURE 8.3-6 ANTENNA PATTERN WITH A SWITCHING -28° PHASE SHIFT (F=9.209GHz)

FIGURE 8.3-5 ANTENNA PATTERN OF THE -28° PHASE SHIFT, HAND TRACED PLOT (F=9.209GHz)

9.0 THE ELECTRODE LIFETIME

As mentioned in the previous section, the lifetime of pure copper electrodes is minimal. That is the reason why the electrodes in the PPS elements were tinned prior to firing them. Bare copper can withstand continuous plasma for a length of 10 minutes only (for a surrounding gas of pure Helium at a pressure of 60Torrs and fired with a DC voltage of 450VDC with a limiting current resistor of 20kOhms). By tinning the electrodes, their lifetime increases by a factor of 3 to approximately 30 minutes. This is the reason that the measurements in the previous section were carried out using a pulse generator, in doing so the lifetime of the tinned electrodes increases many folds.

Some initial research and testing of plated electrodes was conducted. A few different types of material were used to plate the electrodes, these were:

- Tin
- Gold
- Nickel-Tungsten
- Platinum
- Palladium
- Rhenium
- Rhodium

Of these materials some reacted very poorly to the RF, displaying a fairly substantial insertion loss (the Nickel-Tungsten) and others a poor reaction to plasma. In **Table 9.0-1** is given the comparison between the worst case, that of the pure copper electrode, to the tinned electrode and finally the best lifetime result without compromising the RF response of the PPS elements.

TABLE 9.0-1 LIFETIME PERFORMANCE OF PLATED ELECTRODES

Plating Material	Performance	Improvement (%)
Bare Copper (0.75mil)	10 minutes	-
Solder Tinned (6mils)	30 minutes	300%
Rhodium (0.2mil)	15 hours	9000%

10.0 OVERVIEW

This is the final report on the SATCOM Electronic Scan Antenna, SBIR Phase II. All of the major results and critical considerations were presented. They are summarized in the following:

- ➤ Phase I results pointed towards an erroneous conclusion.

- ➤ An extensive theoretical investigation revealed that the plasma skin depth, within the proposed application, is not adequate for the plasma display application.

- ➤ In the process, an alternate plasma array configuration was defined presenting the same major advantages as the initial proposed design.

- ➤ MRA's in-house chamber enabled full control over the plasma parameters in real-time.

- ➤ Lack of hysteresis was a major upset that was solved by using a different gas (close to ideal plasma hysteresis signature was obtained using Helium gas).

- ➤ Shown the ability of plasma to create an efficient RF wall.

- ➤ Shown the ability of plasma to reflect RF with a consistent phase shift.

- ➤ Demonstrated plasma's efficiency in a phase shifting stripline design including the use of hybrids.

- ➤ Demonstrated the plasma phased array antenna scanning capability.

- ➤ Presented the initial electrode lifetime investigation results.

Issues that need to be addressed in the future are:

- Lifetime
    Plated Electrodes
    Outgassing - Ceramic Substrate

- Compactibility

- Ionization Voltage Level

- Different Gasses
    NeAr
    Helium
    Xenon
    Combinations

- Bandwidth (RF)

11.0 REFERENCES

[1]   Zhan R. and Jiang X., "Jumps and Hysteresis Effects in CH4-H2 Plasma

Discharges", *Journal de Physique III France*, vol. 5, February 1995, 197-202.

[2]   Bosh R. and Merlino R., "Sudden Jumps, Hysteresis and Negative Resistance in

an Argon Plasma Discharge; I. Discharges with No Magnetic Field", *Contrib.*

Plasma Phys., vol. 26, 1986, 1-12.

[3]   Cartier S. and Merlino R., "Observations of Nonlinear Behavior in a Low-

Pressure Discharge Column", *IEEE Trans. Plasma Sc.*, PS-12, No. 1, March

1984, 14-18.

Malibu Research

26670 Agoura Road
Calabasas, CA 91302-1974
(818) 880-5494 Fax 880-5499

LCDR Roy Ledesma, PMW 185-9   31 October 2000
APM, Inter-Agency Space Systems
COMSPAWARSYSCOM
4301 Pacific Highway, OT-1, Room 2721
San Diego, CA 92110-3127

Reference: Contract No. N00039-97-C-0069

Subject: Submission of Final Report

Dear LCDR Ledesma:

In accordance with the referenced contract reporting requirements, CDRL Data Item #A002, enclosed please find two (2) copies of Malibu Research Associates' (MRA) Final Report, MRA P354-F, the period covering 04/05/00 through 10/31/00.

Along with this report we are enclosing four (4) copies of the corresponding Final DD250. Upon acceptance, please sign one copy (Item 21B) and forward to my attention.

If you have any questions or need additional information, please don't hesitate to contact the undersigned.

Sincerely,

MALIBU RESEARCH

Frances L. Bohn
Director of Administration

cc: SPAWAR / J. Berkowitz (1c), Kimberly D'Souza (Ltr)
        DCMC-Van Nuys, CA; Attn: Lisa Steg, GVOEW, 4th Floor (Ltr)
        DTIC (4c)
        MRA / D.G. Gonzalez (1c), L. Gravelle (1c), D. Perry (Ltr)